ADVANCES IN FOOD AND NUTRITION RESEARCH, VOL. 42

X-RAY DIFFRACTION OF FOOD POLYSACCHARIDES

RENGASWAMI CHANDRASEKARAN

Whistler Center for Carbohydrate Research
Purdue University
West Lafayette, Indiana 47907

I. INTRODUCTION

A. IMPORTANCE OF FOOD POLYSACCHARIDES

Carbohydrates are molecules composed of carbon, hydrogen, and oxygen atoms. They usually denote simple monosaccharides such as glucose and galactose, disaccharides such as sucrose and lactose, a spectrum of low-molecular-weight oligosaccharides, and a large number of high-molecular-weight polysaccharides that encompass starch and glycogen. In one form

1043-4526/98 $25.00

or another, carbohydrates constitute an important component of human diet: breakfast cereal, bread, snack, and dessert included. Polysaccharides are abundant in plant life. Some examples are cellulose, xylan, glucan, xyloglucan, starch, and pectate. Carrageenan and alginate are copiously produced from marine algae. Likewise, xanthan, curdlan, and gellan are of bacterial origin. Primarily, cellulose is water insoluble, but the rest are water soluble and hence referred to as hydrocolloids. Their aqueous solutions often are either viscous or able to form gels. Such physical properties can be controlled by the addition of co-solutes, by temperature, and also by the amount and type of cations in the case of anionic polymers. If viscosity is exploited for thickening soups, gravies, sauces, and salad dressings, gelation is useful for desserts, confectionery, jams, jellies, and pet foods. Overall, polysaccharides as minor ingredients, i.e., used in small quantities, are essential for texture, stability, and shelf life of a very large number of food products. Polysaccharides of plant, algal, and bacterial origin have so far found excellent practical applications in the food industry (Whistler and BeMiller, 1993, 1997; Ross-Murphy, 1994; Stephen, 1995; Eliasson, 1996). The focus of this chapter is the molecular architecture of these polysaccharides as related to their observed functional properties, which may result from junction zone formation or through specific interactions with the surrounding molecules, as determined by the polymer shapes.

B. STRUCTURE–FUNCTION–PROPERTY CORRELATIONS

Proteins, nucleic acids, and polysaccharides are the three major classes of biopolymers, the building blocks of which are amino acids, nucleotides, and saccharides, respectively. Both proteins and nucleic acids are linear polymers. The polymerization is always from the N-terminal to the C-terminal end in proteins that are composed of 20 different α-L-amino acids, from alanine to lysine, having distinct side chains in terms of size and charge. Depending on the composition and sequence of amino acids, the polypeptide backbone of a protein chain folds a certain way to form a unique molecular shape. In most instances, protein molecules whose functions range from enzyme activity, to polymerization of polynucleotides, to carbohydrate binding, to name a few, take up compact globular forms. In general, the polypeptide chain morphology utilizes α-helical segments, pleated β-sheets and reverse turns, in conjunction with a few loops and some other nonrepetitive conformations in a well-orchestrated combinatorial manner as dictated by its sequence and environment. On the other hand, a spectrum of muscle proteins, collagen, actin, and myosin, adopt long helical forms compatible with their function as structural proteins (Branden and Tooze, 1991).

The skeleton of nucleic acids is the sugar-phosphate backbone. It always proceeds from the 5′ to the 3′ end, the five-membered sugar ring being a β-D-ribose in RNA and a similar 2′-deoxyribose in DNA. One of the four nitrogenous bases (adenine, guanine, cytosine, and thymine or uracil) is a side chain attached to the sugar ring through a glycosyl bond from atom C1′. While DNAs and some RNAs have a preponderance to form antiparallel double helices stabilized by Watson–Crick base pairs, messenger RNAs are known to adopt folded structures with loops and turns, and transfer RNAs occur as fully compact molecules (Saenger, 1984).

Unlike the unidirectional chemical links connecting successive residues in proteins and nucleic acids, carbohydrates utilize multidirectional links. For example, every pyranosyl unit in a hexopyranose-containing polysaccharide may contain up to four (1→n) links, n being 2, 3, 4, or 6. This versatility results in complex branch-on-branch structures similar to that of glycogen that contains only (1→4) and (1→6) links. Further, both L- and D-saccharides occur commonly; and in each case both α- and β-conformers exist. This quadruples the number of available saccharide units as building blocks and enables generation of a large variety of structures. Consequently, it is believed that carbohydrates including polysaccharides are excellent molecules for storage of biological and structural information, perhaps even superior to proteins and nucleic acids.

The shapes of biopolymers at the atomic level, as well as the interactions among biopolymers and the molecules in the environment, are the major determinants of observed functional behavior. Thus, a knowledge of the three-dimensional structures is extremely helpful for understanding the molecular basis of the useful and functional properties. In the case of food polysaccharides, this information is important for enhancing the desired properties at a relatively low cost by chemical modification, addition of cosolutes, or other options.

II. BASIC PRINCIPLES OF SOLVING THREE-DIMENSIONAL STRUCTURES

The spatial arrangement of atoms gives a recognizable shape that is unique to each molecule. There are several experimental techniques that involve the interaction of radiation with atoms in molecules and provide structural details to varying extents. For example, solution light scattering could lead to estimates of the molecular weight and macroscopic dimensions such as the end-to-end distance and radius of gyration (Brownsey *et al.*, 1984; Burchard, 1994; Gunning and Morris, 1990). Ultraviolet and infrared spectroscopy are helpful for diagnosing the presence of ordered structure

and the existence of hydrogen bonds, if any, in the polymer (Arndt and Stevens, 1996; Crescenzi *et al.,* 1987; Morris, 1994). Imaging by electron microscopy can be used to probe peripheral morphologies to a low resolution of about 100 Å, which is relevant for the visualization of gel networks (Hermansson and Langton, 1994). Specifically, the scanning tunneling microscope and the atomic force microscope are gaining momentum in imaging the surfaces of macromolecules at a slightly better resolution (Kirby and Morris, 1994). Since the interatomic distances in a molecule are of the order of an angstrom, diffraction experiments employing electrons, neutrons, and x-rays as radiation sources whose wavelengths are in the region of interest are the tools of choice for exploring the relative positions of atoms in molecules. Among the three, x-ray diffraction is the most powerful experimental technique to date for the determination of three-dimensional structures of biopolymers at high resolution. The fundamentals of x-ray diffraction and results on selected food-related polysaccharides and proteins are reviewed by Clark (1994).

X-ray diffraction is at its best when the polymer specimen is in the crystalline solid state. In other words, it is necessary to induce organization of molecules in a periodic fashion in all three principal directions in space so that the signal-to-noise ratio is high and measurable. Disruption of periodicity as in semi- and noncrystalline regions, or lack of organization within or between molecules as in amorphous regions and in the solution state, is detrimental to the success of the diffraction method.

Like all biopolymers, polysaccharides are living molecules. X-ray diffraction in the solid state helps to elucidate the preferred molecular structure and also the packing arrangement. Most linear polysaccharides consisting of simple repetitive sequences prefer to adopt helical conformations. Unless influenced by external forces in the surroundings, barring minor perturbations, these helical structures are quite stable, particularly over short distances, in solid, solution, and gel states. Gels are composed of an intricate, randomly linked, network of junction zones having tremendous water holding capacity. Each junction zone is a pillar of strength such that a gel can stand on its weight, but a sol cannot. To form a junction zone takes few, say 2 to 10, helices with short-range lateral organization, the details of which are revealed by the three-dimensional structure. The rest of this chater is devoted to the determination and description of the anatomies of polysaccharide helices that are related in some way to food systems.

A. SINGLE CRYSTALS, ORIENTED FIBERS, AND POWDER SPECIMENS

In order to understand some fundamental differences among the best experimental specimens that can be prepared in the laboratory for x-ray

diffraction study, it is necessary to have a good idea about the primary building block, known as the unit cell, of the specimen. The parallelepiped enclosing one or more molecules is called a unit cell. The unit cell shown in Fig. 1 contains a disaccharide molecule. In general, six parameters are needed to define the unit cell: the lengths of the three principal edges *a*, *b*, and *c* in angstrom and the three interaxial angles α, β, and γ in degrees. A large number of building blocks stacked periodically side to side in three dimensions generates a macroscopic single crystal (Fig. 2). The seven crystal systems based on the unit cell dimensions are listed in Table I. Most of the food polysaccharide structures belong to monoclinic, orthorhombic, tetragonal, and hexagonal systems.

Slow evaporation of its saturated solution is a successful approach to growing single crystals for small molecules such as glucose, sucrose, maltose, and some oligopeptides, oligosaccharides, and oligonucleotides. This technique is equally applicable for globular macromolecules, which include proteins and spherical viruses. In general, production of single crystals from concentrated polymer solutions at controlled temperature, pH, humidity, and the like requires almost isotropic growth rate in three dimensions.

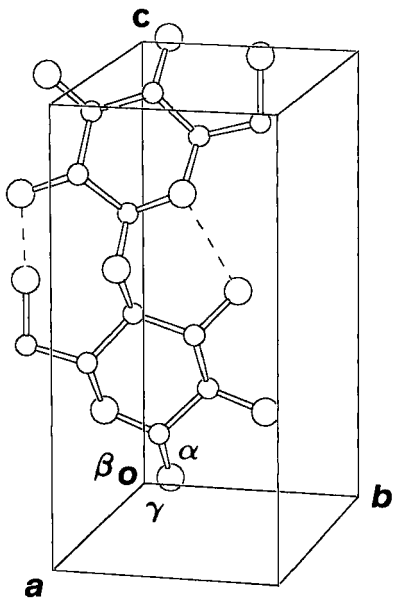

FIG. 1. Schematic drawing of a unit cell whose origin is point O. The volume of the unit cell, defined by lengths *a*, *b*, and *c* and angles α (between *b* and *c*), β (between *c* and *a*), and γ (between *a* and *b*), is given by $V = abc\ (1 - \cos^2\alpha - \cos^2\beta - \cos^2\gamma + 2\cos\alpha\cos\beta\cos\gamma)^{1/2}$. The *c*-axis coincides with the helix axis of the polysaccharide.

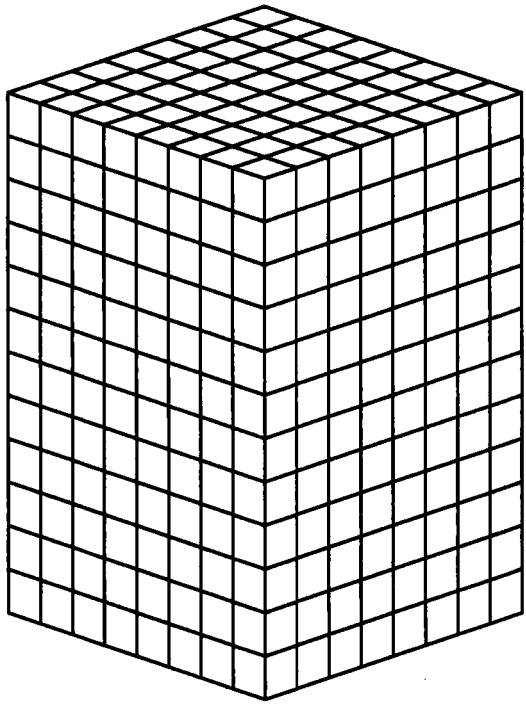

FIG. 2. Periodic stacking of unit cells in three dimensions generates a single crystal.

Unfortunately, crystalline growth of helix-forming polysaccharides is much faster along the longitude than along the transverse direction. This differential development limits the lateral dimensions of crystallites to only a few unit cells and impedes the formation of single crystals. However, under

TABLE I

THE SEVEN CRYSTAL SYSTEMS

System	Sides	Angles
Triclinic	$a \neq b \neq c$	$\alpha \neq \beta \neq \gamma$
Monoclinic	$a \neq b \neq c$	$\alpha = \beta = 90°; \gamma \neq 90°$
Orthorhombic	$a \neq b \neq c$	$\alpha = \beta = \gamma = 90°$
Tetragonal	$a = b \neq c$	$\alpha = \beta = \gamma = 90°$
Trigonal	$a = b = c$	$\alpha = \beta = \gamma \neq 90°$
Hexagonal	$a = b \neq c$	$\alpha = \beta = 90°; \gamma = 120°$
Cubic	$a = b = c$	$\alpha = \beta = \gamma = 90°$

appropriate crystallizing conditions, polycrystalline fibers or films can be obtained. In the case of fibers, a few drops of the polymer solution are placed in the gap of a couple of millimeters between two glass rods in a fiber puller, allowed to dry slowly until a semisolid state is reached, and then gradually stretched to twice or more the original length so that preferential parallelism among several microcrystallites along the molecular axis is induced (Chandrasekaran *et al.,* 1994b). In the case of films, large drops of the polymer solution are placed on Teflon blocks and allowed to dry until films are formed. Since orientation is nonexistent, narrow strips of the required size (about 2×5 mm) are cut and each is suspended in a humidity chamber under hanging weight (a few grams), which helps to invoke preferred alignment due to stretching to almost twice the original length of the strip over a few hours. The extent of longitudinal and lateral organization among the unit cells in such an oriented and polycrystalline specimen is schematically represented in Fig. 3a. This clearly shows that crystallites are nearly aligned parallel along the longitude, but they are rotated to different extents about this axis. Hence, a stationary fiber is considered to be equivalent to a rotating single crystal. On the other hand, when the lateral dimensions of microcrystallites do not exceed a few unit cells, stacking of microcrystallites along the molecular axis dominates (Fig. 3b) and this gives rise to an oriented and noncrystalline specimen. If the microcrystallites in the specimen are randomly oriented in space, the stretching procedure serves no useful purpose at all (Fig. 3c); this is often referred to as a powder sample. In principle, therefore, fibrous polymers may exhibit "polycrystallinity and orientation" to varying extents. The primary goal in specimen preparation is to achieve the most of both in order to collect good quality x-ray data suitable for structure analysis. However, the degree of ordering that can be induced in biopolymer fibers extends over a wide range encompassed by the three distinct types depicted in Fig. 3.

B. X-RAY DIFFRACTION FROM ORDERED MOLECULES

When a narrow beam of x-rays produced by a sealed tube, microfocus or rotating anode, generator is incident on a fiber, electrons surrounding the nuclei in atoms scatter x-rays in specific directions that are dependent on the unit cell dimensions (Fig. 1). This phenomenon is referred to as x-ray diffraction. If the unit cells are stacked as in a single crystal (Fig. 2), the diffraction consists of a series of reflections as shown in Fig. 4. They all conform to the Bragg's law $2d \sin \theta = n\lambda$, where d is an interplanar spacing, 2θ is the angle between the incident and diffracted beams, n is a positive integer, and λ is the wavelength of x-rays. Note that θ is known as the Bragg angle. Each reflection corresponds to a specific d-spacing that

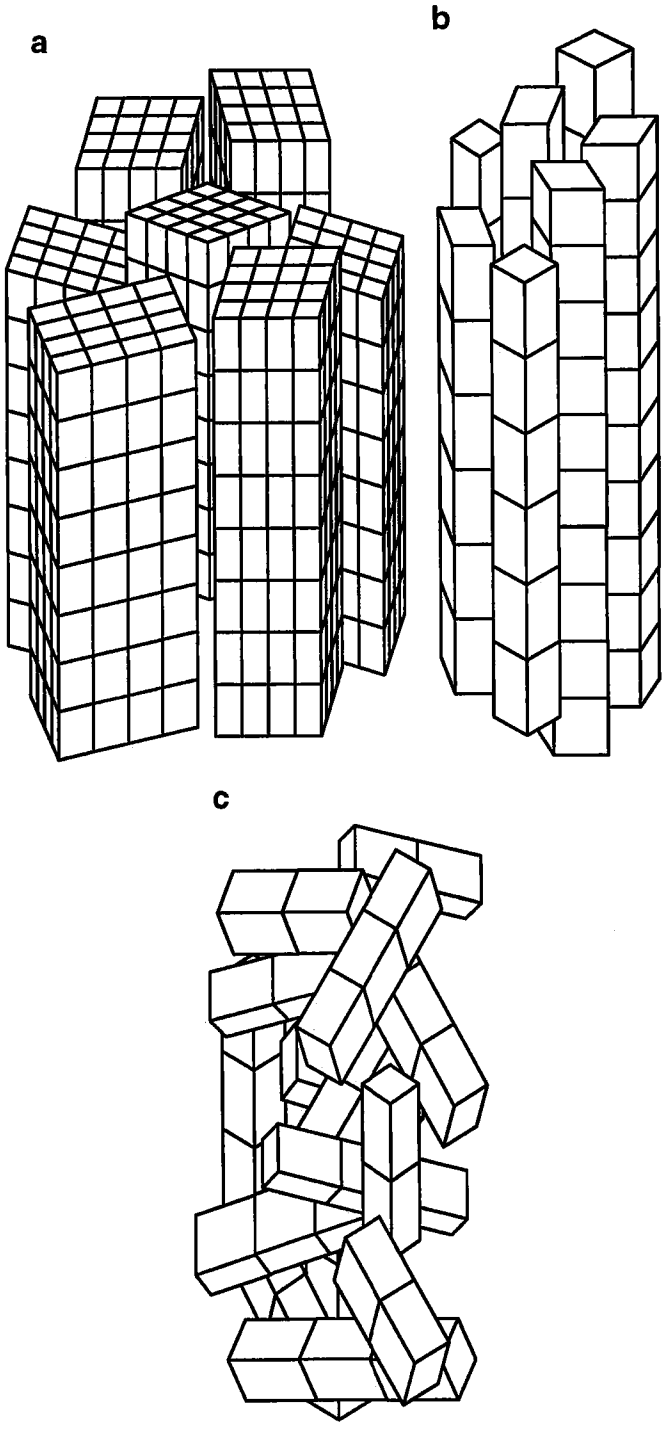
a
b
c

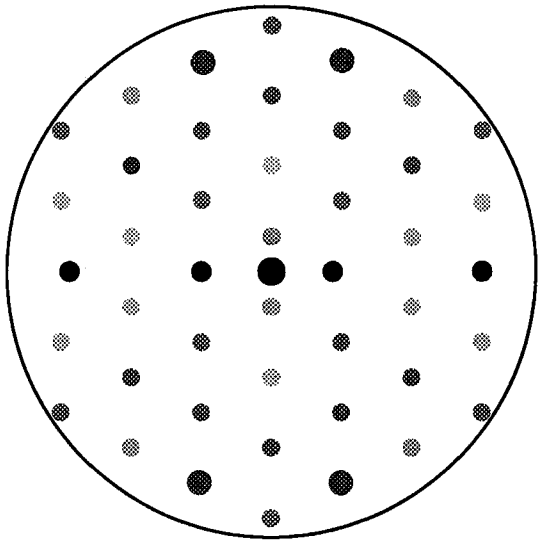

FIG. 4. A section of the diffraction pattern from a single crystal. The positions of discrete Bragg reflections of varying intensities are related to the unit cell dimensions.

is a function of the six unit cell parameters. The intensity of a reflection is distinct and related to the spatial arrangement of atoms in the specimen. The distribution of intensities in a diffraction pattern is commensurate with both the molecular shape and the packing arrangement within and between unit cells. X-ray crystallography deals with the determination of crystal structure from the experimentally measured intensities. It is a common practice to use nickel-filtered CuKα radiation of x-rays (λ = 1.5418 Å) in most crystallographic investigations.

All the fundamental principles of crystallography are fully valid in the case of fibers and films relevant for the polysaccharide structures. Due to a lesser degree of organization described earlier, the number of independent Bragg reflections possible for these systems are unfortunately far less than those from single crystals. Some special care (described in the next section), therefore, must be taken to solve fiber structures. In general, fiber diffraction

FIG. 3. Organization of unit cells in less-ordered systems: (a) The crystallites are preferentially aligned along, and differentially oriented about, the fiber axis in a polycrystalline and orientated specimen, (b) crystallites have preferred orientation but little lateral organization in a noncrystalline and oriented specimen, and (c) microcrystallites are randomly oriented in a powder specimen.

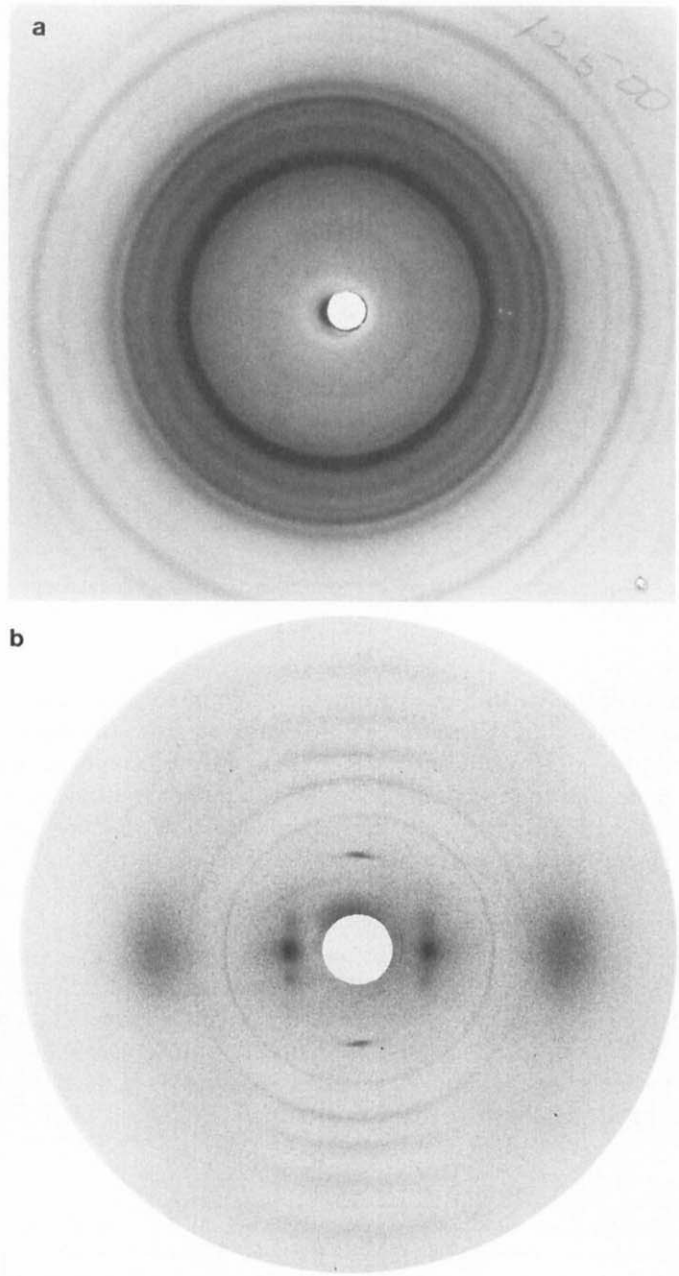

FIG. 5. X-ray fiber diffraction patterns from samples displaying (a) random orientations of microcrystallites as in arabinan, (b) noncrystallinity and orientation for the sodium salt of S-657, and (c) polycrystallinity and orientation for the calcium salt of welan.

patterns are recorded on photographic films in a flat-film camera, typical fiber-to-film distance being 4 cm. During exposure to x-rays, which could range from a few hours to days, a slow and steady stream of helium gas is first bubbled through a chosen saturated salt solution and then flushed through the specimen chamber. This enables not only retention of the fiber at a desired constant relative humidity (r.h.), but also reduction of the otherwise film-fogging due to air scattering.

The diffraction patterns from three different types of polysaccharide fibers shown in Fig. 5 highlight the individual and joint influence of the two parameters, polycrystallinity and orientation, on the x-ray data. When the microcrystallites are randomly oriented as in Fig. 3c, the pattern consists of a series of concentric rings (Fig. 5a) corresponding to the *d*-spacings characteristic of the unit cell of the specimen. The intensity is the same within a ring, but it differs among rings. An oriented, noncrystalline sample depicted in Fig. 3b, on the other hand, gives rise to a series of layer lines normal to the fiber axis. As seen in this diffraction pattern (Fig. 5b), the intensity varies along each layer line. The *d*-spacing of the first layer line

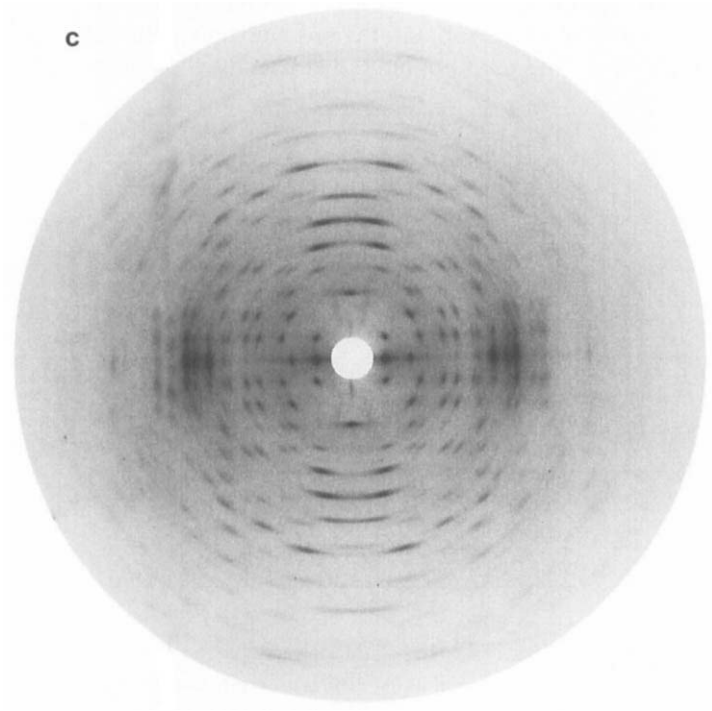

FIG. 5. Continued

represents the c-dimension of the unit cell. In the case of an oriented and polycrystalline specimen as in Fig. 3a, the diffraction pattern displays an array of sharp Bragg reflections (Fig. 5c) at discrete positions where rings intersect layer lines.

Some frequently used terms in fiber diffraction are sketched in Fig. 6. The meridian is the vertical line passing through the center of the pattern where the incident x-ray beam strikes the film and it is parallel to the fiber axis. The horizontal lines are called layer lines, the numbers of which start at $l = 0$ on the equator passing through the center and increase upward and decrease downward. The occurrence of meridional reflections only on $l = \pm 5$ means that the polymer exists as a fivefold helix of pitch c. The two helical parameters, N the number of repeats per turn and h the axial rise per repeat, in this example, are 5 and $c/5$, respectively. Alternately, t the turn angle per repeat is $360/N$ in degrees. By convention, t is positive for right-handed and negative for left-handed helices, and h is always positive. Any stereochemically satisfactory model for consideration must satisfy the observed helical parameters.

In terms of diffraction geometry, it is sufficient to say that the positions of reflections and their distances from the center of the pattern are dependent on the fiber-to-film separation and the unit cell dimensions. This distance information is used not only to determine the unit cell dimensions,

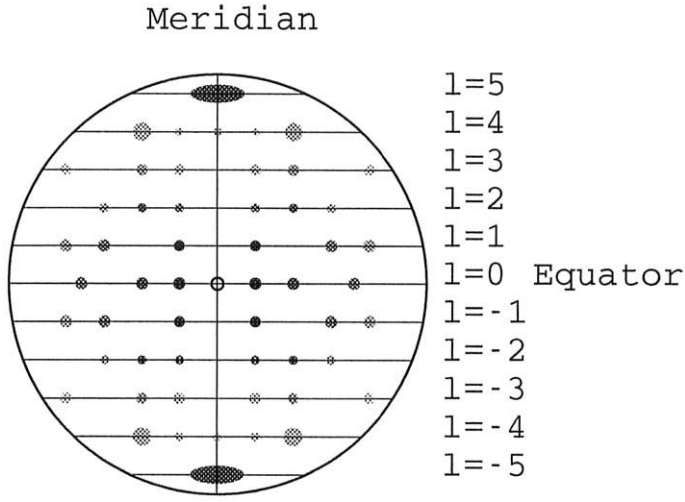

FIG. 6. Some important terms used in fiber diffraction refer to the equator and meridian, which are the horizontal and vertical lines, respectively, passing through the center of the pattern. Each layer line is roughly parallel to the equator and contains Bragg reflections.

but also to assign a set of three integers, h, k and l, as Miller indices (l being the layer line number) that uniquely specify the diffraction direction of each reflection. Subsequently, the intensities of reflections are measured using a microdensitometer or by digitizing with an optical film scanner and then converted into structure amplitudes after applying appropriate geometrical corrections for Lorentz and polarization effects (Millane and Arnott, 1985a,b; Millane, 1989). Note that intensity is proportional to the square of amplitude. This experimental x-ray data set is the key to determining and refining the molecular and packing models and to conducting objective comparisons among alternatives.

Stout and Jensen (1989), for instance, have elegantly described the details of x-ray crystallography to solve structures. The basic principles are mentioned here briefly for convenience. The structure factor F_c for reflection h, k, l is the resultant of M waves scattered by the M atoms in the unit cell. Each wave has an amplitude proportional to the respective atomic scattering factor and a phase ε relative to the unit cell origin. The structure factor is hence calculated using the expression

$$F_c\,(h\ k\ l) = \sum_j f_j \exp 2\pi i\,(hx_j + ky_j + lz_j), \tag{1}$$

where f_j is the atomic scattering factor of the jth atom positioned at fractional coordinates x_j, y_j, and z_j in the unit cell and all M atoms in it are included in the summation. The scattering factor depends on Bragg angle θ and, starting from a value of Z (atomic number) at $\theta = 0$, f decreases as θ increases. Equation (1) can be rewritten in the form

$$F_c\,(h\ k\ l) = |F_c\,(h\ k\ l)|\exp i\delta = A + iB, \tag{2}$$

which gives the structure amplitude $|F_c\,(h\ k\ l)| = (A^2 + B^2)^{1/2}$ and phase of the reflection $\delta = \tan^{-1} B/A$.

Alternately, if amplitudes and phases are known for all reflections, the electron density ρ at any point x, y, z in the unit cell of volume V can be calculated by using the Fourier summation

$$\rho\,(x, y, z) = (1/V) \sum_h \sum_k \sum_l F\,(h\ k\ l) \exp -2\pi i\,(hx + ky + lz). \tag{3}$$

An important extension of Eq. (3) is called the difference Fourier or difference electron density ($\Delta\rho$) map, which can be computed and used to locate missing atoms or relocate wrongly placed atoms. In this synthesis,

the coefficients are $\Delta F = (|F_o| - |F_c|) \exp i\delta$, where δ is based on the current model, and $|F_o|$ and $|F_c|$ are the observed and calculated structure amplitudes, respectively. Thus,

$$\Delta\rho\,(x, y, z) = (1/V) \sum_{h}\sum_{k}\sum_{l} \Delta F\,(h\ k\ l) \exp -2\pi i\,(hx + ky + lz). \quad (4)$$

C. STRUCTURAL ANALYSIS OF HELICAL POLYSACCHARIDES

Even the best fiber diffraction pattern seldom contains over 100 reflections up to about 3 Å resolution, in contrast to a couple of thousand reflections from a single crystal having comparable unit cell dimensions. This drastic reduction is due to the following reasons. First, since the fiber is equivalent to a rotating crystal, systematic superposition of equivalent reflections, from the four *hk*-quadrants (++, +−, −+ and −−), as in an orthorhombic system, on any layer line *l* gives rise to a single spot instead of four. Second, fortuitous overlap of two or more independent reflections with different intensities having the same *l* and the same Bragg angle θ cannot be avoided. Third, a few adjacent reflections might be too close to separate analytically. Under these circumstances, all overlapping reflections have to be considered individually in structure factor calculation and compounded properly for comparison with the observed composite reflection. Unobserved reflections that are too weak to see are assigned threshold values based on the lowest measured intensities. Still, the available x-ray data alone are far less than the number of atomic coordinates in a repeat of the helix, and hence inadequate to solve a fiber structure.

This pitfall is somehow overcome by appropriately embedding stereochemical information derived from the crystal structures of related monomers into the polymer as well (Scott and Arnott, 1972). This includes bond lengths, bond angles, and some conformation angles. On this basis, an average or a standard geometry for a sugar ring is an excellent starting point for polysaccharide structure analysis. Thus, when the ring shape in a monosaccharide is known, only three conformation angles and the bond angle at the glycosyl bridge oxygen atom between the sugar rings are required to describe the helix geometry, instead of 33 coordinates for 11 nonhydrogen atoms as variables. The conformation angles are ϕ and ψ around the glycosyl bonds and χ, which defines the orientation of hydroxymethyl group about the C5–C6 bond. An order of magnitude reduction in the number of variables significantly increases the data-to-parameter ratio and fiber structure analysis becomes meaningful.

D. MODEL BUILDING AND REFINEMENT TECHNIQUES

Linked-atom least-squares (LALS) analysis (Smith and Arnott, 1978) and the variable virtual bond (PS79) method (Zugenmaier and Sarko, 1980) are two major computer programs developed on the same basic principles for the generation and refinement of helical structures using x-ray data from fibers. The LALS program has been instrumental in unraveling well over 100 structures including polysaccharides, polypeptides, polynucleotides, and polyesters. This program requires information on precursor atom, scattering type, bond length, bond angle, and conformation angle to describe a tree geometry for every atom in one repeat plus three adjoining atoms in the next repeat. The extra three-atom plane is essential for establishing helix connectivity. In addition to refining the main chain and other relevant conformation angles, the positioning of the repeat is simultaneously adjusted by refining three Eulerian angles and a distance from the helix axis (z-axis) for a conveniently chosen root atom, until adjacent repeats conform to the desired N and h values of the helix.

The function minimized by the LALS program is given by

$$\Omega = \sum w_m \Delta F_m^2 + \sum u_n \Delta T_n^2 + \sum e_i \Delta \theta_i^2 + \sum k_j \Delta c_j^2 + \sum \lambda_h G_h \quad (5)$$

$$= X + Y + E + C + L. \quad (6)$$

The first term (X) on the right-hand side accounts for the sum of squares of the differences ΔF_m between observed (F_o) and calculated (F_c) x-ray structure amplitudes of Bragg reflections. The second term (Y) accounts for the sum of squares of the differences ΔT_n between observed (T_o) and calculated (T_c) x-ray structure amplitudes of continuous diffraction. Either or both terms can be used as necessary. The third term (E) minimizes the differences $\Delta\theta_i$ between expected/standard values (θ_o) and corresponding conformation and bond angles (θ_c) in the model. The fourth term (C) includes both intra- and interchain hydrogen bonds, and the differences Δc_j between acceptable (d_o) and calculated nonbonded distances (d_c) for those contacts that are smaller than the acceptable limiting values; this is designed to keep the model free from steric compression. The weights associated with these four types of observations are w_m, u_n, e_i, and k_j, respectively. Finally, the fifth term imposes constraints (G_h, with Lagrange multipliers λ_h) for ring closure and helix connectivity, and it reaches zero when the constraints are obeyed. For an unobserved reflection to be included in the refinement, its F_c must be larger than F_o.

Alternative molecular models to be examined in order to select the best include (a) both right- and left-handed helices and (b) single as

well as multistranded helices with parallel and antiparallel strands. The packing arrangement in the unit cell is considered next. If two or more helices can account for the measured fiber density, their positions, orientations and relative polarities are individually tested. Hamilton's significance test is used to assess the relative merits of competing models on the basis of Ω, E, X, Y, or C, or in terms of the crystallographic R-values, $R = \sum|F_o - F_c|/\sum F_o$ and $R'' = \{\sum|F_o - F_c|^2/\sum F_o^2\}^{1/2}$ (Hamilton, 1965).

If good Bragg data are available, difference Fourier maps in the last stages of structure analysis are helpful in locating ordered water molecules and/or cations responsible for the integrity of helix and in the association of helices. The positions of guest atoms are refined to enhance the fit of the augmented crystal structure with the x-ray data. Also, sugar rings are flexed by refining the endocyclic conformation angles along with the endocyclic bond angles and bond angle at the bridge oxygen atom. The accuracies of the final atomic coordinates are within a few tenths of an angstrom and the R-values are typically around 0.25 in many polysaccharide structures determined by this methodology. It should be pointed out that most structures reported prior to 1980 did not include hydrogen atoms mainly because of inadequate computing power.

III. MOLECULAR SHAPES AND INTERACTIONS

The three-dimensional structures of a number of food polysaccharide helices of interest have been determined to date. The repeating units range from a simple monosaccharide to a branched hexasaccharide. This includes only mono, di, tetra, penta, and hexasaccharide repeats. On the basis of linkage, it is convenient to sort the polymers into five distinct groups. The first deals with (1→4)-linked polysaccharides, the second with (1→3), the third with alternating (1→3) and (1→4), the fourth with the gellan family of gel-forming polysaccharides, and the fifth with some branched polysaccharides. Some of these results have been extrapolated to related systems that are more complex in terms of chemical repeat and type of linkage.

The monosaccharide unit shown in Fig. 7 is to help with atom labels. Descriptions of the molecular features in the following sections include specific details on the helical parameters, unit cell dimensions, number of helices per unit cell and the relationship between them, conformation angles in the main chain and side chain, orientation of the hydroxymethyl or carboxylate group in the repeating unit, hydrogen bonds within and between helices, and much more. The subsequent stereo drawings are intended to reveal clearly many of these aspects; hydrogen bonds are indicated by

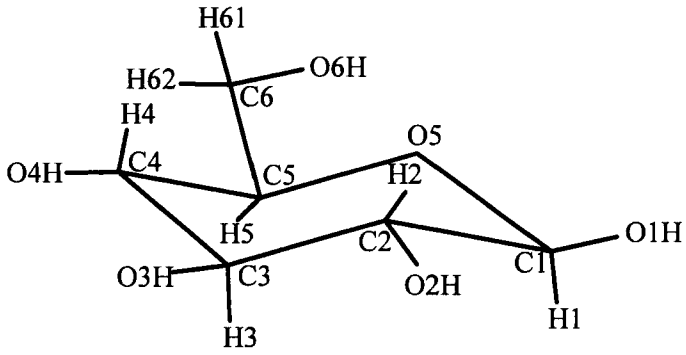

FIG. 7. Atom labeling in a monosaccharide unit.

dashed lines and hydrogen atoms, even when available in the original papers, are omitted to minimize crowding of atoms and maximize clarity. Each major conformation angle cited in the text refers to the dihedral angle between planes ABC and BCD in a four-atom segment A–B–C–D; the eclipsed *cis* conformation sets this angle to zero and clockwise rotation of the farthest bond while looking along the middle bond is reckoned positive (IUPAC-IUB, 1971). For the (1→*n*) linkage, *n* being 2, 3 or 4, ϕ and ψ refer to O5–C1–O*n*′–C*n*′ and C1–O*n*′–C*n*′–C*n*+1′, respectively, where the primes denote atoms belonging to the reducing end of the chain. However, for the (1→6) linkage, ϕ and ψ are O5–C1–O6–C6 and C1–O6–C6–C5, respectively. Unless otherwise specified, the hydroxymethyl group orientation, as in glucose, refers to C4–C5–C6–O6; the carboxylate group orientation, as in glucuronate, refers to C4–C5–C6–O61. For sulfate attachment in carrageenan to atom O*n*, the two dihedral angles are θ_1 = C*n*+1–C*n*–O*n*–S and θ_2 = C*n*–O*n*–S–OS1. However, if $n = 6$, θ_1 = C*n*–1–C*n*–O*n*–S. The bond angle C1–O*n*′–C*n*′ at the glycosyl oxygen atom, referred to as the bridge bond angle τ, is usually refined during structure analysis. Unless otherwise specified it is 116.5°.

A. (1→4)-LINKED POLYSACCHARIDES

Polysaccharides with monosaccharide repeating units may be divided into three distinct groups. The first group includes cellulose and mannan, which are structural polysaccharides that display similar extended ribbon-like molecular morphologies. If the structure of cellulose is important with regard to those of microcrystalline cellulose and some derivatives of cellulose amply used in many food products, the structure of mannan is equally important in the context of an entire series of galactomannans that are

utilized extensively as thickening agents in soups and sauces. The second group includes amylose and amylopectin, which are the basic constituents of starch deposited in the form of granules of varying shapes and sizes depending on the botanical source. A series of amylose derivatives adopt numerous polymorphic forms. The third group contains alginate and pectate, which are gel-forming polysaccharides used in the food industry. All polymers carry $^4C_1$ pyranose rings in their main chains with the exception of polyguluronic acid, which consists of $^1C_4$ pyranose rings. Their three-dimensional structures are presented below and correlated with the observed physical properties.

1. Cellulose

The repeating unit of cellulose is →4)-β-D-glucose-(1→. Native cellulose fibers from *Valonia, ramie,* cotton, and woods are referred to as cellulose I. The material obtained from native cellulose either by a solution regeneration process or by mercerization involving a swelling treatment with alkali is referred to as cellulose II. Two other minor forms, III (Sarko *et al.,* 1976) and IV (Gardiner and Sarko, 1985), are derived by heat or alkali treatment from I and II, respectively, and their structural details remain elusive. Historically, the first x-ray diffraction study (Meyer and Misch, 1937) established that (a) cellulose chain forms a twofold helix of pitch 10.3 Å; (b) the monoclinic unit cell, $a = 8.35$, $b = 7.9$, $c = 10.3$ Å, and $\gamma = 96°$, accommodates two chains (total of four glucosyl units) passing through (0 0 0) and ($a/2$ $b/2$ 0), respectively; and (c) an antiparallel packing is preferred over a parallel alignment of both chains. Since then, these molecular features have been widely accepted and confirmed by other independent studies. However, the original packing arrangement has been criticized, specifically in relation to the biosynthesis of cellulose.

a. Cellulose I. Gardner and Blackwell (1974) used the LALS program to define the molecular structure and to propose the correct packing arrangement of *Valonia* cellulose I. The ribbon-like twofold helix ($t = 180°$) of pitch 10.38 Å ($h = 5.19$ Å) is stabilized by a series of O3H···O5 (2.75 Å) hydrogen bonds formed across each glycosidic oxygen atom ($\tau = 114.8°$). The main chain conformation angles ($\phi = -98°$, $\psi = -143°$) are near the global energy minimum for an isolated cellulose chain. The x-ray data consist of 36 of 39 reflections that fit the monoclinic unit cell ($a = 8.17$, $b = 7.86$, $c = 10.38$ Å, and $\gamma = 97.0°$). On the basis of a significantly lower R-value of 0.18, compared to 0.21 for the antiparallel packing, the parallel model was judged to be the best for cellulose I.

The lateral ordering of the parallel chains produces hydrogen-bonded sheets parallel to the *ac*-plane as shown in Fig. 8a. Each hydroxymethyl group adopts a *tg* (i.e., C6–O6 *trans* to C5–O5 and *gauche* minus to C5–C4) conformation ($\chi = -81°$) so that intrachain O2H···O6 (2.87 Å) and interchain O6H···O3 (2.79 Å) hydrogen bonds are maintained simultaneously. An axial projection of the unit cell is shown in Fig. 8b. The relative displacement of the corner from center chains (sheets) along the fiber axis is $0.27c$ and it leads to excellent stacking between adjacent pyranosyl rings. These

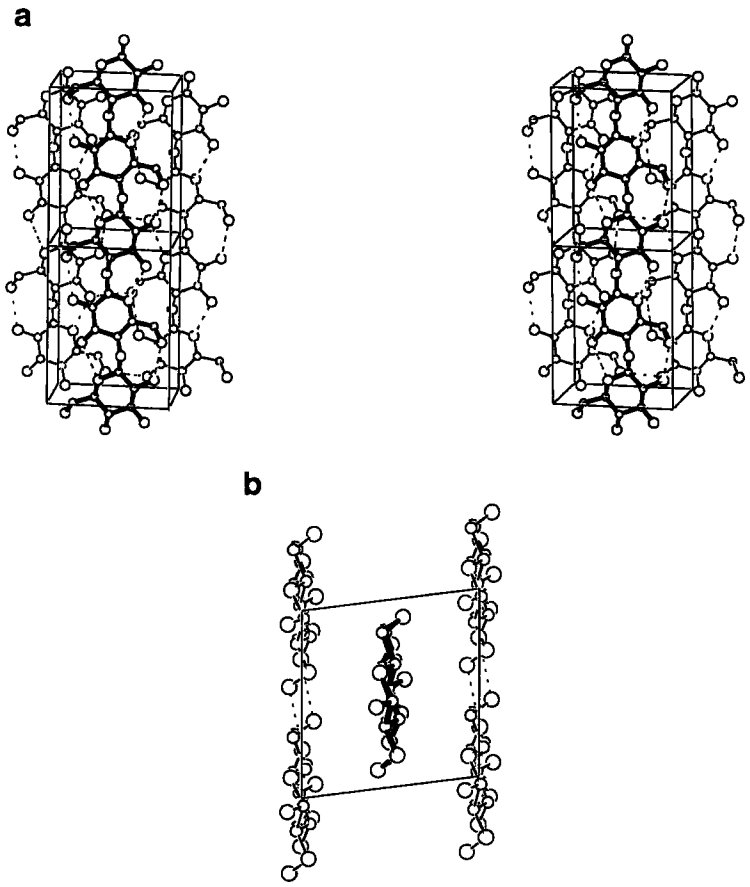

FIG. 8. Parallel packing arrangement of the twofold cellulose I helices. (a) Stereo view of two unit cells roughly normal to the *ac*-plane (*c*-axis is vertical). The corner chains (thin bonds), separated by *a*, in the back are connected by hydrogen bonds to form a sheet. The center chain is drawn in thick bonds. (b) Projection of the unit cell along the *c*-axis, with *a* down the page. Only van der Waals attraction is present between the corner and center chains.

structural features are responsible for the self-association of cellulose chains, which in turn explains the strength and rigidity displayed by the crystalline regions of cellulose. Similar results were simultaneously published by Sarko and Muggli (1974). Comparison shows that differences, if any, are only marginal.

b. Cellulose II. Fiber diffraction analysis of this crystalline form (Kolpak and Blackwell, 1976) has produced a twofold helix ($t = 180°$ and $h = 5.18$ Å) as its molecular structure and its backbone ($\tau = 114.8°$, $\phi = -96°$, $\psi = -145°$) is isomorphous with that of cellulose I. Its unit cell is also monoclinic ($a = 8.01$, $b = 9.04$, $c = 10.36$ Å, and $\gamma = 117.1°$). Two cellulose chains pass through the unit cell the same way as in cellulose I except that they run antiparallel. Both chains maintain O3H···O5 (2.69 Å) hydrogen bonds. The x-ray results (final R-value = 0.17 for 44 observed reflections) show that the hydroxymethyl orientations are *gt* and *tg*, respectively, for the corner ($\chi = 174°$) and center ($\chi = -70°$) chains. Consequently, O2H···O6 (2.73 Å) hydrogen bonds are possible only in the "down" center chains, which form a sheet in the 020 plane and exhibit interchain O6H···O3 (2.67 Å) hydrogen bonds (Fig. 9a). The "up" corner chains, connected by O6H···O2 (2.76 Å) hydrogen bonds, also form a sheet structure; their O2H groups make a new set of O2H···O2 (2.77 Å) hydrogen bonds in the 110 (diagonal) plane with a neighboring center chain. In other words, adjacent antiparallel sheets are now connected. Due to this additional linkage, cellulose II is energetically more stable than cellulose I. The relative orientations of the corner and center chains, which are significantly different from those of cellulose I, can be visualized from the axial projection of the unit cell (Fig. 9b). Results of the same sort have also been published by Stipanovic and Sarko (1976). It is now well known that the transformation of cellulose I to cellulose II, from parallel to antiparallel packing, is irreversible. Therefore, I and II are the metastable and stable forms of cellulose.

c. Cellulose Derivatives. Despite conformational similarity in the backbone, which remains rigid due to regular interresidue O3H···O5 hydrogen bonds, there are structural differences between cellulose I and II in fibers. For example, due to freedom of rotation about the C5–C6 bonds, the hydroxymethyl groups are not restricted to the same orientation, but are found in two distinct domains; also, cellulose chains are able to aggregate in parallel and antiparallel modes and are stabilized by alternate intra- and interchain hydrogen bonds. In any case, this self-association is so strong that cellulose is insoluble in most solvents.

However, there are ample food applications for cellulose in one form or another (Coffey *et al.,* 1995). The noncrystalline region of cellulose in wood

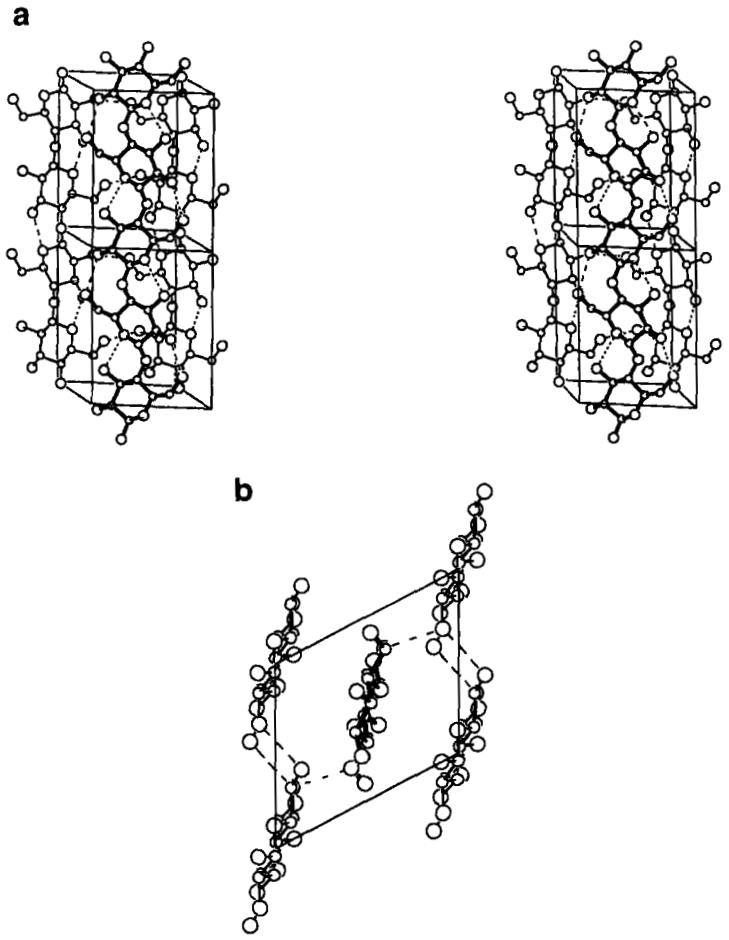

FIG. 9. Antiparallel packing arrangement of the twofold cellulose II helices. (a) Stereo view of two unit cells roughly normal to the *ac*-plane (*c*-axis is vertical). The corner chains (thin bonds), separated by *a*, in the back are connected by hydrogen bonds to form a sheet. The center chain is drawn in thick bonds. (b) Projection of the unit cell along the *c*-axis, with *a* down the page. The corner and center chains are joined by O2H···O2 hydrogen bonds.

pulp is hydrolyzed into fringed crystallites, which in turn are converted to microcrystalline particles less than 1000 Å in diameter by spray drying or mechanical shearing. This type of microcrystalline cellulose (MCC) is used in shredded cheese to carry flavor, in high-fiber bakery products for reduced calories, and in the production of extruded snacks. Also, dispersion of MCC in water develops appreciable viscosity. Derivatization of cellulose at atoms

O2, O3, or O6 lends water solubility. While the reactivity is high and nearly the same at O2 and O6, it is very low at O3, perhaps due to its involvement in intrachain hydrogen bond with O5. Methyl, hydroxypropyl, and carboxymethyl substituents, as ether groups, are introduced to one or more sites by treating alkali cellulose with methylchloride, propylene oxide, and sodium salt of chloroacetic acid, respectively. By controlled reaction, the degree of substitution (DS) is monitored and a variety of derivatives with DS in the range 0.02 to 0.95 are prepared for use as water-soluble food gums (Desmarais and Wint, 1993; Feddersen and Thorp, 1993; Grover, 1993). Hydroxypropylmethyl cellulose (HPMC) is prepared by reacting alkali cellulose with propylene oxide and methyl chloride at the same time and is also referred to as methyl cellulose (MC). As the four panels in Fig. 10 indicate, the substituents in MC, caboxymethyl cellulose (CMC), hydroxypropyl cellulose (HPC), and HPMC stick out laterally from the main chains to increasing extents. For example, the width of a cellulose chain is only about 7.9 Å compared to 9.1, 10.3, 10.7, and 10.9 Å in the four derivatives, respectively. In the case of HPC and HPMC, the hydroxyl moiety in hydroxypropyl group is also a possible additional substitution site that will further increase the lateral dimension to values greater than 11.0 Å. Thus, due to bumps along the chain at the modified sites, the strong intermolecular hydrogen bonds between the main chains are no longer possible and the association of polymer molecules becomes weaker, leaving the interstices accessible to solvent molecules. In all cases, the interactions between the substituents and the environment will dominate and result in solubilizing the polymer. These food gums are used in ice cream, pancake syrup, onion rings, sandwich spreads, extruded products, and frozen desserts, to name a few.

2. *Mannan*

The repeating unit of mannan is →4)-β-D-mannose-(1→. Microfibrils of mannan are the major constituents of the cell walls of ivory nut endosperm and date seeds; mannan also occurs in a granular form in siphoneous green algae (Frei and Preston, 1968). As in the case of cellulose, two distinct crystalline forms, I and II, are known for the native and alkali-treated materials, respectively. They both have orthorhombic unit cells with quite different dimensions and hence their packing arrangements are not the same. Antiparallel chains are the common features. The mannan chains are twofold helices, very similar to those of cellulose, although the O2H group in mannose is axial instead of equatorial as in glucose.

a. Mannan I. Early x-ray studies (Frei and Preston, 1968; Nieduzynski and Marchessault, 1972) followed by more recent electron diffraction

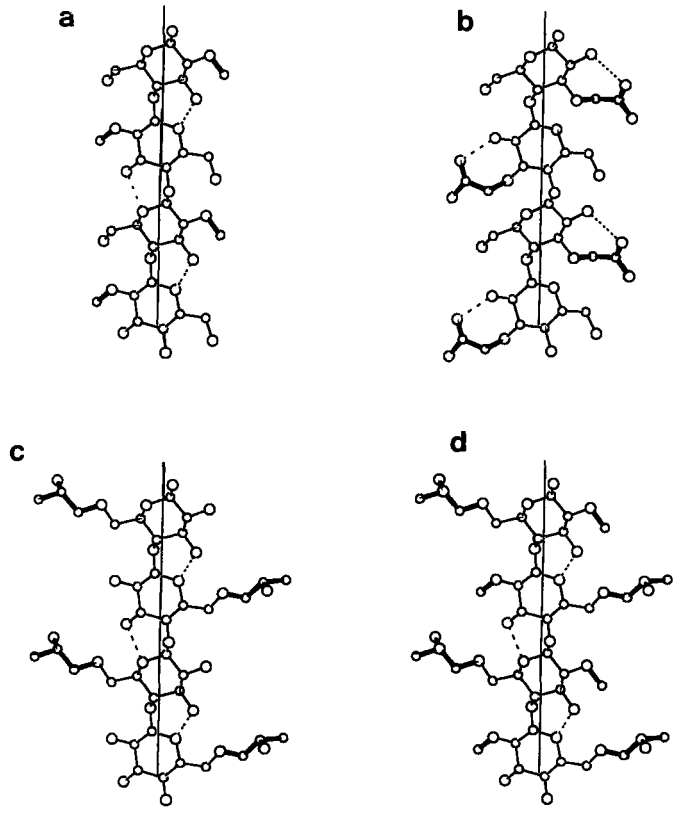

FIG. 10. Side views of two turns of cellulose derivatives. (a) O2-Methyl cellulose, (b) O3-caboxymethyl cellulose, (c) O6-hydroxypropyl cellulose, and (d) O6-hydroxypropyl–O2-methyl cellulose.

(Chanzy *et al.*, 1987) and x-ray (Atkins *et al.*, 1988) analyses show that the mannan I helices (t = 180° and h = 5.14 Å) crystallize in a two-chain orthorhombic unit cell (a = 8.92, b = 7.21, and c = 10.27 Å). The chains passing through (0 0 0) and (a/2 b/2 0) are related by twofold screw axes perpendicular to the chain direction and hence are antiparallel. According to the x-ray results, the backbone conformation angles are $\phi = -90°$ and $\psi = -149°$, and τ is 117.0°; the hydroxymethyl group orientation is *gt* (*gauche, trans*), but χ alternates between 175 and −175° in successive residues. The molecule is stabilized by two intrachain hydrogen bonds, O3H···O5 (2.58 Å) and O6H···O3 (3.0 Å). The molecular features and intermolecular interactions are shown in Fig. 11a. The corner and center chains are con-

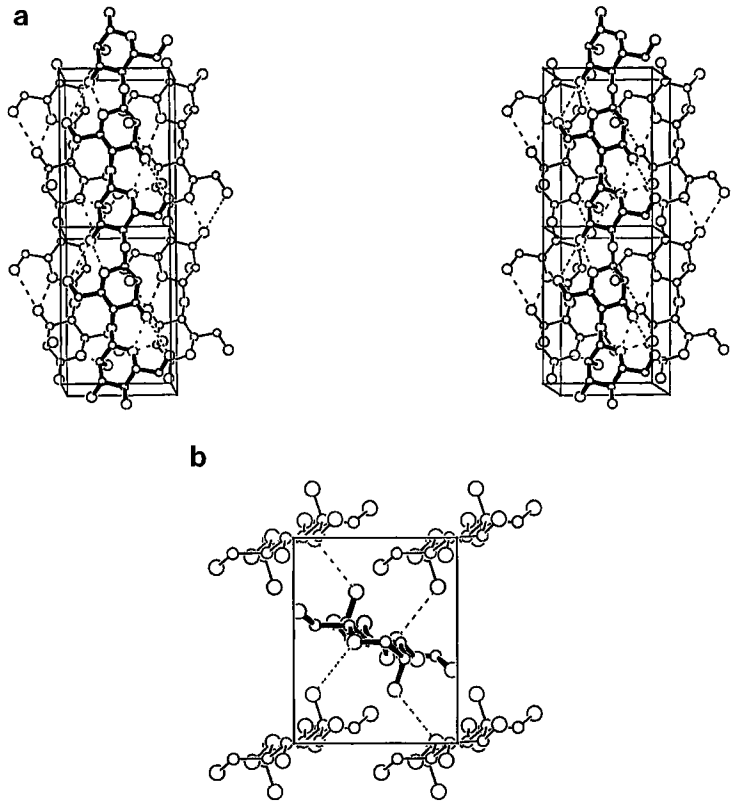

FIG. 11. Antiparallel packing arrangement of the twofold helices of mannan I. (a) Stereo view of two unit cells approximately normal to the *bc*-plane. The two corner chains (thin bonds) in the back, separated by *b*, are not hydrogen bonded to each other. Instead, the antiparallel center chain (thick bonds) in the middle is linked to the corner chains by O2H···O5 hydrogen bonds. (b) Projection of the unit cell along the *c*-axis; the *a*-axis is down the page. This highlights the hydrogen bonds between corner and center chains.

nected by O2H···O5 (2.93 Å) hydrogen bonds. The axial projection (Fig. 11b) shows that the sugar rings are somewhat rotated from the *bc*-plane.

b. Mannan II. Based on two x-ray analyses (Frei and Preston, 1968; Millane and Hendrixson, 1994), mannan II crystallizes in a four-chain orthorhombic unit cell (a = 9.00, b = 16.65, and c = 10.35 Å) that is twice as large as that of mannan I. There are four helices (t = 180° and h = 5.18 Å), two up and two down, related by crystallographic dyads normal to the c-axis, and all are conformationally identical (τ = 116.5°, ϕ = −88°,

$\psi = -153°$). The molecular structure is essentially the same as that of mannan I except that the hydroxymethyl group is in the *tg* conformation ($\chi = -23°$). The antiparallel strands are connected by O6H···O6 (2.6 Å) hydrogen bonds and they form sheets almost parallel to the *bc*-plane. In addition, there is a water molecule (W) on a twofold rotation axis per mannose residue that forms an intersheet O2···W···O2 bridge (O···W = 2.9 Å) and provides additional stability to the mannan II structure.

3. *Galactomannans*

Since self-association of mannan helices in the solid state is as strong as that in cellulose, it is not a bit surprising that mannan also is insoluble in most solvents. Of course, derivatization of mannan is a way of inducing solubility, but nature has provided a better course by producing an abundant supply of a number of galactomannans in plants. Water solubility increases with the amount of substitution of (1→6)-linked α-D-galactose residues as random side chains on the mannan backbone. Depending on its source, the galactose/mannose ratio varies from 0.3 in carob gum, 0.45 in tara gum, 0.6 in guaran, to 0.95 in water-insoluble fenugreek. The galactomannans produce extremely viscous aqueous solutions and hence are used extensively as thickening agents in food products. A mixture of carob gum and xanthan, however, forms gels.

X-ray fiber diffraction patterns from any of these galactomannans resemble that of mannan, implying twofold helix symmetry ($t = 180°$) and a pitch of 10.3 or $h = 5.15$ Å (Chien and Winter, 1985). Guaran, for instance, has an orthorhombic unit cell ($a = 9.3$, $b = 30.8$, and $c = 10.3$ Å) and the four helices in it are related by twofold screw axes parallel to the *a*- and *b*-axes. According to a recent x-ray study (Chandrasekaran *et al.*, 1998), the guaran helix has a mannan-like backbone ($\phi = -100°$, $\psi = -149°$, and $\chi = -109°$) and the galactose side chain conformation is $\phi = 32°$ and $\psi = -123°$. The polymer chain with galactosyl unit on alternate mannose residues, shown in Fig. 12, is stabilized by a series of O3H(Man)···O5(Man), O3H(Man)···O5(Gal), and O6H(Gal)···O3(Man) hydrogen bonds. The four galactomannan chains in the unit cell are packed similar to those of mannan II and are stabilized by hydrogen bonds between the side chains. The galactose residues are further important in hindering the otherwise self-association of the mannan skeletons. Also, the side chains are in orientations that promote favorable interactions with the surrounding solvent molecules. This is the structural reason for the solubility of some of the galactomannans in water that results in highly viscous solutions.

The food applications of galactomannans are very extensive (Maier *et al.*, 1993). Guaran is easily water soluble at room temperature. Because of

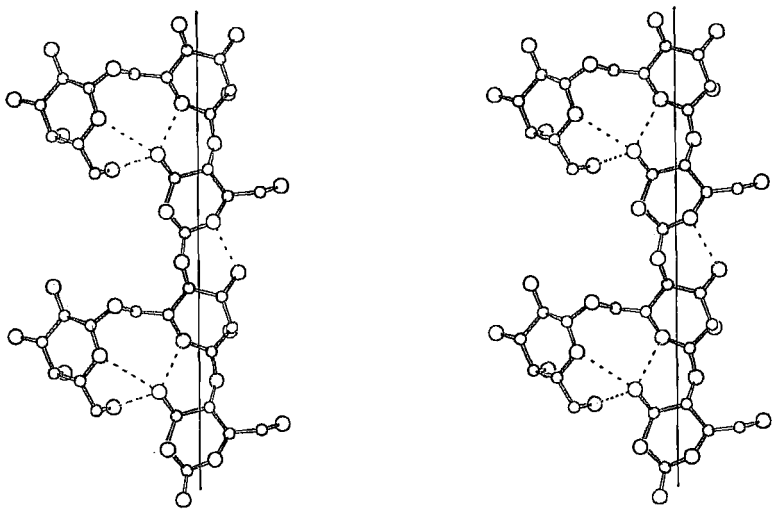

FIG. 12. Stereo view of two turns of a twofold galactomannan helix. The vertical line is the helix axis and the side chains appear on one side.

the thickening caused by enhanced viscosity, this gum is used as the most economical thickening agent in a variety of food products, including dips, salad dressings, and cheese, which require an acidic environment, and sauces, soups, and related canned food items. Carob, also known as locust bean gum, due to its lower *G/M* ratio, is only slightly water soluble even at an elevated temperature of 85°C, but develops good viscosity when cooled down to 25°C. This behavior leads to its ample use in dairy and frozen food desserts, including ice cream, cheese spreads, sour cream-based dips, and yogurts. Tara gum, nearly 70% soluble in water at room temperature, has viscosity intermediate between carob and guaran. Its limited availability has restricted its use mainly to processed seafoods, frozen meats, ice cream, and frozen yogurt, where water binding and emulsion stability are important. Fenugreek, with its *G/M* content nearing 1.0, is not known for its viscosity like the other galactomannans. Instead, the ground seed is used as a spice in curry powder, chutneys, and corn bread. Fenugreek extract is added to maple syrup for flavor.

4. Amylose

Starches in large quantities are commercially produced from corn, potatoes, rice, sorghum, and tapioca, to name a few. They are water soluble, form viscous dispersions, and are gel formers at low concentrations. In

addition to being the major food for human consumption, native as well as modified starches are commonplace in a variety of food applications (BeMiller, 1993). Each starch granule in plants stores the polysaccharide made up of α-D-glucose. Its two major components are the linear amylose or (1→4)-α-D-glucan and the branched polysaccharide amylopectin, which contains both (1→4) and (1→6) links. The relative amount of the two components varies with species and hybrid starch. For example, high-amylose corn starch has up to 70% amylose, and waxy maize starch has about 98% amylopectin and less than 2% amylose, while potato starch has 21% amylose.

The linear polymer amylose has a molecular weight ranging from 160,000 to 2.6 million Da and the degree of polymerization (DP) varies from 1000 to 16,000 in a single chain. In contrast, amylopectin is a branch-on-branch polymer in which the (1→6) links are the branch points from the main chain, each of which may also be connected to a bunch of short stretches of amylose having only 20 to 30 units. The molecular weight can be as high as 400 million Da, which accounts for a net DP of 2.5 million. Within the starch granules, it is believed that the three-dimensional ordering of amylopectin segments is responsible for the observed crystallinity, whereas the amylose segments account for the amorphous domains (Imberty *et al.,* 1991).

Two principal types of crystalline starch granules are the A-starch of cereals and B-starch of tubers. On the basis of x-ray diffraction patterns, Wu and Sarko (1978a,b) were the first to suggest that starch molecules exist as helices in both cases and that their packing arrangements are different. A third type, C-starch, found in some plants such as arrow root, pea, and tapioca, yielding distinctive diffraction patterns, is proposed to be a mixture of A- and B-forms, but remains to be fully characterized. Further, amylose can be regenerated in the presence of solvents or complexed with molecules such as alcohols, fatty acids, and iodine; the molecular structures and crystalline arrangements in these materials are classified under V-amylose. When amylose complexes with alkali or salts such as KBr, the resulting structures (Sarko and Zugenmaier, 1980) are surprisingly far from those of V-amyloses.

a. A-Amylose. Wu and Sarko (1977) prepared a pure sample of A-amylose by solid-state deacetylation of oriented and crystalline amylose triacetate fibers with 0.2 *M* KOH in 75% ethanol, followed by exposure to 80% or higher r.h. at temperatures of 85°C or higher. A good quality x-ray diffraction pattern from this specimen was indexed (Wu and Sarko, 1978a) on an orthorhombic unit cell (a = 11.9, b = 17.7, and c = 10.52 Å). Consistent with the presence of meridional reflection on the third layer

line, a sixfold, right-handed ($t = 60°$), "half-staggered parallel double helix" of pitch $2c$ or 21.04 Å ($h = 3.51$ Å) was proposed as a possible molecular model. In this type of double helix, the two helices are coaxially interwound; sliding one along the helix axis by c leads to exact superposition on the other. One problem with Wu and Sarko's model is the relatively low bond angle ($\tau = 105°$) at the glycosidic bridge oxygen atom. They proposed that the two double helices passing through (0 0 0) and ($a/2$ $b/2$ 0) of the cell were packed in an antiparallel fashion such that each unit cell accommodated half-a-turn per double helix and eight water molecules. Another problem is the antiparallel packing of helices, which has been severely criticized because of biosynthetic considerations that favor only the all-parallel amylose chains (French, 1984; Wild and Blanshard, 1986).

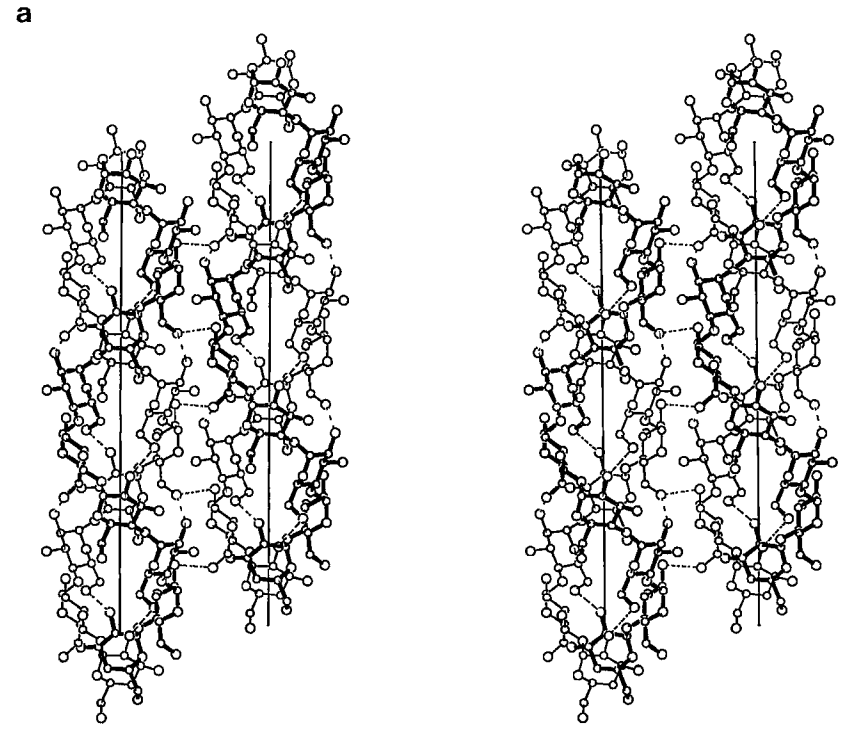

FIG. 13. Parallel packing arrangement of A-amylose. (a) Stereo side view of less than two turns of two sixfold double helices separated by 10.62 Å along a. The two strands in each helix are in thin and thick bonds for clarity, and the helix axis is vertical. Atom O6 mediates both intra- and inter-double helix hydrogen bonds. (b) A c-axis projection of the unit cell contents, with a down and b across the page. A water molecule (crossed circle) per trisaccharide bridges three surrounding helices.

To set the record straight, Imberty *et al.* (1988) collected their own x-ray powder and electron microcrystal diffraction data and used them along with the x-ray fiber data of Wu and Sarko (1978a) to reexamine the previous model. Powder patterns were from pure amylose (DP 15) obtained after mild hydrolysis of potato starch. Electron diffraction data were from micro single crystals grown from the same material. According to the revised results, the reindexing of the original fiber data is compatible with a monoclinic unit cell (a = 21.24, b = 11.72, c = 10.69 Å, and γ = 123.5°) that accommodates 12 glucose residues and 4 water molecules in order to be compatible with the fiber density of 1.51 g/ml. The final structure corresponds to a sixfold, left-handed (t = −60°), parallel double helix of pitch 21.38 Å (h = 3.56 Å). The inner and outer diameters of the helix are 3.4 and 10.4 Å, respectively. Two double helices, having the same polarity, pass through (0 0 0) and (a/2 0 c/2) per cell. A side view of this pair is shown in Fig. 13a. The crystal structure has been refined against the observed x-ray intensities, which include 34 fiber data and 21 powder peaks extracted from the one-dimensional 2θ scan; the corresponding final R-values are 0.27 and 0.21. The electron diffraction data have not been used in the refinement.

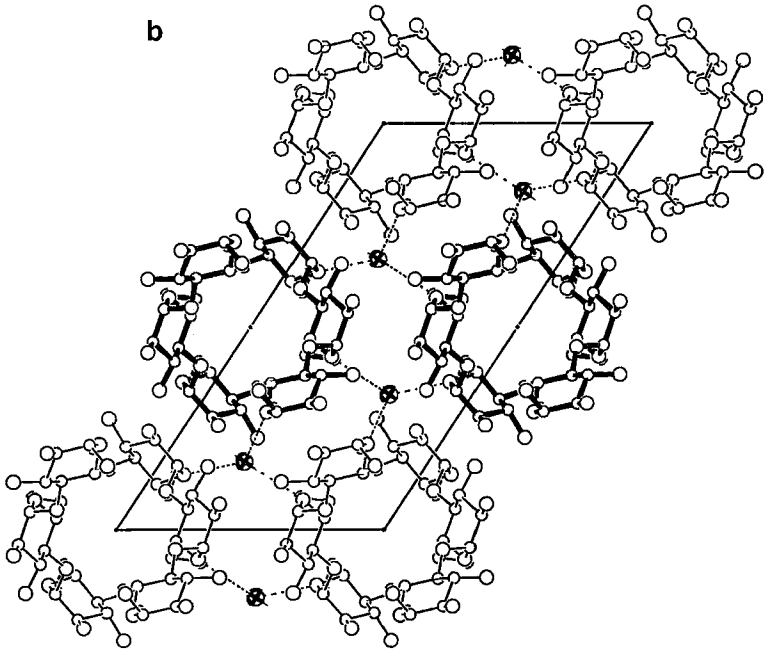

FIG. 13. Continued

Since Imberty *et al.* (1988) described the A-amylose double helix in terms of a maltotriose repeating unit that corresponds to $t = -180°$ and $h = 10.69$ Å, the three glucose residues, confined to identical $^4C_1$ ring geometries, are no longer required to retain conformational identity. Three sets of four angles (τ, ϕ, ψ, χ) given by (117.0, 92, −153, 50), (113.6, 86, −145, 62), and (123.0, 93, −150, 56) in degrees define the resulting helix. There is no intrachain hydrogen bonding, but the *gg* (*gauche, gauche*) orientations of all hydroxymethyl groups result in interchain hydrogen bonds between atoms O2 and O6 within the double helix and among atoms O2, O3, and O6 between double helices. The one and only water molecule per maltotriose is also involved in hydrogen bonds with three double helices surrounding it as shown in Fig. 13b. The hydrogen bond distances range from 2.6 to 2.9 Å.

b. B-Amylose. Material preparation similar to that for A-amylose, but through two stages of 3 days each of 80 and 100% r.h., at room temperature and a third stage of annealing in hot water at 90°C for 1 hr produces B-amylose from amylose triacetate fibers (Wu and Sarko, 1978b). X-ray diffraction patterns correspond to a hexagonal unit cell ($a = b = 18.5$, $c = 10.4$ Å, and $\gamma = 120°$). Similar to their results on A-amylose (Wu and Sarko, 1978a), these authors proposed an antiparallel packing of two sixfold, right-handed ($t = 60°$), half-staggered, parallel double helices ($h = 3.47$ Å) passing through (2*a*/3 *b*/3 0) and (*a*/3 2*b*/3 0) of the unit cell. Half-a-turn per double helix and 36 water molecules were located in the cell. Again, as in the case of A-amylose, the antiparallel packing was criticized from the point of view of starch biosynthesis (French, 1984; Wild and Blanshard, 1986).

Subsequently, Imberty and Pérez (1988) used the x-ray data of Wu and Sarko (1978b) to demonstrate that the correct B-amylose helix essentially resembles the revised A-amylose structure (Imberty *et al.* 1988) described above, but the packing arrangement differs. The pitch of the half-staggered, parallel, sixfold, left-handed double helix is 20.8 Å. The helix is described in terms of a maltose repeating unit in which $t = -120°$ and $h = 6.93$ Å are twice those for a monomer. The inner and outer diameters of the helix are 3.0 and 10.6 Å, respectively. The final *R*-value after refinement of this structure against 34 reflections is 0.15. Two sets of (τ, ϕ, ψ, χ), namely (115.8, 84, −144, 53) and (116.3, 84, −144, 68) in degrees, define the disaccharide conformation. As Fig. 14a shows, hydrogen bonds are absent within, but are present between chains connecting atoms O2 and O6 and they stabilize the double helix. Two double helices of the same polarity pass through (2*a*/3 *b*/3 0) and (*a*/3 2*b*/3 0) of the unit cell. Six water molecules per disaccharide repeat, or 36 per cell, have been located. The two helices in

the hexagonal cell are related by a crystallographic twofold screw parallel to c passing through ($a/2$ $b/2$ 0). This setup leads to a hexagonal network of amylose helices as shown in Fig. 14b. The channel in the middle, almost as wide (10 Å) as the helix itself, is filled with ordered water molecules that are hydrogen bonded to one or more of the six surrounding helices. Exchange of these water molecules with another amylose double helix is all it takes to reproduce the A-amylose packing arrangement shown in Fig. 13b.

With regard to molecular morphology, in both A- and B-amylose, there is no room for a water or similar molecule of radius about 2 Å to pass through the inner core of the relatively extended helix. Coaxial intertwining of two such rod-like helices obviously leads to a tight complex and hence low solubility, as observed.

c. Amylopectin. The (1→6) branching point of amylopectin has been modeled based on a 6-glucosylmaltotriose unit by energy calculations (Imberty and Pérez, 1989). The glucose side chain is attached to the second residue in the backbone. The maltotriose conformation is minimally altered from the A- or B-helix when the side chain folds back on the main chain in an orientation in which the branched tetrasaccharide unit falls in place to form a parallel double helical segment, as during the process of twinning of short amylopectin chains. Such a finding is consistent with the cluster model proposed for amylopectin aggregation in the growth of starch granules (French, 1984).

d. V-Amylose. Following an initial x-ray study of Zobel *et al.* (1967), later investigations under suitable experimental conditions have characterized the structures of a family of sixfold, left-handed ($t = -60°$), single helices for V-amylose with very low h values around 1.35 Å. They include certain allomorphs for amylose fibers obtained from solution in Me_2SO (French and Zobel, 1967; Winter and Sarko, 1974a; Rappenecker and Zugenmaier, 1981), iodine (Bluhm and Zugenmaier, 1981), or butanol (Booy *et al.,* 1979) in anhydrous, hydrous, or intermediate states. The structure of anhydrous V-amylose (Winter and Sarko, 1974a) is chosen here to represent the entire family. Its unit cell is orthorhombic ($a = 12.97$, $b = 22.46$, and $c = 7.91$ Å). The left-handed sixfold helix ($t = -60°$ and $h = 1.32$ Å) is very shallow as shown in Fig. 15a. The main chain conformation angles, $\phi = 115°$ and $\psi = -131°$, are up to 30° away from those in A- and B-amylose, and τ is 119.7°. The hydroxymethyl group has *gt* orientation ($\chi = -168°$). The inner and outer diameters of the helix are about 7.1 and 13.7 Å, respectively. The helix looks like a hollow cylinder (Fig. 15a) and is stabilized by intrachain O3H···O2 (2.8 Å) and O2H···O6 (2.9 Å) hydrogen

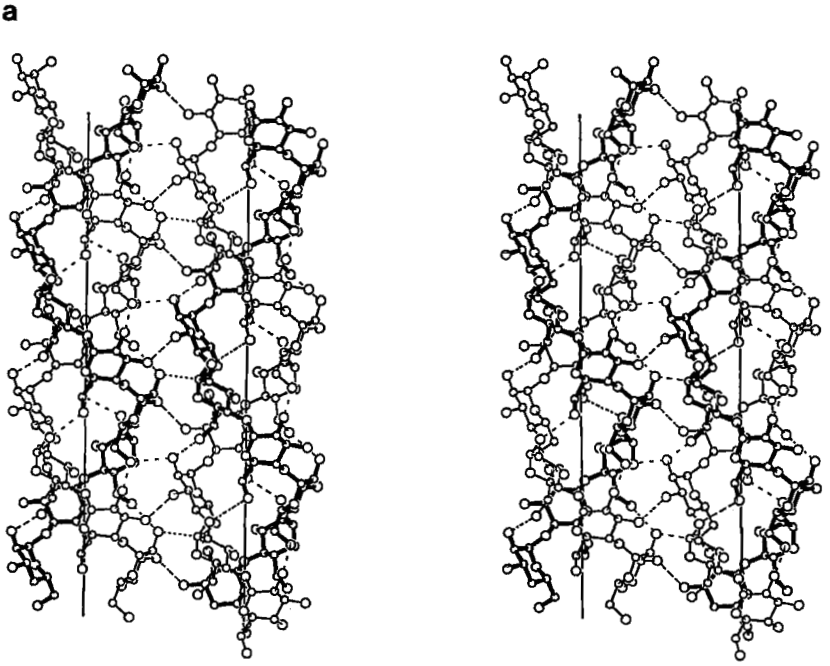

FIG. 14. Parallel packing arrangement of B-amylose. (a) Stereo side view of slightly less than two turns of two sixfold double helices 10.7 Å apart along the long diagonal of the *ab*-plane. The two strands in each helix are in thin and thick bonds for clarity, and the helix axis is vertical. Atom O6 mediates both intra- and inter-double helix hydrogen bonds. (b) A *c*-axis projection of the unit cell contents plus four other helices surrounding a cluster of six water molecules (crossed circles) per disaccharide in the middle.

bonds that link adjacent residues and turns, respectively. Related by crystallographic twofold screw axes parallel to *a* and *b*, the two helices in the unit cell are antiparallel and connected by intermolecular O2H···O2 (2.9 Å) hydrogen bonds (not shown). An axial projection of the unit cell contents is shown in Fig. 15b. Variations among the known V-amylose molecular structures are marginal. The helical cavity is wide enough to accommodate guest molecules such as water, ion, alcohol, lipid chain, and others of similar size. Depending on the complexing agent or solvent used, the full range of flexibility available to the hydroxymethyl group is exploited. As a consequence, there are changes in packing arrangements of helices among the various examples studied to date (Zobel *et al.*, 1967; Hinkle and Zobel, 1968; Winter and Sarko, 1974a,b; Zugenmaier and Sarko, 1976; Booy *et al.*, 1979; Bluhm and Zugenmaier, 1981; Rappenecker and Zugenmaier, 1981).

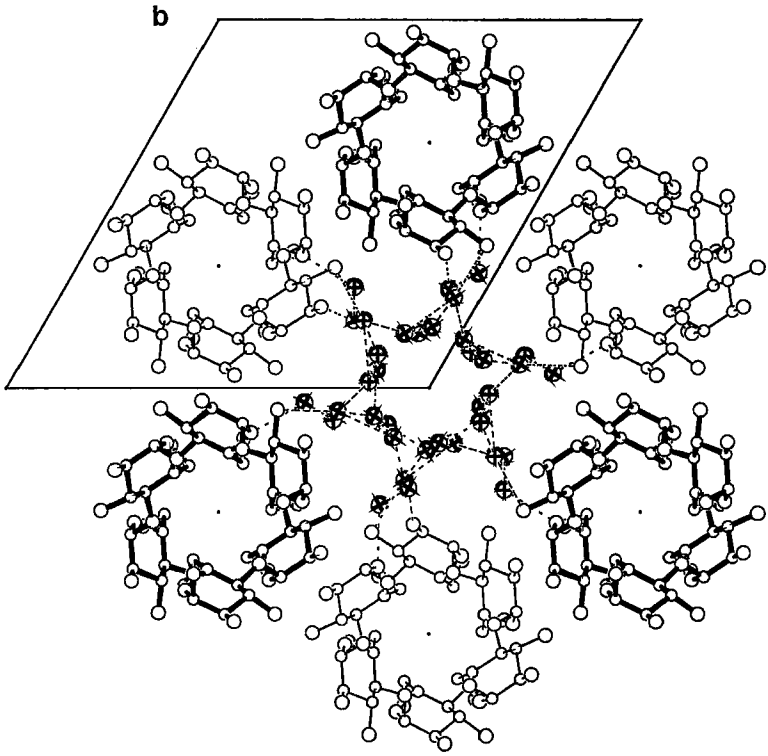

FIG. 14. Continued

Further reduction of pitch from that of V-amylose is stereochemically disallowed, but a sudden jump to zero is quite appropriate in the case of a short amylose chain with a DP of 6. This doughnut-like circular structure corresponds to α-cyclodextrin, which retains the central cavity, 5 Å wide, similar to that in V-amylose and forms inclusion complexes with various guest molecules that range from acetic acid, benzoic acid, iodine, hexanol, to tyrosine (Clarke *et al.*, 1988). Similar cyclic structures having DP 7 and 8 have increasing cavity sizes (6.2 to 8.0 Å) and are known as β- and γ-cyclodextrin, respectively. Although cyclodextrins are not approved for food use in the United States, they are of immense importance and interest to the pharmaceutical industries. For example, the strong binding property of β-cyclodextrin to cholesterol is used to remove the latter from dairy products.

Investigation of the complex of amylose with lipids is highly relevant toward understanding the structure and interactions of starch with food constituents (Biliaderis, 1991). In the presence of fatty acids, single-helical

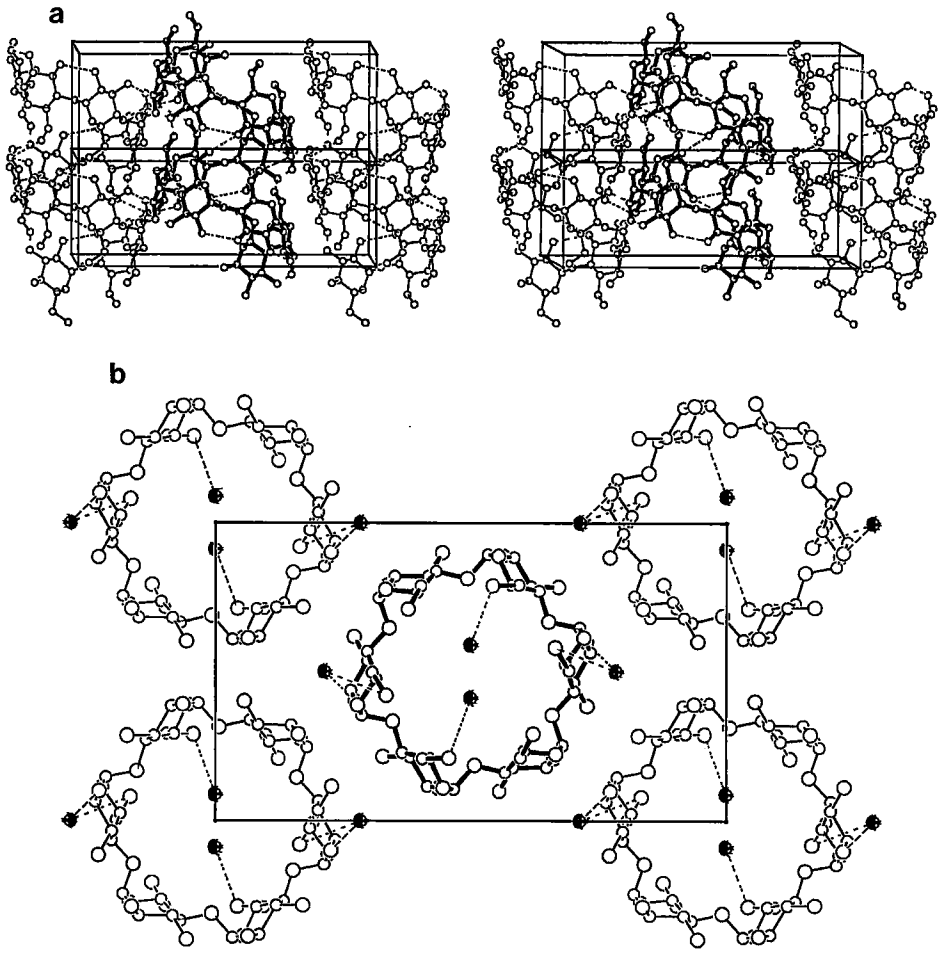

FIG. 15. Packing arrangement of shallow, sixfold, V-amylose helices. (a) Stereo view of two unit cells approximately normal to the *bc*-plane. The helix at the center (thick bonds) is antiparallel to the two helices (thin bonds) back at the corners. Intrachain hydrogen bonds (O3H···O2 and O2H···O6) stabilize each helix. (b) A *c*-axis projection of the unit cell shows that three water molecules (crossed circles) per monosaccharide, inside and between helices, are involved in the organization of helices.

V-amylose is apparently the active form, according to several independent investigations. For example, thermal behavior of the complex is consistent only with V-amylose allomorphs (Biliaderis *et al.*, 1985; Biliaderis and Galloway, 1989). X-ray powder diffractograms and differential scanning calorimetry coupled with molecular modeling indicate that a lipid inclusion

complex consists of a left-handed sixfold V_h-helix whose interior cavity is large enough to accommodate the aliphatic portion of the lipid in a *trans* conformation; the polar group cannot enter the cavity at all due to steric and electrostatic repulsion (Godet *et al.*, 1993a,b, 1995). Thus, although the double helix represents the native form of starch, it is now well known that the single-chain V-helix prevails when amylose interacts with fatty acids to form an inclusion complex.

e. KOH–Amylose Complex. In sharp contrast to the shallow V-helix, amylose can be induced to adopt an extended single helix under certain circumstances. For instance, a sixfold, left-handed ($t = -60°$) helix with $h = 3.74$ Å is formed when amylose complexes with KOH (Sarko and Biloski, 1980). The unit cell is orthorhombic with dimensions $a = 8.84$, $b = 12.31$, and $c = 22.41$ Å. The repeating motif is compatible with a maltotriose repeat in the final model, similar to that in A-amylose (Imberty *et al.*, 1988). Each trimer is associated with a KOH and three water molecules. The main chain conformation angles ϕ and ψ for the three saccharides are less than 1° off from 93° and −150°, respectively. The corresponding values of τ are 115.6, 116.3, and 113.7°. Because of structural similarity, it is not surprising that the amylose chain in KOH complex (Fig. 16a) is almost superimposable on a chain in the A- or B-amylose double helix. Due to its slightly larger pitch, the inner and outer diameters of the single helix (3.0 and 10.2 Å) are a bit smaller than those in the latter. The orientations of the three hydroxymethyl groups are two *gg* ($\chi = 57$ and 68°) and one *tg* ($\chi = -68°$). There are two helices organized in an antiparallel mode in the unit cell (Fig. 16b) and they are related by crystallographic twofold screw axes parallel to *a* and *b*. Adjacent helices are linked by a potassium ion involving two oxygen atoms as ligands from each helix. The close packing of helices is further stabilized by a water molecule per monosaccharide.

f. Amylose Derivatives. Several amylose derivatives in which all three potential hydroxyl groups are substituted are of special interest in relation to the structure of chemically modified starch and further extends its practical applications to food products. They include amylose triacetate (Sarko and Marchessault, 1967), trimethylamylose (Zugenmaier *et al.*, 1977), triethylamylose (Bluhm and Zugenmaier, 1979a), and its complexes with solvents (Bluhm and Zugenmaier, 1979b). All of them generally conform to fourfold, left-handed helices ($t = -90°$) whose h values vary from 3.75 to 4.05 Å. Since intrachain hydrogen bonds are not possible in these helices, their packing arrangements are controlled by van der Waals interactions only. The structure of triethylamylose (Bluhm and Zugenmaier, 1979a) having $h = 3.87$ Å is described here as an example. Its main chain conformation

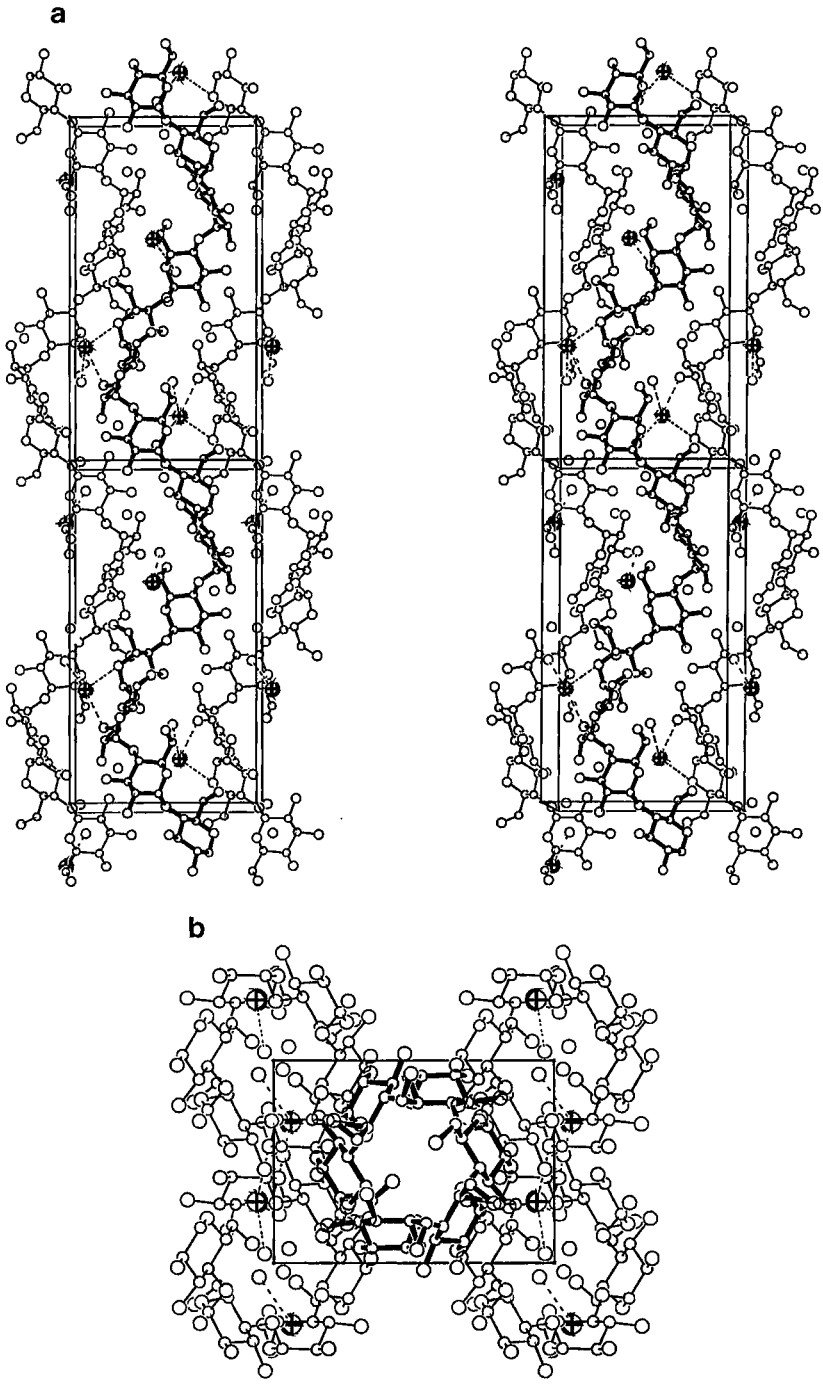
a
b

angles are $\phi = 64°$ and $\psi = -162°$ and τ is 122.1°. While χ is −94°, all three ethyl groups adopt roughly extended conformations, as shown in Fig. 17a. The orthorhombic unit cell ($a = 15.36$, $b = 12.18$, and $c = 15.48$ Å) accommodates two antiparallel helices that are related by crystallographic twofold screw axes parallel to a and b. An axial projection of the unit cell contents (Fig. 17b) shows clearly the interdigitation of substituents from neighboring helices. Consistent with the large t (−90°) and regular substitution, the inner and outer diameters of the helix are 2.8 and 13.4 Å, respectively. The closure of the helical cavity shows that it has no room to capture guest molecules as the V-form does.

The polymorphism of amylose helices in oriented fibers is a remarkable observation. The spectrum of structures covers single and double helices, all of which are left-handed; h values range from 1.35 to 3.8 Å; the shallow helices are excellent candidates for inclusion complexes, but the extended helices are not. The variety of intra- and interchain hydrogen bonds is clear testimony to the structural flexibility for transition between helical states and for transition from helix to coil under the influence of new interactions that amylose chains might encounter within their surroundings. These events in starch-based foods involve amylose, amylopectin, cations, water molecules, lipids, proteins, and the rest, and they undergo continuous changes in a dynamic fashion due to variations in temperature, pressure, shear, and so on. The structural details preceding gelation, gelatinization, and retrogradation of starch are indeed complex to visualize, but worthy of understanding through further investigation.

5. *Pectin*

Pectin is a heterogeneous complex structural plant polysaccharide that is part of the human diet. Depending on its source (e.g., apple pomace or citrus peel) and isolation procedure, pectin is polydisperse and polymolecular. The backbone of pectin is made up of (1→4)-linked α-D-galacturonic acid repeating units and some of the carboxyl groups are methyl esterified. Often, (1→2)-linked α-L-rhamnose residues interrupt the regular main chain. The high viscosity and cation-dependent gelling properties of pectin are exploited by the food and pharmaceutical industries. Moreover, the

FIG. 16. Packing arrangement of extended, sixfold, KOH–amylose helices. (a) Stereo view of two unit cells approximately normal to the *bc*-plane. The helix at the center (thick bonds) is antiparallel to the two helices (thin bonds) back at the corners. Water molecules (open circles) and hydroxyls from amylose helices are ligands to potassium ions (crossed circles). (b) A *c*-axis projection of the unit cell shows that amylose helices are packed tightly aided by ions and water molecules.

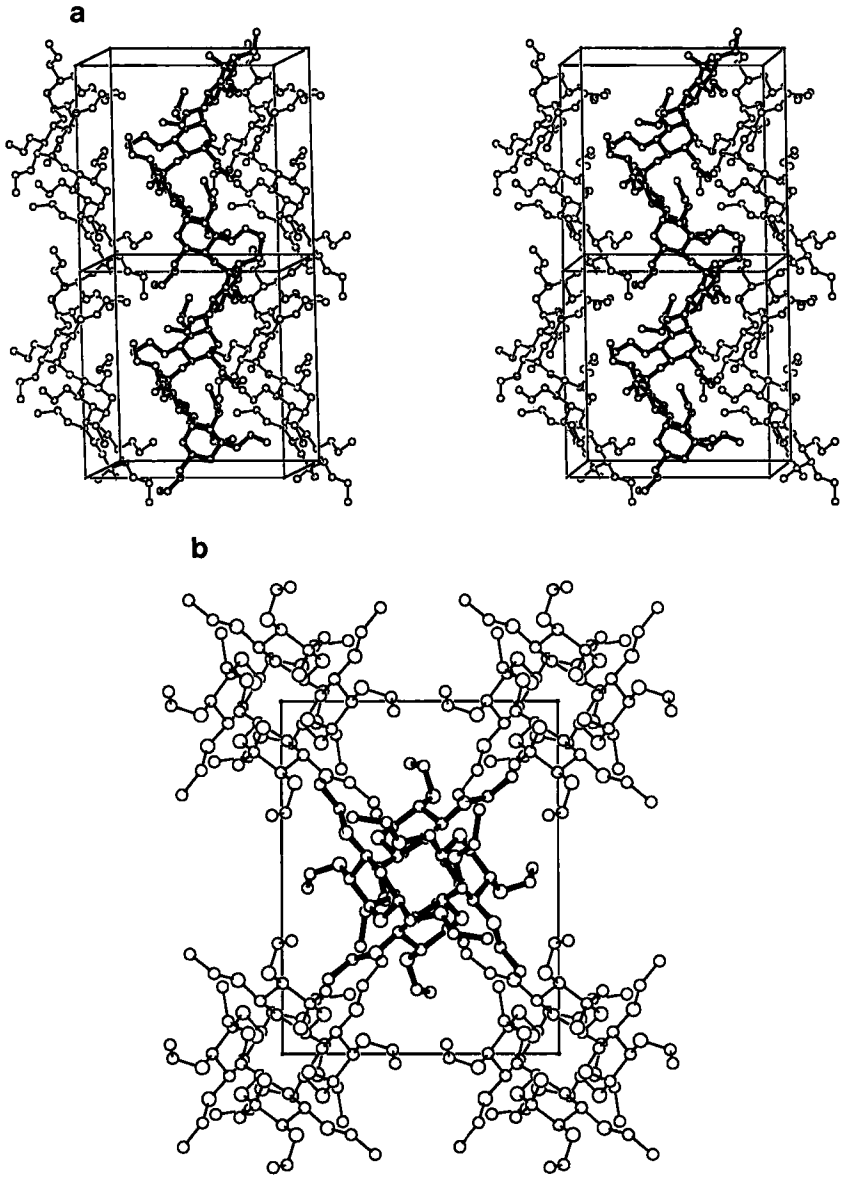

FIG. 17. Antiparallel packing arrangement of extended, fourfold, 2,3,6-tri-*O*-ethylamylose helices. (a) Stereo view of two unit cells approximately normal to the *bc*-plane. The helix at the center (thick bonds) is antiparallel to the two helices (thin bonds) at the back corners. There is no intra- or interchain hydrogen bond, and only van der Waals forces stabilize the helices. (b) A *c*-axis projection of the unit cell shows that the ethyl groups extend into the medium in radial directions.

rheological properties of pectin can be controlled by the degree of esterification (Rolin, 1993). X-ray studies on pectic acid (polygalacturonic acid), sodium pectate, calcium pectate (salts of polygalacturonic acid), and pectinic acid (100% methyl ester of pectic acid) have led to their structural details to varying extents.

a. Sodium Pectate. The x-ray diffraction pattern of sodium pectate (Walkinshaw and Arnott, 1981a) shows that the polymer forms a threefold helix of pitch 13.36 Å as evident from meridional reflections on the third and sixth layer lines. The unit cell is monoclinic (a = 8.39, b = 14.27, c = 13.36 Å, and γ = 90°). The 1,4-diaxial links, coupled with $^4C_1$ chair conformation for the galacturonate repeat, generate a right-handed helix (t = 120°) with h = 4.45 Å that fits the x-ray data (26 reflections) much better (R = 0.23) than a competing left-handed (t = −120°) model. Its conformational parameters τ, ϕ, and ψ are 116.5, 80, and 90°, respectively. The three residues per turn have, however, slightly different carboxylate group orientations: 115, 97, and 99° for χ. The helix is stabilized by intrachain O2H···O61 hydrogen bonds (2.8 Å) across each bridge oxygen atom and its inner and outer diameters are 0.4 and 7.0 Å, respectively. There are two water molecules and one sodium ion (near the carboxylate group) per monomer. The two rod-like helices in the unit cell are packed antiparallel and related by crystallographic twofold screw symmetry parallel to the b-axis; they are laterally separated by 8.4 Å and their carboxylate groups are bridged by sodium ions and water molecules. These structural features are shown in Fig. 18.

b. Pectic Acid. According to the x-ray study on the acid form (Walkinshaw and Arnott, 1981a), pectic acid crystallizes in a monoclinic unit cell (a = 9.9, b = 12.3, c = 13.3 Å, and γ = 90°). Similar to sodium pectate, it forms a threefold helical structure (t = 120° and h = 4.43 Å) stabilized by O2H···O61 (2.62 Å) hydrogen bonds between adjoining residues. The conformational parameters of a monomer unit are τ = 116.5°, ϕ = 73°, ψ = 97°, and χ = 93°. The two helices in the unit cell are antiparallel and related by twofold screw symmetry along the b-axis. Due to the absence of ions in this case, however, the interhelical association is directly through O3H···O62 (2.8 Å) and O61H···O61 (2.8 Å) hydrogen bonds (Fig. 19a). The resulting packing arrangement (Fig. 19b) is somewhat different from that of sodium pectate (Fig. 18b) due to changes in lateral dimensions of their unit cells.

c. Calcium Pectate and Pectinic Acid. Neither calcium pectate nor pectinic acid has produced decent diffraction patterns for detailed structure

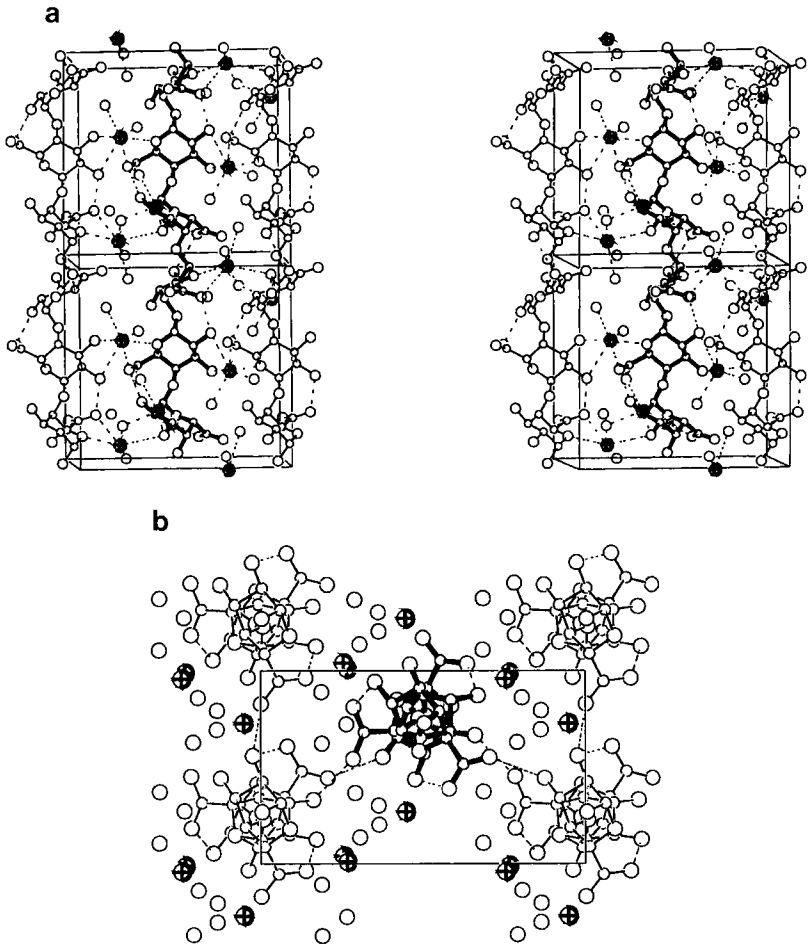

FIG. 18. Antiparallel packing arrangement of threefold sodium pectate helices. (a) Stereo view of two unit cells roughly normal to the *bc*-plane. The helix at the center (thick bonds) is antiparallel to the two in the front (thin bonds). Intrachain hydrogen bonds stabilize each helix. Sodium ions (crossed circles) and water molecules (open circles) connect adjacent helices. (b) A *c*-axis projection of the unit cell contents shows that ions and water molecules are located between helices.

analysis. Preliminary x-ray analysis of calcium pectate (Walkinshaw and Arnott, 1981b) favors the same molecular structure and packing arrangement as pectic acid except that the O61H···O61 hydrogen bond is replaced by an O61···Ca^{2+}···O61 interaction. Pectinic acid is also a threefold helix, but it has a hexagonal packing arrangement with only one helix per trigonal unit cell ($a = b = 8.37$ and $c = 13.0$ Å). In this idealized 100% methylester

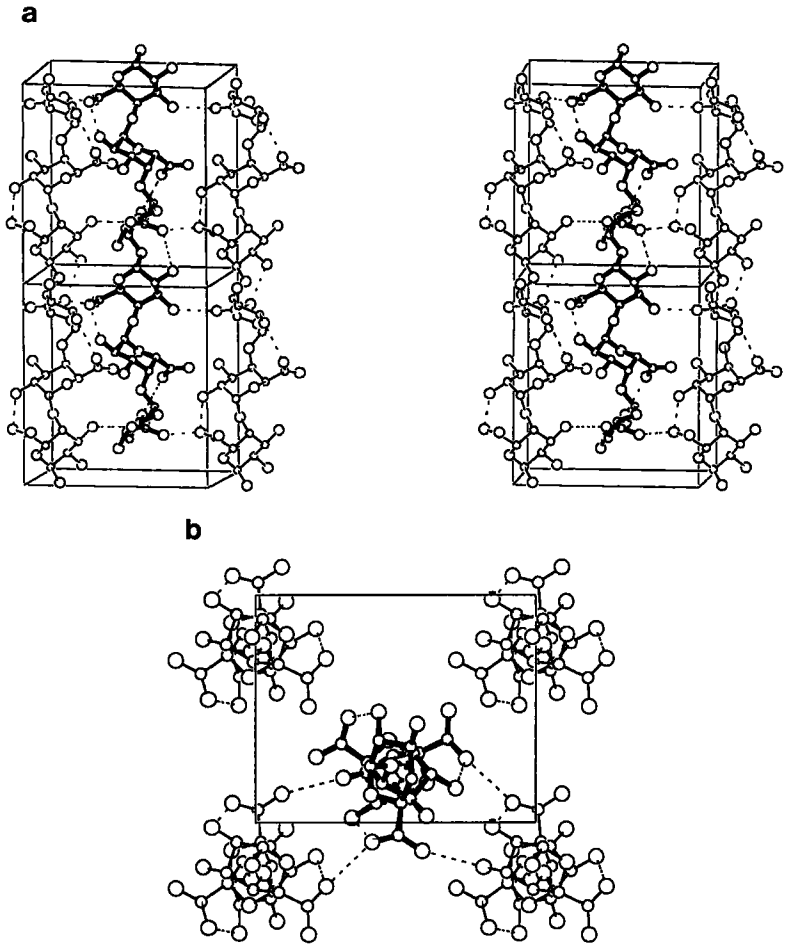

FIG. 19. Antiparallel packing arrangement of threefold pectic acid helices. (a) Stereo view of two unit cells roughly normal to the *bc*-plane. The helix at the center (thick bonds) is antiparallel to the two in the front (thin bonds). Intrachain hydrogen bonds stabilize each helix. Association of helices is through direct hydrogen bonds involving the carboxyl groups. (b) A *c*-axis projection of the unit cell contents highlights the interactions among three helices.

form of pectinic acid, the unit cell has a triangular column of methyl (hydrophobic) groups, enclosed by three helices, and a similar channel filled with water molecules hydrogen bonded to the surrounding polymer chains (Walkinshaw and Arnott, 1981b). The network formed by alternating hydrophobic and hydrophilic channels embedded among the helices provides an interesting motif in the formation of junction zones, which are implicated in the gelation process. If reducing the degree of methylation would increase

the amount of water within the network, addition of co-solute would not only compete for this water but also disrupt the formation of the hydrophobic cage. Both strategies, in conjunction with pH and temperature as variables, are commercially exploited to alter the gelation properties to suit current needs (Rolin, 1993).

Jams and jellies containing desired levels of sugar are always associated with pectins, fruits and plants being their respective origins. Pectins are also used in fruit sauces, fruit yogurts, milk drinks, and heat-resistant bakery glazing. In all cases, the pH is very acidic (3.0 to 5.5).

6. *Alginic Acid*

Alginic acid constitutes one of the structural polysaccharides of marine brown algae and some bacteria. Although a homopolymer of D-mannuronic acid (M) is the starting fermentation product, mannuronan C5 epimerase converts β-D-mannuronic acid to α-L-guluronic acid (G) in certain blocks (Clare, 1993). Therefore, the (1→4)-linked polymer contains blocks of β-D-mannuronic acid alternating with blocks of α-L-guluronic acid of varying size. The composition and block lengths are species dependent. For example, the sample from *Fucus* or *Asophyllum* species is 97% polymannuronic acid and that from *Lamineria hyperborea* is rich in polyguluronic acid (Atkins *et al.*, 1973a). Alginic acid is useful to the food industries because of its cation-dependent gelling properties. Since M and G adopt $^4C_1$ and $^1C_4$ chair conformations, respectively, and since the linkages are diequatorial for M and diaxial for G, morphologies of the two polymers are quite unrelated.

a. Poly(β-D-Mannuronic Acid). The x-ray diffraction pattern (Atkins *et al.*, 1973a) recorded from a bundle of fibers prepared from *Fucus vesiculosius* is reminiscent of those from mannan I. The orthorhombic unit cell dimensions are $a = 8.6$, $b = 7.6$, and $c = 10.4$ Å. The molecule is an extended ribbon-like twofold helix ($t = 180°$ and $h = 5.2$ Å) similar to that of mannan stabilized by O3H···O5 hydrogen bonds (2.7 Å) across each glycosidic bridge oxygen atom. The conformational parameters τ, ϕ, ψ, and χ are 117.1, −94, −145, and 94°, respectively. The two helices located at (a/4 0 0) and (3a/4 b/2 0) in the unit cell are antiparallel and related by crystallographic twofold screw axes parallel to a and b as shown in Fig. 20a. One of the carboxylate oxygen atoms is hydrogen bonded (2.7 Å) to atom O3 of a neighboring chain of the same polarity, separated by the b-axis. The antiparallel chains are connected by O2H···O5 hydrogen bonds (3.0 Å). The c-axis projection (Fig. 20b) shows that the sugar rings are oriented roughly parallel to the bc-plane. In all respects, this molecular

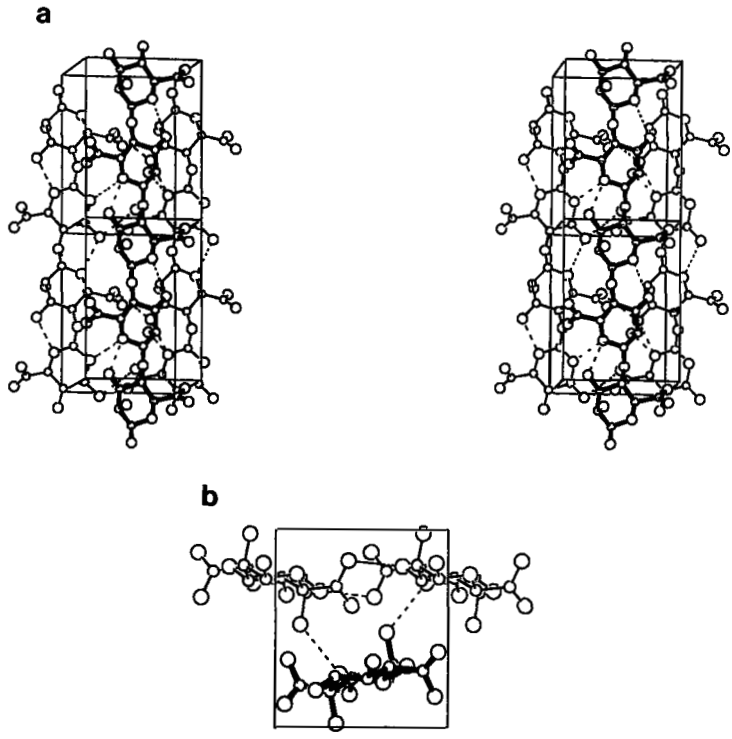

FIG. 20. Antiparallel packing arrangement of twofold poly(mannuronic acid) helices. (a) Stereo view of two unit cells roughly normal to the *bc*-plane. The helix at the center (thick bonds) is antiparallel to the two (thin bonds) in the back. Intrachain hydrogen bonds stabilize each helix. Association of helices through direct hydrogen bonds involves carboxylate groups for parallel, and the axial 2-hydroxyl groups for antiparallel chains. (b) A *c*-axis projection of the unit cell contents highlights hydrogen bonds between helices.

structure and packing arrangement are very similar to those previously described for mannan I (Atkins *et al.*, 1988).

a. Poly(α-L-Guluronic Acid). The x-ray diffraction pattern (Atkins *et al.*, 1973b) shows a meridional reflection on the second layer line, which is diagnostic of a twofold helix (t = 180° and h = 4.35 Å). The unit cell is orthorhombic (a = 10.7, b = 8.6, and c = 8.7 Å). The 8.7 Å pitch is 1.7 Å shorter than that of cellulose or mannan. The guluronate residue is in the preferred $^1C_4$ chair conformation. Because of the 1,4-diaxial C–O bonds, the helix is a buckled ribbon (Fig. 21a) that does not resemble the poly(mannuronic acid) structure. The conformational parameters τ, ϕ, ψ, and χ are 117.6, −108, −134, and 99°, respectively. The helix is stabilized by

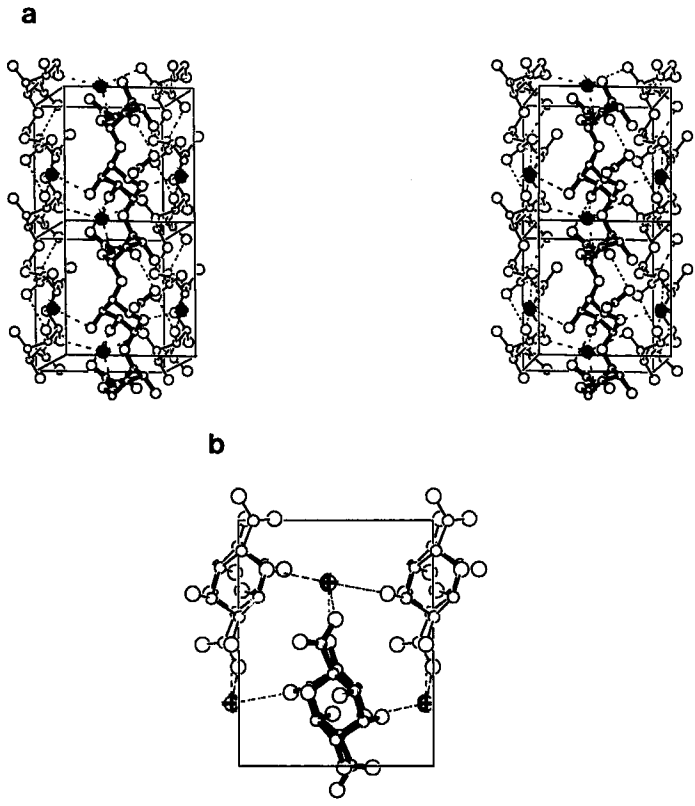

FIG. 21. Antiparallel packing arrangement of twofold poly(guluronic acid) helices. (a) Stereo view of two unit cells roughly normal to the *bc*-plane. The helix at the center (thick bonds) is antiparallel to the two (thin bonds) in the back. Intrachain hydrogen bonds stabilize each helix. Association of antiparallel helices involves carboxylate groups and water molecules (crossed circles). (b) A *c*-axis projection of the unit cell contents shows that helices are connected via water molecules. Due to a buckled shape of the helix, there is complete overlap between adjacent sugar rings.

O2H···O61 (2.7 Å) hydrogen bonds across every glycosyl bridge oxygen atom. The two chains in the unit cell, located at (*a*/4 0 0) and (3*a*/4 *b*/2 0) and related by crystallographic twofold screw symmetry parallel to *a* and *b*, are antiparallel. Adjacent helices are connected by water molecules, one per guluronate residue, via O2···*W*···O3 and O5···*W*···O3 interactions. Figure 21b suggests that adjacent sugar rings in the chain overlap completely when projected down the helix axis.

The carboxylate oxygen atoms are farthest from the helix axis at 3.7 Å in both poly(mannuronic acid) and poly(guluronic acid) so that they can

easily interact with ions and water molecules in the environment. It is believed that pairs of carboxylate groups may be connected by calcium ions. The pairwise association of helices mediated by an array of calcium ions in the middle bears certain resemblance to a Styrofoam box packed with eggs. This similarity is the basis for the "egg-box" model (Grant *et al.,* 1973), which depicts the junction zone in guluronate-rich alginate gels. According to computer modeling, a pair of chains can associate in parallel as well as antiparallel mode with the help of calcium ions (Mackie *et al.,* 1983). The thickening effect and calcium-dependent gelation properties of alginate are extensively utilized in pimento-stuffed olives, salad dressings, fruit drinks, and coatings on food to prevent bacterial contamination (Clare, 1993).

B. (1→3)-LINKED POLYSACCHARIDES

β-Glucan and scleroglucan are the two polysaccharides in this group having food applications. The former, known as curdlan, has excellent gelling properties and is used in numerous Japanese foods. It adopts at least three different helical structures. The latter is (1→6)-branched and its backbone retains one of the curdlan structures.

1. β-Glucan

Curdlan, the extracellular microbial polysaccharide having (1→3)-linked β-D-glucose as its repeating unit, forms resilient gels from aqueous solutions at 95°C. X-ray diffraction patterns from oriented specimens (Marchessault *et al.,* 1980) identified three distinct forms, I, II, and III, representing the native specimen, the hydrated form after annealing at 140°C, and the dehydrated form after annealing, respectively. This investigation assigned similar triple helical structures to all three, but Curdlan I is now known to exist as a single helix (Okuyama *et al.,* 1991).

a. Curdlan I. According to a recent x-ray reexamination (Okuyama *et al.,* 1991), the unit cell of form I is monoclinic (a = 28.8, b = 18.6, c = 22.8 Å, and γ = 90°). Consistent with a meridional reflection on the sixth layer line in the diffraction pattern, the molecular structure is a sixfold, right-handed, single helix (t = 60° and h = 3.8 Å). Its conformational parameters τ, ϕ, ψ, and χ are 116.5, −71, 126, and −54°, respectively. As illustrated in Fig. 22a, the helix is rather extended (pitch = 22.8 Å) and is stabilized by O4H···O5 (3.14 Å) hydrogen bonds connecting adjacent residues. With reference to atomic centers, the inner diameter is too small (2.0 Å) to hold any guest molecules, but the outer diameter of the helix is

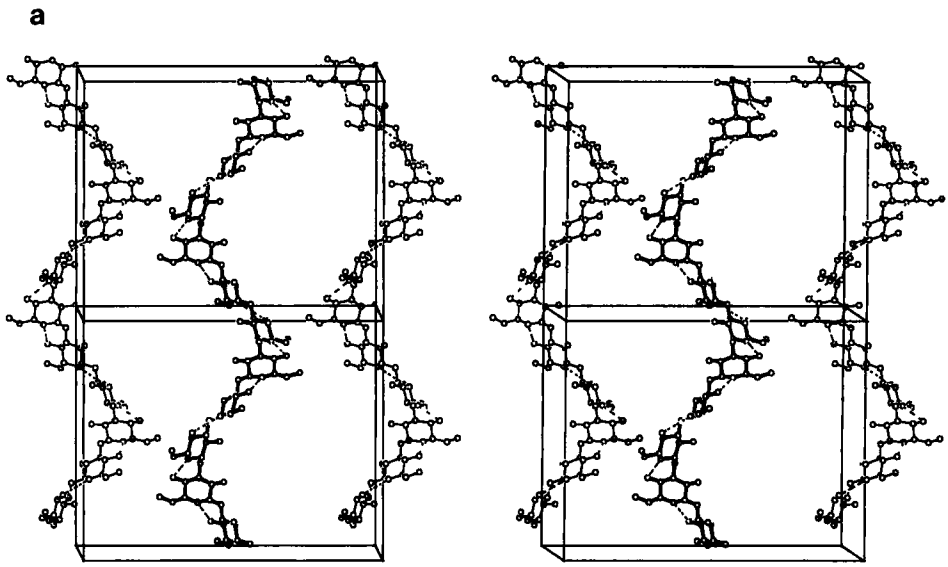

FIG. 22. Parallel packing arrangement of sixfold, curdlan I helices. (a) Stereo view of two unit cells approximately normal to the *bc*-plane. The helix is stabilized by intrachain O4H···O5 hydrogen bonds. There are only van der Waals interactions between helices. (b) A *c*-axis projection of the unit cell shows large gaps between helices which are alleged to be filled with 250 water molecules.

large (14.3 Å). Two helices pass through (0 0 0) and (*a*/2 *b*/2 0) of the unit cell in a parallel mode. There are no interhelical hydrogen bonds and the large interstitial space in the unit cell, clearly seen in Fig. 22b, is reported to be filled with about 250 water molecules. The final *R*-value is 0.14 for 40 reflections.

b. Curdlan III. The dehydrated form III is structurally well organized and its x-ray analysis (Deslandes *et al.*, 1980) reveals that the polymer chains crystallize in a hexagonal cell ($a = b = 14.41$, $c = 5.87$ Å, and $\gamma = 120°$). The meridional reflection occurs on the second layer line and there are six glucose residues per cell. A sixfold, parallel, triple helix of pitch $3c = 17.61$ Å ($h = 2.94$ Å), in which the three chains are related by c translation along the helix axis, is consistent with these observations. The pitch (17.61 Å) is 5.2 Å shorter than that of curdlan I. A right-handed helix ($t = 60°$) corresponding to a final *R*-value of 0.23 for 21 reflections is superior to any left-handed alternative. The conformational parameters τ, ϕ, ψ, and χ of the triple helix shown in Fig. 23a are 110.6, −92, 126, and −82°, respectively. Both its inner and outer diameters are 1 Å larger than those in curdlan I, so that triads of interchain O2H···O2 (2.72 Å) hydrogen

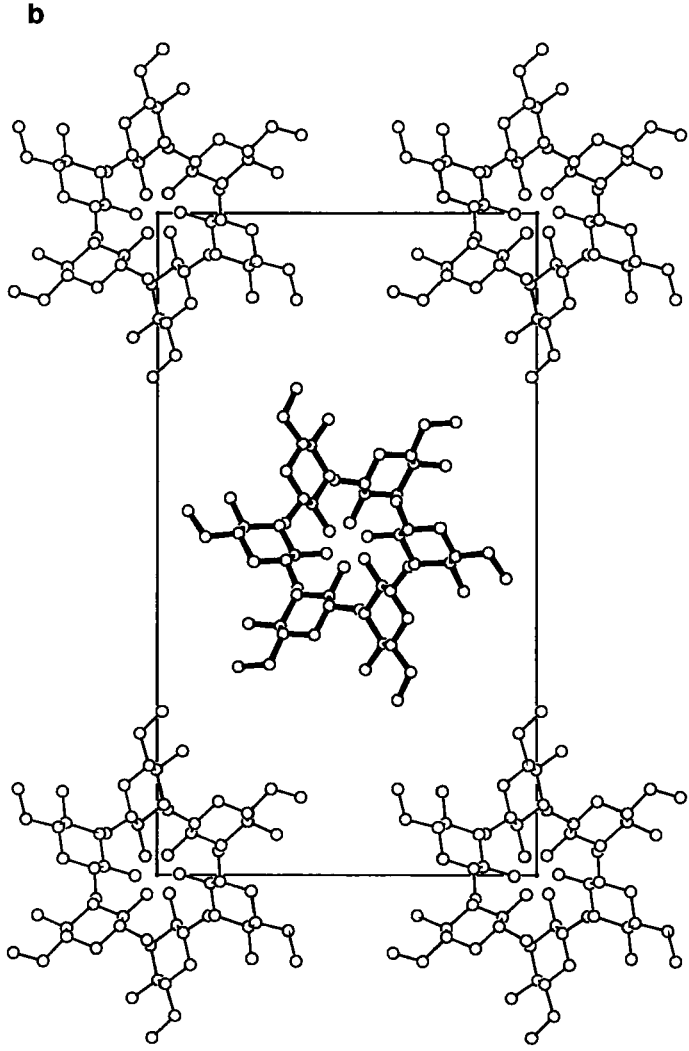

FIG. 22. Continued

bonds are formed at successive levels separated by h in the central wider core. As a result, the triple helix appears like a solid cylinder. The intrachain O4H···O5 distance of 3.18 Å between adjacent residues represents a weak hydrogen bond. The packing of molecules in the unit cell (Fig. 23b) is facilitated by a series of strong hydrogen bonds (2.70 to 2.75 Å) between neighboring triple helices involving atoms O4 and O6.

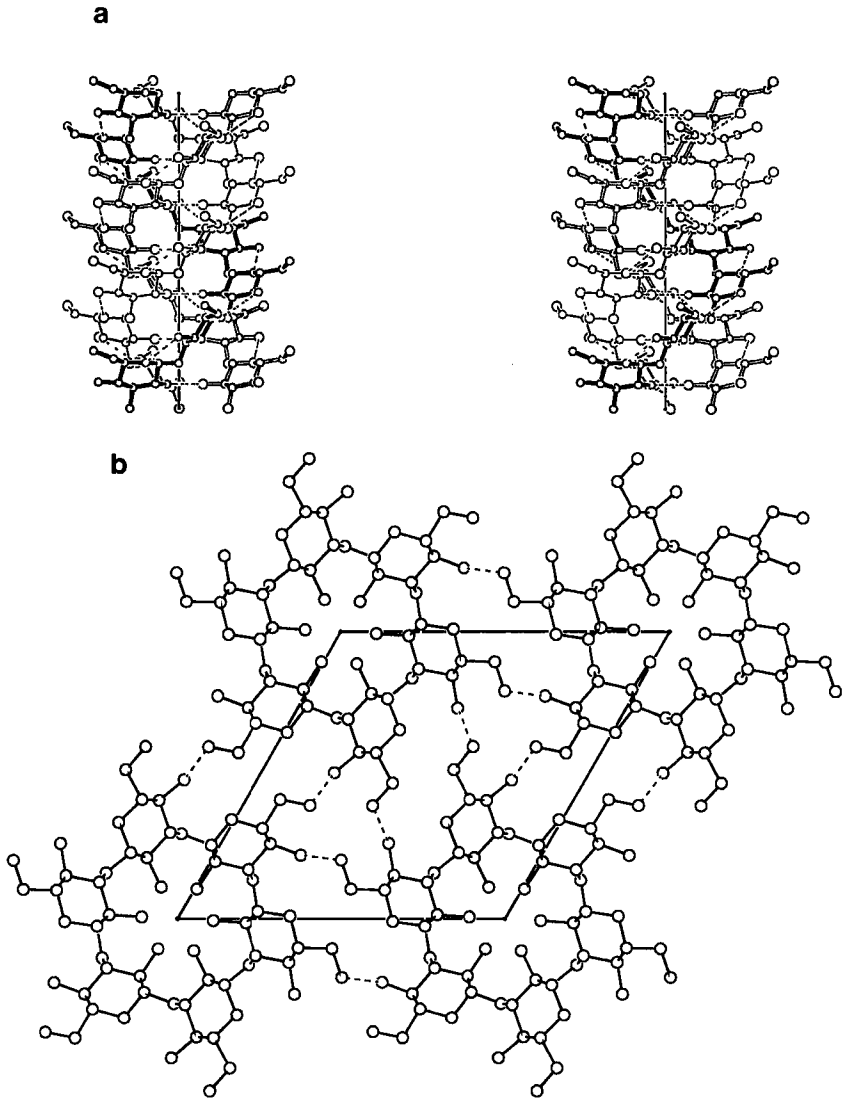

FIG. 23. Structure of the sixfold anhydrous curdlan III helix. (a) Stereo view of a full turn of the parallel triple helix. The three strands are distinguished by thin bonds, open bonds, and filled bonds, respectively. In addition to intrachain hydrogen bonds, the triplex shows a triad of O2H···O2 interchain hydrogen bonds around the helix axis (vertical line) at intervals of 2.94 Å. (b) A *c*-axis projection of the unit cell contents illustrates that O6H···O4 hydrogen bonds between triple helices stabilize the crystalline lattice.

c. Curdlan II. The hydrated form II is not quite like the ordered structure of curdlan III. According to its x-ray analysis (Chuah *et al.,* 1983), the hexagonal unit cell ($a = b = 15.56$, $c = 18.78$ Å, and $\gamma = 120°$) of II is somewhat larger than, and the intensity distribution in the diffraction pattern is slightly different from, that of III. In order to account for the 18.78 Å layer line, the final model for curdlan II compromises with a triple helical backbone as in III, and distinct orientations covering the entire range of staggered domains for the 18 hydroxymethyl groups in one turn. This arrangement is feasible by revising the conformational parameters τ, ϕ, and ψ to 104.6, −87, and 127°, respectively. Six water molecules per monosaccharide are involved in connecting triple helices in the unit cell through hydrogen bonds. The final R-value is 0.17 for 79 reflections.

The water-mediated hexameric aggregation of curdlan triple helices is strong enough to result in micelle formation. The interaction of these micelles with each other is believed to be responsible for gelation (Fulton and Atkins, 1980). The dependence of gelation on high temperatures is an attractive feature of curdlan for food applications (Harada *et al.,* 1993). For instance, gels formed by heat treatment at 120°C have remarkable fat-adsorbing properties. Curdlan helps to improve the texture of soy bean curd, sweet bean paste jelly, boiled fish paste, Japanese noodles, sausage, jellies, and jams. It is also used as a stabilizing agent in ice cream and a thickener in sauces and soup.

2. *Scleroglucan*

Scleroglucan has a branched tetrasaccharide repeating unit composed of a trisaccharide fragment like that of curdlan and an (1→6)-linked β-D-glucoside as side chain. X-ray diffraction of oriented fibers of scleroglucan coupled with molecular modeling (Bluhm *et al.,* 1982) suggests considerable morphological similarity with curdlan III. The unit cell is hexagonal ($a = b = 17.3$, $c = 6.0$ Å, and $\gamma = 120°$) but the poor quality of the x-ray data has not permitted an independent structure determination. Based on a conformational analysis of gentobiose, the preferred orientation of the side chain is given by $\chi = 60°$, $\phi = 60°$, and $\psi = -130°$. Incorporation of a side chain in this conformation on every third glucoside residue in a curdlan III triple helix generates a plausible model for scleroglucan as shown in Fig. 24. The peripheral side chains increase the outer diameter to 24.2 Å from 15.3 Å for the main chains alone, and thus hinder main chain–main chain association of scleroglucan helices. However, aggregation is promoted by side chains and a large number of water molecules are trapped between helices. This structural feature is important for the observed gelation properties.

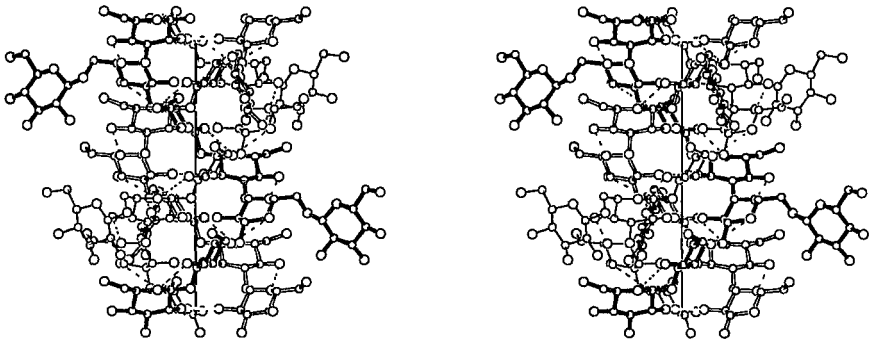

FIG. 24. A stereo view of a full turn of the sixfold scleroglucan triple helix. The three strands are distinguished by thin bonds, open bonds, and filled bonds, respectively. As in curdlan III, the triad of O2H···O2 interchain hydrogen bonds stabilize the triple helix. Peripheral side chains shield the main chains appreciably.

Scleroglucan is used as a stabilizer in frozen and aerated desserts, creams, and sauces. As in the case of curdlan, Japan is the foremost country to use scleroglucan in cakes, steamed foods, rice crackers, and bakery products (Brigand, 1993).

C. ALTERNATING (1→3) AND (1→4)-LINKED POLYSACCHARIDES

This group includes carrageenans and agarose, which are useful as gelling agents. These polysaccharides are exclusively built with galactopyranosyl units with disaccharide motifs, which utilize both L- and D-sugars; and α- and β-anomers. While carrageenans are sulfated to varying extents, agarose and related polymers are not sulfated at all. Both polymers tend to be double helical. In contrast with the monotonous monosaccharide repeat and the same type of linkage in the previously described polysaccharides, due to their disaccharide repeats, carrageenan and agarose helices display greater conformational flexibility and hence more interesting morphology.

1. Carrageenans

Carrageenans belong to a family of gel-forming sulfated polysaccharides found in the marine red algae *Rhodophyceae.* Two principal members, known as ι- and κ-carrageenan, chemically differ in degree of sulfation (Therkelsen, 1993). The disaccharide repeat (A–B) for each case is

A B

ι-carrageenan: →3)-β-D-Gal4SO_3^--(1→4)-3,6-anhydro-α-D-Gal2SO_3^--(1→

κ-carrageenan: →3)-β-D-Gal4SO_3^--(1→4)-3,6-anhydro-α-D-Gal-(1→

Two sets of parameters are needed to describe the disaccharide conformation: τ_1, ϕ_1, ψ_1 refer to A(1→4)B and τ_2, ϕ_2, ψ_2 to B(1→3)A linkage; χ_A and χ_B are the orientations of the hydroxymethyl groups. Note that in the case of κ-carrageenan, the anhydrogalactose residue B is not sulfated. Both polymers form thermally reversible gels that exhibit substantial differences in their physical properties. For example, ι-carrageenan forms very clear and elastic gels that neither synerese nor undergo hysteresis effects. In contrast, κ-carrageenan gels are hazy and brittle and exhibit syneresis as well as hysteresis effects. Consistent with their chemical differences, their molecular structures are not the same, resulting in distinct physical properties in the presence of a variety of ions.

a. ι-Carrageenan. X-ray diffraction patterns from polycrystalline and well-oriented fibers of Ca^{2+} ι-carrageenan have meridional reflections on the third and sixth layer lines (Arnott *et al.*, 1974a). The unit cell is trigonal ($a = b = 13.73$, $c = 13.28$ Å, and $\gamma = 120°$). The x-ray data are best fitted by a threefold, right-handed ($t = 120°$), parallel, half-staggered, double helix. The pitch is $2c = 26.56$ Å so that $h = 8.85$ Å. The helix, shown in Fig. 25a, incorporates the preferred $^4C_1$ and $^1C_4$ chair geometries in residues A and B, respectively, and contains both sulfate groups on its outside. The molecule is extremely sinuous due to its disaccharide motif. The conformational parameters (τ_1, ϕ_1, ψ_1) and (τ_2, ϕ_2, ψ_2) are (116.5, −87, 94) and (116.5, 75, 79), respectively, and $\chi_A = 176$, all in degrees. The sulfate group orientations (θ_1, θ_2) are (115°, −159°) in A and (−140°, −165°) in B. The galactose residues are connected by six interchain O6H···O2 (2.7 Å) hydrogen bonds per turn. The trigonal unit cell accommodates only one helix. In terms of coordinates published for nonhydrogen atoms alone (Arnott *et al.*, 1974a), its inner and outer diameters are 3.4 and 14.2 Å, respectively. A packing arrangement with up- and down-pointing molecules distributed randomly at each cell corner, similar to that shown in Fig. 25b, explains the presence of both Bragg reflections and layer line streaks in the diffraction pattern. The two sulfate groups on the anhydrogalactose residues of adjacent helices, linked through direct $SO^{4-}\cdots Ca^{2+}\cdots SO^{4-}$ interactions, are believed to be responsible for polymer aggregation during gel formation.

b. κ-Carrageenan. Fibers prepared from the potassium salt of κ-carrageenan are less oriented and less crystalline than those of ι-carrageenan. The diffraction pattern exhibits only continuous intensities

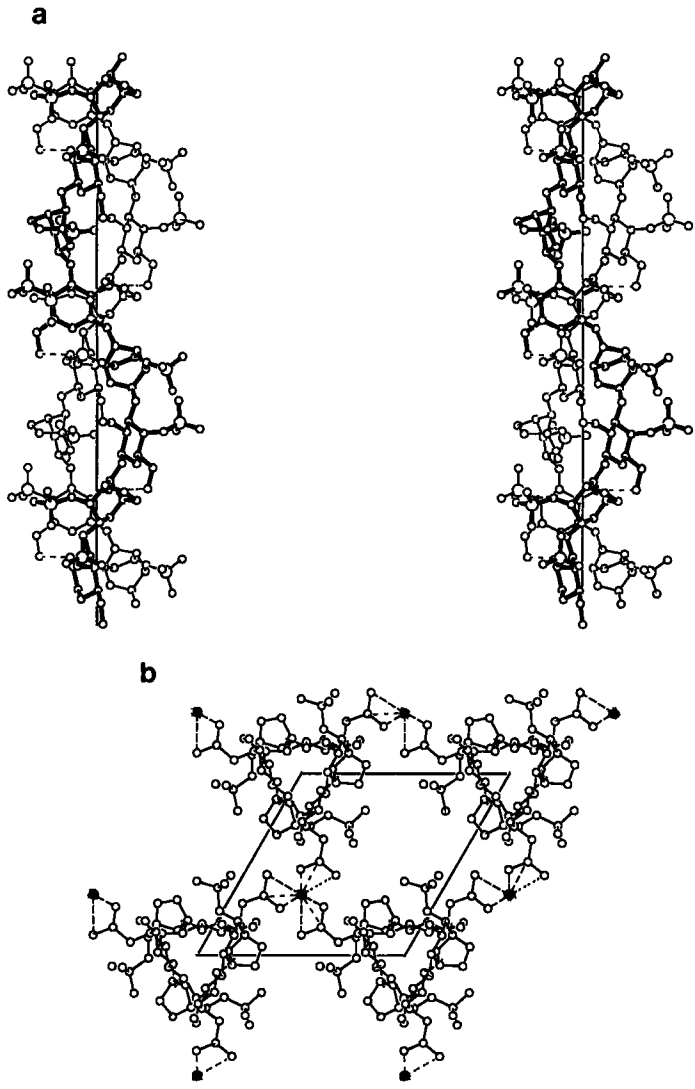

FIG. 25. (a) Stereo view of slightly over a turn of the threefold double helix of ι-carrageenan. The two chains are distinguished by thin and thick bonds for clarity. The vertical line is the helix axis. Six interchain hydrogen bonds per turn among the galactose residues stabilize the double helix. The sulfate groups lined up near the periphery are crucial for intermolecular interactions. (b) An axial projection of the unit cell contents. The helix at each corner can be either "up-" or "down-pointing" in terms of the x-ray data. All are, however, up in this diagram so that a calcium ion (crossed circle) is connected to the sulfate groups in three surrounding helices.

on layer lines, indicating that there is no lateral organization of polymer molecules in the fiber (Millane *et al.*, 1988). The first layer line spacing (25 Å) is roughly twice that observed for ι-carrageenan (i.e., c = 13.28 Å), and meridional intensity is seen on the sixth and ninth layer lines. On the basis of modest similarity in overall intensity distribution with that of ι, and as a reasonable fit with the observed x-ray intensities, κ-carrageenan is also double helical. As shown in Fig. 26, the two chains in the threefold, right-handed (t = 120°), parallel, double helix of pitch 25 Å (h = 8.33 Å) are offset from the half-staggered position by 1.1 Å along, and 28° about, the common helix axis. Due to this offset, the 25 Å layer line is not extinguished in the diffraction pattern, and there are only half the number of interchain O6H···O2 (2.5 Å) hydrogen bonds connecting the galactose residues. The main chain conformational parameters (τ_1, ϕ_1, ψ_1) and (τ_2, ϕ_2, ψ_2) are (116.5, −98, 108) and (116.5, 61, 81), respectively, and χ_A = −178, all in degrees. The two angles θ_1 and θ_2 for the sulfate group orientation in residue A are 118° and −155°, respectively. Due to a shorter pitch, the outer diameter of the helix is about 1 Å larger than that in ι-carrageenan. Details of the interactions among helices and the structural role of potassium ions are beyond the scope of this analysis.

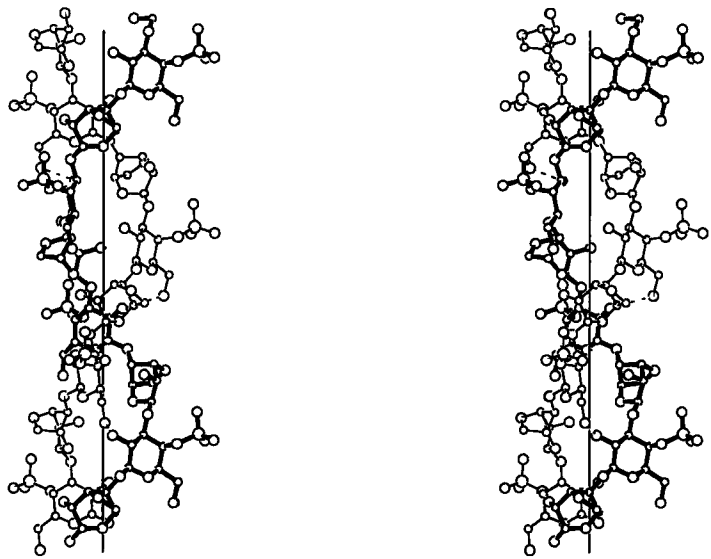

FIG. 26. Stereo view of about a turn of the threefold double helix of κ-carrageenan. The two chains are distinguished by thin and thick bonds for clarity. The vertical line is the helix axis. Only three interchain hydrogen bonds per turn among the galactose residues stabilize the helix. The peripheral sulfate groups are crucial for intermolecular interactions.

Consistent with their chemical differences, the molecular structures of ι- and κ-carrageenans are not identical. A shorter pitch and an offset positioning of the two chains in the κ-helix is compatible with the absence of sulfate groups on its anhydrogalactose residues. The variations in molecular structures mirror the types of junction zones formed by these polymers and relate to differences in the observed gelation properties (Therkelsen, 1993). Carrageenans, known also for stabilizing and viscosity building beyond gelation, are routinely used in dairy products, including ice cream, chocolate milk, and custards to name a few. Water desserts incorporating fruit constituents, glazing of hot tart berry fillings, processed cooked ham, and canned meat and fish are other examples of foods that contain carrageenans exclusively or in combination with other food gums.

2. *Agarose*

Agarose, a member of the agar family of galactan polysaccharides found in red seaweeds, is an excellent gel-forming agent extracted from *Rhodophyceae.* The only difference in covalent structure between agarose and carrageenan is in inversion of the anhydrogalactose residues from D to L. Also agarose carries no sulfate groups. Its disaccharide repeat (A–B) is $\rightarrow$3)-β-D-Gal-(1$\rightarrow$4)-3,6-anhydro-α-L-Gal-(1$\rightarrow$. As in the case of κ-carrageenan, agarose films and fibers used in the x-ray study are oriented and noncrystalline. Therefore, its diffraction patterns consist of only continuous intensities on layer lines. The first layer line spacing c is 9.5 Å and meridional intensity is on the third layer line. Arnott *et al.* (1974b) proposed a threefold, left-handed ($t = -120°$), half-staggered, parallel, double helix of pitch $2c$ = 19.0 Å (h = 6.33 Å) as the best model and it contains both monomers in the same $^4C_1$ chair conformation. This helix, as shown in Fig. 27, is much shorter than the carrageenan helices (Figs. 25a and 26). Its inner and outer diameters are 4.2 and 13.6 Å, respectively, in terms of nonhydrogen atoms alone. The conformational parameters (τ_1, ϕ_1, ψ_1) and (τ_2, ϕ_2, ψ_2) are (116.5, −124, −113) and (116.5, −52, 157), respectively, and $\chi_A = -69$, all in degrees. There are no hydrogen bonds either within or between chains and the double helix is stabilized only by van der Waals forces. The inner cavity is just wide enough to hold water molecules, which can mediate interchain hydrogen bonds with the oxygen atoms O2A and O5B positioned in the interior.

Although sharper diffraction patterns from agarose films dried at about 100°C are in favor of extended single helices, h ranging from 8.9 to 9.7 Å (Foord and Atkins, 1989), such models are incompatible with chiroptical data (Shafer and Stevens, 1995) that are consistent only with the double helical model derived from the original x-ray analysis (Arnott *et al.*, 1974b)

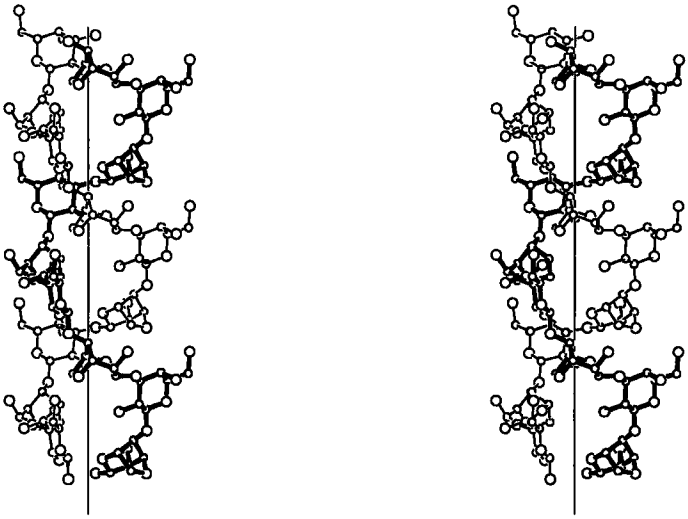

FIG. 27. Stereo view of about a turn of the threefold double helix of agarose. The two chains are distinguished by thin and thick bonds for clarity. The vertical line is the helix axis. Only van der Waals forces stabilize the double helix.

or from a later energy minimization procedure (Jimenez-Barbero *et al.*, 1989).

Despite the absence of internal hydrogen bonds in the double helix, agar gels have a high melting point (75–85°C). This superiority over carrageenan gels is particularly useful in bakery products, for instance, cake icing, cream cheeses, candies, cookies, and pie fillings. Although nondigestible, agar jelly noodles are widely consumed in Japan (Selby and Whistler, 1993; Stanley, 1995).

D. THE GELLAN FAMILY OF POLYSACCHARIDES

Up to eight anionic polysaccharides, including gellan, welan, S-657, and rhamsan, are secreted by unrelated bacteria and, barring substituents, their main chains have the same tetrasaccharide repeat (A–B–C–D) as the parent polymer gellan (Chandrasekaran and Radha, 1995). Chemically, barring the difference between CH_2OH and COOH groups, 75% of the gellan backbone (i.e., A–B–C) is cellulose-like. As shown below, the native polymer secreted by *Pseudomonas elodea* has both glyceryl and acetyl substituents and is referred to as native gellan. Commercial deesterification of native gellan by hot alkali treatment removes the substituents and the resulting material is called gellan. The branched polysaccharide welan (with

side chain E, Rha:Man being 2:1) is an excellent viscosifier. Since it has the potential for food applications, it is included in this review.

Crystal structures are now well established for native gellan, gellan, and welan. Most other members including S-657 and rhamsan are branched like welan. The side chains in them are flexible disaccharides and their diffraction patterns are of poor quality. Hence structural details are elusive, but through computer modeling, they are believed to exist as gellan-like helices (Lee and Chandrasekaran, 1991).

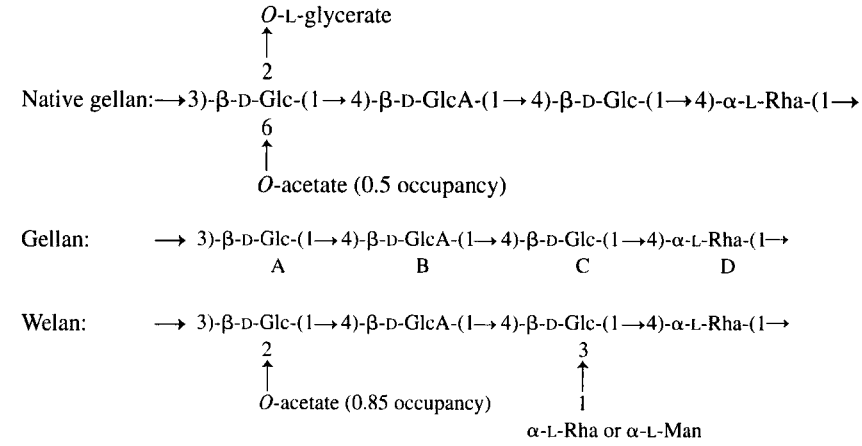

The high-acyl native gellan and the acyl-free gellan are both gel-forming and texturing polysaccharides. While the former forms only soft and spongy gels, the latter forms hard and brittle gels. By combining the two in proper ratios, and by the use of appropriate cations, gels of desired quality can be prepared. X-ray analyses reveal only subtle differences in molecular morphology between the two polymers. Altered packing arrangements, however, are able to explain their respective gelling behaviors.

a. Potassium Native Gellan. An x-ray study (Chandrasekaran *et al.*, 1992) revealed that native gellan helices are packed in a trigonal unit cell ($a = b = 16.47$, $c = 28.42$ Å, and $\gamma = 120°$). The molecule forms a parallel, threefold, left-handed ($t = -120°$) double helix of pitch $2c = 56.84$ Å ($h = 18.95$ Å) as shown in Fig. 28a. Among the four monomers, α-L-rhamnose adopts $^1C_4$, and the other three have $^4C_1$ chair geometry. The inner and outer diameters of the helix are 1.2 and 20.7 Å, respectively, implying that there is no hole along the helix axis. Four sets of conformational parameters (in degrees) at the linkages A–B, B–C, C–D, and D–A define the main chain geometry. They are specified by (τ_1, ϕ_1, ψ_1) = (116.1, −99, −150),

(τ_2, ϕ_2, ψ_2) = (116.6, −134, −148), (τ_3, ϕ_3, ψ_3) = (115.9, −141, 98), and (τ_4, ϕ_4, ψ_4) = (116.4, −119, 64), respectively; the hydroxymethyl or carboxylate orientations in the four saccharides are $\chi_A = -82°$, $\chi_B = 24°$, $\chi_C = 62°$, and $\chi_D = 91°$. Parameters defining the orientation of the glyceryl group at O2A are: θ_1(C3-C2-O2-C9) = 42°, θ_2(C2-O2-C9-C10) = −166°, θ_3(O2-C9-C10-C11) = 78°, and θ_4(C9-C10-C11-O11) = 96°. Those for the acetate group at O6A are: θ_5(C5-C6-O6-C7) = 159° and θ_6(C6-O6-C7-C8) = 73°. The nearly extended polysaccharide chain exhibits one hydrogen bond across every glycosyl bridge oxygen: cellulose-like O3HB···O5A (2.73 Å), O2HB···O6C (2.92 Å), O3HD···O2C (2.99 Å), and O4HA···O5D (3.10 Å). The glycerate group also participates in two intrachain hydrogen bonds: O10HA···O61B (2.59 Å) and O11HA···O3D (3.08 Å). Crucial to stability of the double helix are the three interchain hydrogen bonds O6HC···O62B (3.08 Å), O6HC···O10A (2.55 Å), and O2HB···O10A (3.11 Å), of which the latter two involve the glycerate moiety. This setup leads to partial shielding of the carboxylate group so that the potassium ion located nearby has only half occupancy; also the ion has just three ligands, instead of about six as normally observed for potassium. They are atoms O62B, O5B, and O3C in disaccharide B–C. Unable to reach out both chains in the helix, each ion dangles to one chain only. Two double helices pass through (*a*/3 2*b*/3 0) and (2*a*/3 *b*/3 0) of the unit cell in an antiparallel fashion (Fig. 28b), the lateral separation between them being 9.5 Å. There are two ordered water molecules per tetrasaccharide repeat that form water bridges and help to stabilize the packing arrangement, which includes only a few direct hydrogen bonds. The final *R*-value of this structure is 0.17 for 42 reflections. Since their positions are not conducive to linking the carboxylate groups of neighboring helices, the ions are unable to strengthen the junction zones in the case of native gellan.

The structural roles of the acetyl and glyceryl groups can be readily extracted from these results. For example, the axial view of the unit cell contents (Fig. 28b) indicates that the acetyl groups on the periphery protrude into neighboring unit cells, but do not interfere with the association of double helices. On the other hand, each glycerate group screens an adjacent carboxylate group from efficient ion binding, thereby making ion-mediated interhelical association less probable or fragile at best. Hence, it seems that native gellan's soft and spongy gelling behavior stems from its glycerate and not acetate groups. This is further corroborated by experimental observations (Baird *et al.*, 1992).

b. Potassium Gellan. Diffraction patterns from polycrystalline and well-oriented fibers of potassium gellan (Chandrasekaran *et al.*, 1988b) contain nearly 40 sharp Bragg reflections up to 3 Å resolution that can be

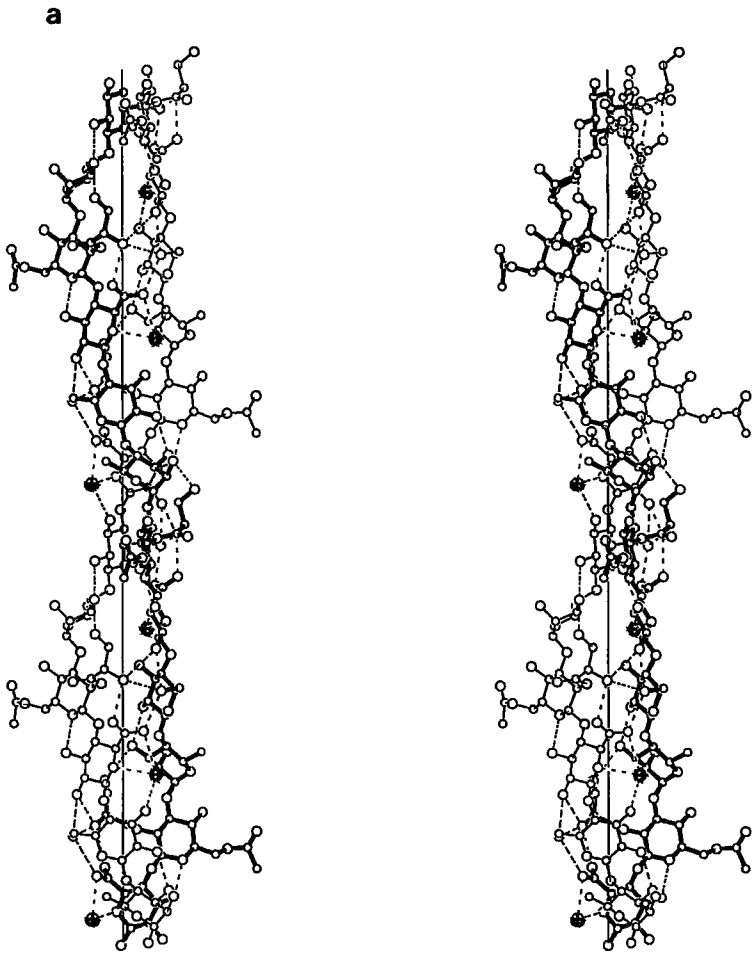

FIG. 28. (a) Stereo view of about a turn of the threefold double helix of native gellan. The two chains are drawn in thin and thick bonds for distinction. Both intra- and interchain hydrogen bonds stabilize the helix. The vertical line is the helix axis. Potassium ions (crossed circles) have only half occupancy at each site. (b) A *c*-axis projection of the trigonal unit cell contents showing an antiparallel packing arrangement of two double helices drawn in thin and thick bonds.

indexed on a trigonal unit cell ($a = b = 15.75$, $c = 28.15$ Å, and $\gamma = 120°$). The x-ray analysis has (a) confirmed that the previously determined molecular structure and packing arrangement of lithium gellan (Chandrasekaran *et al.*, 1988a) are valid for potassium gellan also, and (b) yielded structural details on several ordered water molecules in the unit cell and on the tight binding of potassium ion to gellan helix. This information was

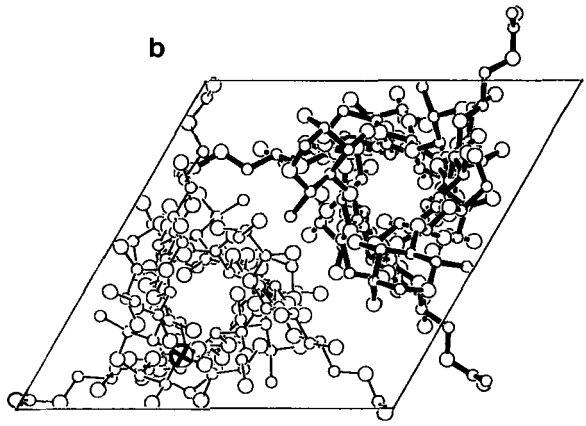

FIG. 28. Continued

beyond the reach of the lithium gellan investigation owing to the very low scattering power of lithium ion. With its slightly shorter axial rise per tetrasaccharide repeat (h = 18.78 Å), the potassium gellan helix ($t = -120°$) shown in Fig. 29a is isomorphous to that of native gellan described before. The parallel, half-staggered, double helix is stabilized by both intra- and interchain hydrogen bonds. The flexibility of the chain is tempered by three bonds per tetrasaccharide, O3HB···O5A (2.92 Å), O2HA···O61B (2.51 Å), and O2HB···O6C (2.45 Å), but there are none across C–D or D–A. Apart from the interchain O6HC···O62B (3.04 Å), both chains in the double helix are strongly linked through six ligands to a potassium ion with full occupancy near each carboxylate group. The roughly octahedral coordination is generated by atoms O2A, O61B, and O62B, in one chain, O2C and O6C in the other, and an ordered water molecule (W). This ion cage seems to be a symbol of robustness of the gellan molecule in the presence of monovalent ions such as lithium, sodium, potassium, and rubidium. The inner and outer diameters of this rod-like helix are 1.1 and 15.8 Å, respectively, and the latter corresponds to atom O6A. The backbone geometry and the side group orientations are given by (τ_1, ϕ_1, ψ_1) = (116.5, −101, −136), (τ_2, ϕ_2, ψ_2) = (116.5, −154, −144), (τ_3, ϕ_3, ψ_3) = (115.9, −150, 86), and (τ_4, ϕ_4, ψ_4) = (117.7, −124, 88); $\chi_A = -79°$, $\chi_B = 10°$, $\chi_C = 58°$, and $\chi_D = 77°$. The R-value for the final model is 0.18 for 51 reflections, of which 38 are observed.

Two double helices pass through (2a/3 b/3 0) and (a/3 2b/3 0) per cell in an antiparallel fashion (Fig. 29b). They are laterally separated by 9.1 Å, which is 0.4 Å less than in native gellan. Four structured water molecules per tetrasaccharide repeat have been located in the unit cell. Each ion cage

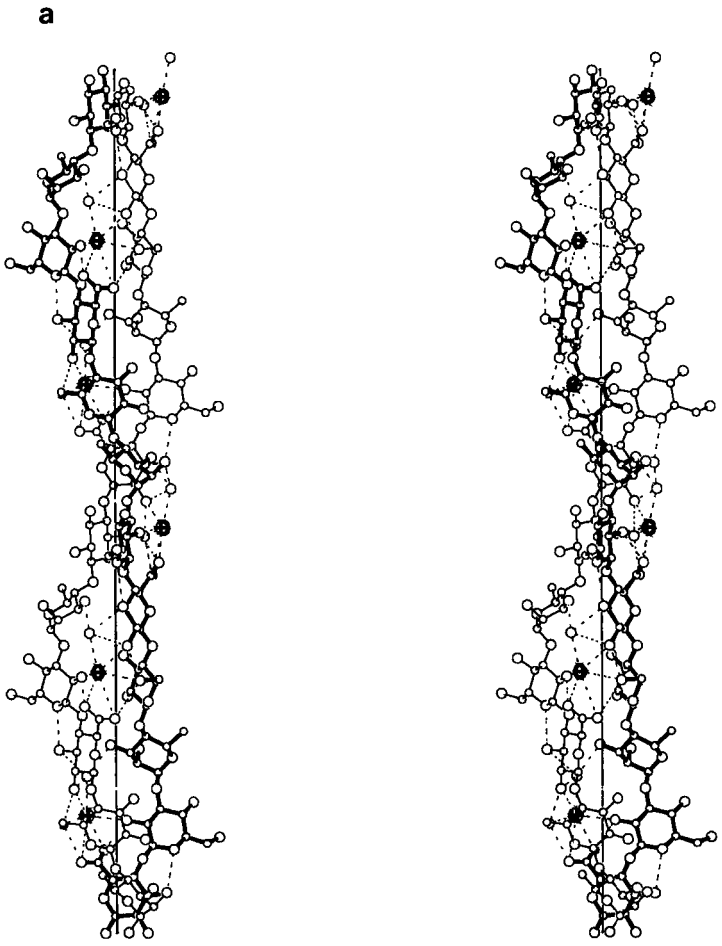

FIG. 29. (a) Stereo view of about a turn of the threefold double helix of potassium gellan. The two chains are drawn in thin and thick bonds for distinction. Both intra- and interchain hydrogen bonds stabilize the helix. The vertical line is the helix axis. Octahedrally coordinated potassium ions (crossed circles) and triply hydrogen-bonded water molecules (open circles) located above each ion are part and parcel of gellan. (b) A *c*-axis projection of the trigonal unit cell contents showing an antiparallel packing arrangement of two double helices, drawn in thin and thick bonds.

is juxtaposed to another in a neighboring helix so that distance between the two cations is only 4.3 Å. This allows interhelical association through strong carboxylate–potassium–water–potassium–carboxylate interactions in every tetrameric repeat, which in turn strengthens the junction zones

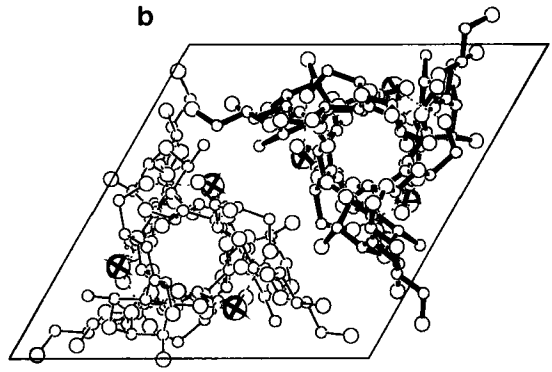

FIG. 29. Continued

responsible for gelation. Extrapolation of these experimental results by computer modeling (Chandrasekaran and Thailambal, 1990) shows that calcium gellan double helices would associate even stronger due to direct carboxylate–calcium–carboxylate interactions. This appears to be the molecular basis for the strong and brittle gelation behavior of calcium gellan even at low ionic strength.

Although gellan gum was discovered in 1977, approval for food applications in the United States and several other countries was not granted until the middle of this decade. It is not just another gelling agent, it is also a texturizing, stabilizing, film-forming, viscosifying, and flavor-releasing polysaccharide. Its versatility is obvious from its use in puddings, dessert gels, frostings, beverages, dairy products, fruit spreads, bakery fillings, glazes, confections, sauces, batters, and breadings (Kang and Pettitt, 1993).

2. *Welan*

X-ray diffraction patterns from well-oriented and polycrystalline fibers of calcium welan (Fig. 5c) closely resemble those of gellan and contain excellent intensity data, about 80 reflections up to 2.5 Å resolution (Chandrasekaran *et al.*, 1994a). The unit cell is trigonal ($a = b = 20.83$, $c = 28.69$ Å, and $\gamma = 120°$) and much larger than that of gellan. Detailed structure analysis reveals that welan also exists as a gellan-like double helix whose pitch, $2c = 57.38$ Å, is 1 Å higher ($h = 19.1$ Å) than that of gellan. The backbone is stiffened by a total of six intrachain hydrogen bonds per pentasaccharide repeat, including O3HB···O5A (2.46 Å), O3HD···O2C (3.06 Å), and O4HA···O5D (2.93 Å) within the main chain. The other three are through the rhamnose/mannose side chain

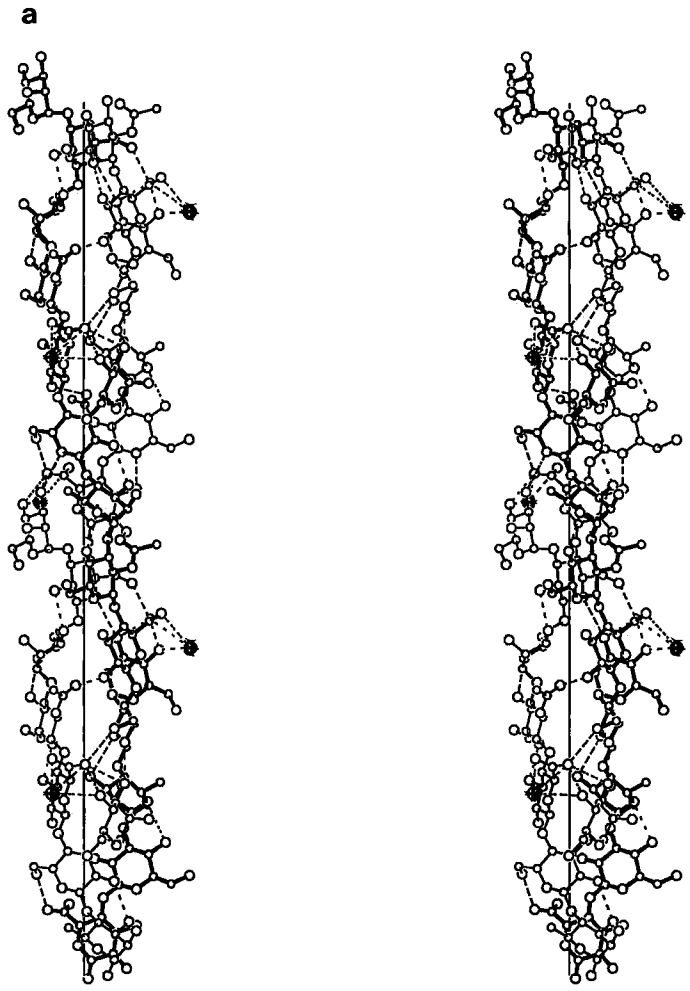

FIG. 30. (a) Stereo view of one turn of the threefold welan double helix. The two chains are drawn in thin and thick bonds for distinction. The vertical line represents the helix axis. Both intra- and interchain hydrogen bonds and side chains hydrogen bonded to carboxylate groups stabilize the double helix. Calcium ions (crossed circles) are present near the carboxylate groups, but outside the helix in order to make inter-double helical connections. (b) A *c*-axis projection of the trigonal unit cell contents shows the packing arrangement of three welan double helices. The helix drawn in solid bonds is antiparallel to the remaining helices (thin and open bonds). Note that calcium ions are positioned between helices and each water molecule (large open circle) shown here is connected to all three surrounding helices. Several other ordered water molecules (not shown) have been located in the interstitial space.

(E), namely, O3HE···O62B (3.04 Å), O4HE···O62B (2.58 Å), and O2HC···O5E (2.84 Å). Gellan-like O6HC···O62B (3.08 Å) and side chain-promoted O3HE···O5C (3.16 Å) and O2HB···O7A (2.49 Å) are interchain hydrogen bonds. Consequently, the welan double helix (Fig. 30a) is very sturdy. Its inner and outer diameters are 1.2 and 13.0 Å, respectively. Surprisingly, in spite of its side chains, the welan helix is marginally slimmer than native gellan and gellan helices. The five sets of conformational parameters in degrees are given by (τ_1, ϕ_1, ψ_1) = (116.6, −90, −157), (τ_2, ϕ_2, ψ_2) = (116.6, −147, −157), (τ_3, ϕ_3, ψ_3) = (115.9, −155, 96), (τ_4, ϕ_4, ψ_4) = (117.6, −104, 90), and (τ_5, ϕ_5, ψ_5) = (116.5, −35, 168) for the side chain; the hydroxymethyl or carboxylate orientations are χ_A = −70°, χ_B = 37°, χ_C = 85°, χ_D = 84°, and χ_E = 37°. The orientation of the acetyl substituent at O2A is given by θ_1(C3–C2–O2–C7) = −66° and θ_2(C2–O2–C7–O7) = −21°. The *R*-value for the final model is 0.22 for 102 reflections, of which 76 are observed.

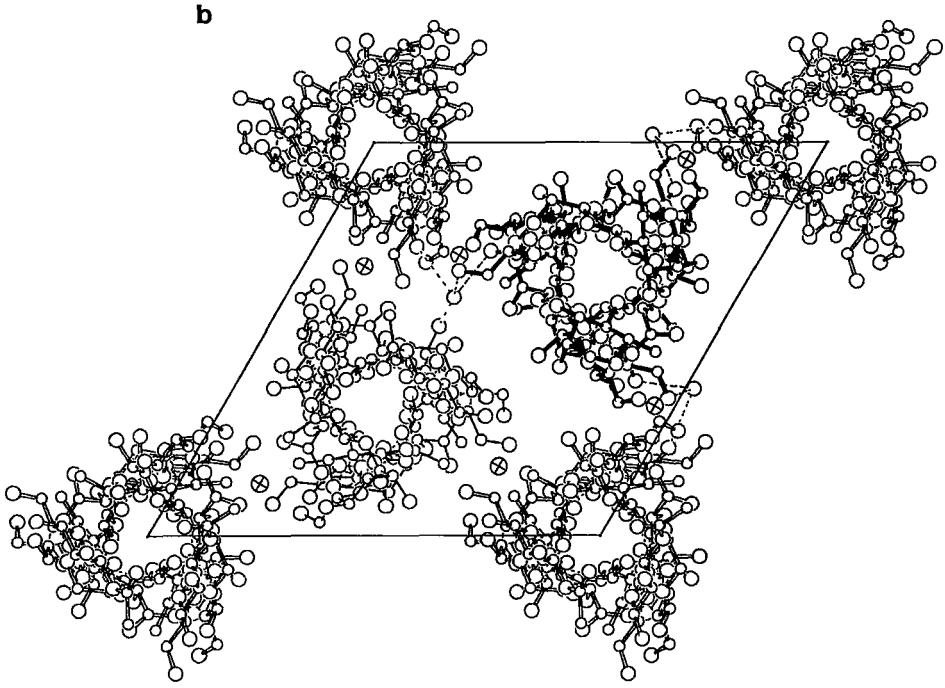

FIG. 30. Continued

Three welan helices pass through the unit cell as shown in Fig. 30b. Two of them, I and II, respectively at (2*a*/3 *b*/3 0) and (*a*/3 2*b*/3 0), are antiparallel as in gellan and the third, III, at (0 0 0), is new and parallel to the first. They are equidistant (12.0 Å) from each other, 2.9 Å farther than in gellan. The unit cell accommodates 9 pentasaccharides, 6 calcium ions, and 75 ordered water molecules. The experimental results (Chandrasekaran *et al.,* 1994a) show that welan helices interact via side chains and surrounding guest molecules. Specifically, I and II are linked only by side chain···side chain hydrogen bonds involving atoms O2 and O4. I and III, aligned parallel, are connected by carboxylate–calcium–water–carboxylate interactions in addition to hydrogen bonds between residues A and E. II and III, aligned antiparallel, are held together by very strong carboxylate–calcium–carboxylate interactions in addition to side chain···main chain hydrogen bonds. Largely facilitated by ordered water molecules, these interactions are responsible for the intense viscosifying behavior of welan in solutions up to 130°C. Thus, the crystal structure of welan is an excellent comprehensive visualization of the constructive role of side chains to the stability of a branched polysaccharide helix whose favorable associative interactions at the molecular level relate to its macroscopic properties.

E. BRANCHED POLYSACCHARIDES

Side chains in polysaccharides can have stabilizing as well as destabilizing influences on structural organization. The structure of welan just described attests to the stabilizing effect of side chains on secondary structure and intermolecular ordering. The gel-forming, doubly branched, capsular polysaccharide (CPS) from *Rhizobium trifolii* having a hexasaccharide repeat also has an ordered helical structure; the side chains stabilize the molecular structure but not its packing arrangement. The monosaccharide side chains in galactomannans are flexible (Section III,A,*3*). Xanthan has a pentasaccharide repeat that includes a trisaccharide side chain that is far more flexible than the monosaccharide side chain in welan or galactomannan, and hence its structure remains elusive. Long side chains are susceptible to conformational fluctuations, resulting in less ordered structures. Such systems are invariably difficult to solve.

1. Rhizobium trifolii CPS

The doubly branched galactose-rich gel-forming capsular polysaccharide from *R. trifolii* consists of a hexamer repeat composed of main chain

–A–B–C– and two side chains, a monosaccharide D and a disaccharide F–E; both D and E are attached to A as shown below:

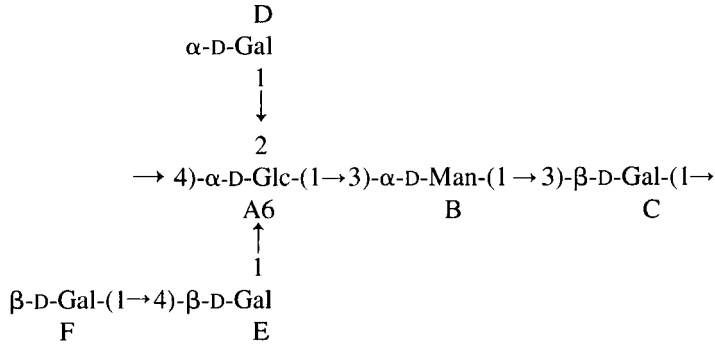

The neutral polysaccharide is water soluble and thermoreversible gels are formed in the temperature range 42 to 49°C in the absence of ionic co-solutes. For this reason it has the potential for food applications. Consistent with the x-ray data consisting of predominantly continuous intensities on layer lines and one or two Bragg reflections, the polymer forms a right-handed twofold helix (t = 180°) of pitch 20.2 Å (h = 10.1 Å). The molecular structure has been determined and refined against the continuous intensities to a final R-value of 0.28 (Lee and Chandrasekaran, 1992). As illustrated in Fig. 31a, the helix is very sinuous and it progresses with a right-handed twist. The six sets of conformational parameters in degrees at A–B, B–C, C–A, D–A, E–A, and F–E are given by (τ_1, ϕ_1, ψ_1) = (116.6, 67, 101), (τ_2, ϕ_2, ψ_2) = (116.8, 65, 100), (τ_3, ϕ_3, ψ_3) = (116.9, −84, −135), (τ_4, ϕ_4, ψ_4) = (116.7, 101, −94), (τ_5, ϕ_5, ψ_5) = (116.6, −90, −100), and (τ_6, ϕ_6, ψ_6) = (116.6, −132, 113), respectively; the hydroxymethyl orientations are χ_A = −85°, χ_B = −172°, χ_C = 70°, χ_D = −65°, χ_E = 79° and χ_F = 83°. There are eight hydrogen bonds per repeat, of which four are bifurcated. The interior main chain is stabilized by O3HA···O5C/O5D (2.72/2.79 Å) and O6HB···O2C (3.00 Å). The peripheral mono- and disaccharide side chains are connected to successive repeats by O2HD···O3F (3.03 Å) and O4HF···O2D/O3D (3.03/3.08 Å). The disaccharide side chain is internally stiffened by O6HE···O5F (2.80 Å) and O2HF···O3E (2.52 Å). The extensively hydrogen-bonded polymer chain has the appearance of a double helix whose inner and outer diameters are 2.2 and 19.8 Å, respectively.

A putative packing arrangement in a monoclinic unit cell (a = 16.8, b = 9.7, c = 20.2 Å, and γ = 90°) is shown in Fig. 31b. It reveals that there are no direct interactions among main chains of adjacent helices, but side chains may generate hydrogen bonds. Such an ordered picture is, however,

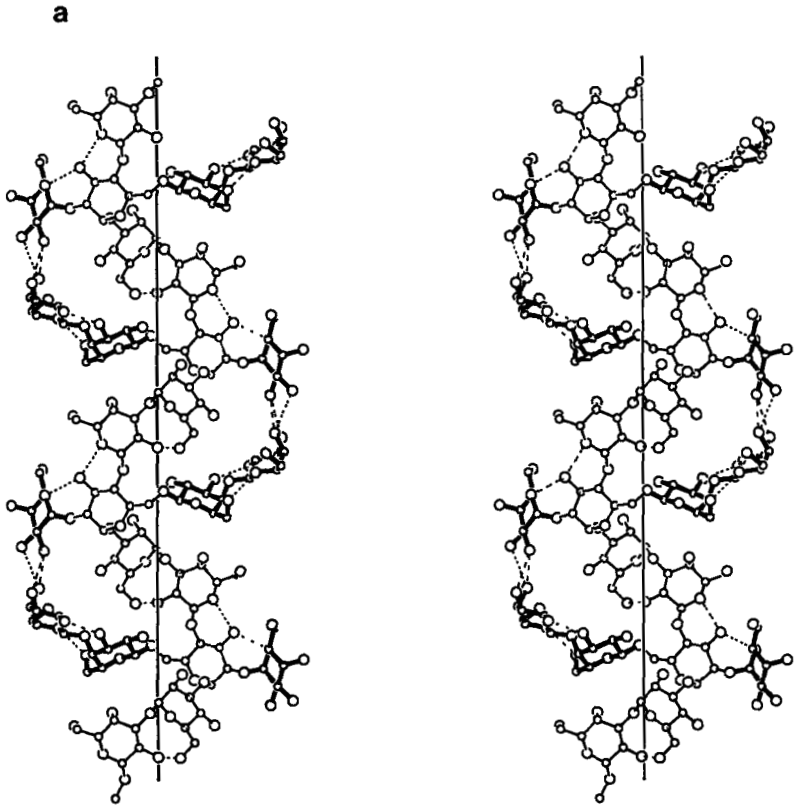

FIG. 31. (a) Stereo view of two turns of the right-handed, twofold helix of *R. trifolii* CPS. The mono- and disaccharide side chains (thick bonds) generate intrachain hydrogen bonds so that the molecule has the appearance of a double helix composed of two, inner and outer, strands. The vertical line represents the helix axis. (b) A *c*-axis projection of a monoclinic unit cell shows the putative packing arrangement of helices promoted by hydrogen bonds involving side chains.

not supported by the diffraction pattern. Perhaps the side chains in this CPS promote helix stability, but not interhelical association.

2. *Xanthan*

The microbial polysaccharide xanthan from *Xanthomonas campestris* has a pentasaccharide repeat composed of a cellobiose (disaccharide) in the main chain and an anionic trisaccharide side chain as shown below:

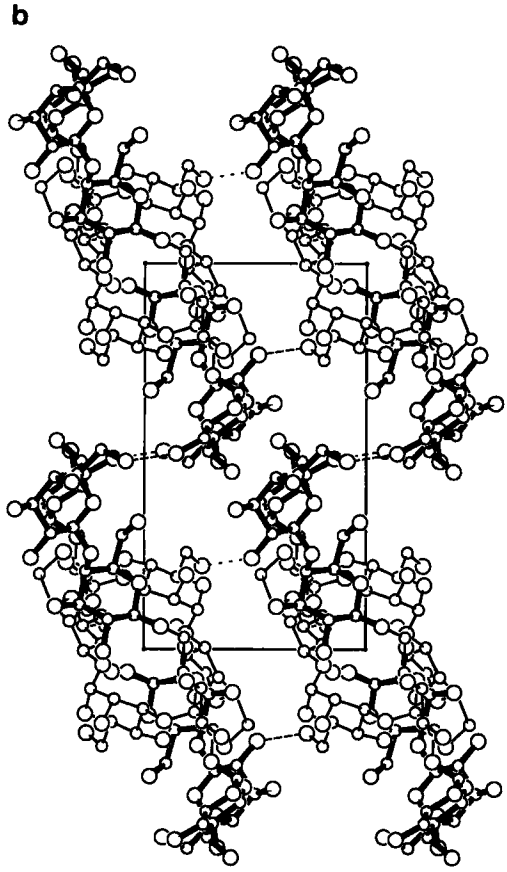

FIG. 31. Continued

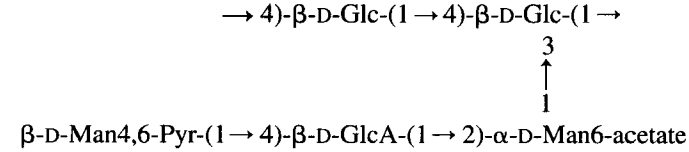

Xanthan is extensively used in many food applications because of its unique rheological properties (Kang and Pettitt, 1993; Morris, 1995). For example, its very high viscosity in aqueous solution is independent of pH in the range 2 to 12, and insensitive to salt effects and temperature from 18 to 80°C. Xanthan is added as an emulsifier in salad dressings and as a dispersion agent in desserts, gravies, sauces, and beverages. It is used in syrups, toppings, and relishes for enhancing consistency and flow properties.

Batters for baked goods are often mixed with xanthan in order to achieve required pseudoplastic properties.

X-ray diffraction patterns from xanthan fibers show much diffuse continuous intensity on layer lines and very few Bragg reflections (Moorhouse *et al.,* 1977; Okuyama *et al.,* 1980). Although the intensity data are not conducive to conducting detailed structure analysis, meridional spots on the $5n$ layer lines and their spacings indicate that the polymer has five-fold helix symmetry and a pitch of 47.0 Å; the cellobiose repeat in the main chain has h = 9.4 Å, which is 0.8 Å shorter than that of cellulose. From a knowledge of the helical parameters alone, several speculative models have been proposed so far. They include single and double helices; parallel and antiparallel chains; left- and right-handed chiralities; and up to four chains in the unit cell. However, none of the models provide an acceptable x-ray fit. Consequently, the molecular details of xanthan remain unknown. A right-handed (t = 72°) antiparallel duplex, generated by molecular modeling, is shown in Fig. 32 as an example of the various possibilities. Since the side chain is longer than the main chain in each repeat, it has greater flexibility to wrap around the main chain, reach out neighboring side chains, or extend out radially as much as possible. The range of interactions among adjacent side chains is perhaps so overwhelming that it may never be feasible to trap xanthan molecules in an ordered state for detailed diffraction study.

F. ARABINAN

Arabinan, a plant polysaccharide commonly found in large quantities in sugar beet, various seeds and roots, has a main chain composed of (1→5)-linked α-L-arabinofuranose residues. It occurs as a side chain attached to a long pectate chain through a rhamnose residue. Arabinan itself is a branched polymer containing arabinofuranose monomers as side chains at random. The enzymatically debranched linear polymer (DP 50–80), called araban, has very low water solubility, forms a spreadable gel similar to maltodextrins, and exhibits rheological properties like those of high-fat products and thus can be used in food applications as fat mimetics (Cooper *et al.,* 1992). It has also been reported that an L-arabinan obtained from apple juice is essentially linear (Churms *et al.,* 1983). Conformational analysis has led to six probable models, two-, three-, four-, and six-fold helices with distinct values of pitch, for arabinan (Cros *et al.,* 1994).

Oriented fibers of araban diffract like a microcrystalline powder sample, as shown in Fig. 5a. The spacings of the concentric rings in this pattern are consistent with a monoclinic unit cell of dimensions a = 5.55, b = 6.14, c = 8.74 Å, and γ = 90°, which could accommodate only two monomers (Chandrasekaran *et al.,* 1994b). This implies that a twofold helix of pitch

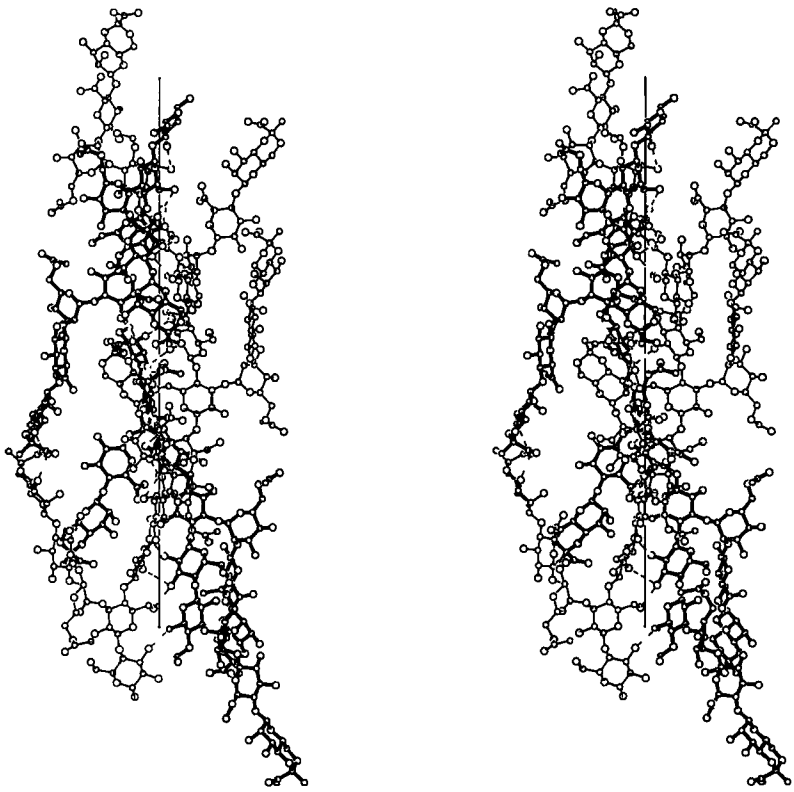

FIG. 32. Stereo view of about a turn of an antiparallel, right-handed, double helix as a probable molecular model of xanthan. The two strands are in thin and thick bonds for clarity. Both intra- and interchain hydrogen bonds are present. The side chains are turned toward the nonreducing end and aligned almost parallel to the helix axis (vertical line). The helix is further stabilized by hydrogen bonds between side chains.

a, b, or *c* is a good possibility if the araban chain adopts a regular structure. Conventional structure determination of a helical polymer is not possible with powder diffraction data. Hence, molecular modeling based on energy calculations has been employed to explore both C2′-*endo* and C3′-*endo* pentose conformations as viable options; the three conformation angles ϕ(C2-C1-O5′-C5′), ψ(C1-O5′-C5′-C4′), and χ(O5-C5-C4-C3) are the other variables. This has given rise to seven low-energy molecular models, all with the same pitch (c = 8.74 Å). There are considerable differences among them in terms of molecular geometry and crystal packing arrangement. Three of them correspond to C2′-*endo* and the other four to C3′-*endo* sugar rings. Two selected models, having the lowest energy within each

kind, are shown in Fig. 33. The C2′-*endo* helix (Figs. 33a, 33b) characterized by (τ, ϕ, ψ, χ) = (116.5, 116, 132, −66°) is stabilized by intrachain hydrogen bond O2H···O4 (2.82 Å) across the glycosidic oxygen atom. It has inner and outer diameters of 1.4 and 6.0 Å, respectively. Crystalline packing is facilitated by interhelix hydrogen bonds O3H···O4/O2 (2.70/2.82 Å). On the other hand, the C3′-*endo* helix (Figs. 33c, 33d) characterized by (τ, ϕ, ψ, χ) = (116.5, 54, −119, −59°) does not have intrachain hydrogen bonds. Its inner and outer diameters are 0.7 and 6.5 Å, respectively. Its crystalline packing arrangement is facilitated by O3H···O2 (3.0 Å) hydrogen bonds. Similar variations are present in the other twofold helical models (Radha and Chandrasekaran, 1997).

Due to the small energy difference between any pair, transition from one allomorph to another could be easily induced by breaking old and making new hydrogen bonds within and between helices. This polymorphism and tendency to form microcrystals in the solid state, as evident from the x-ray diffraction pattern, might confer upon arabinan or araban the observed fat mimetic properties.

IV. MIXED POLYSACCHARIDES

The quest for new polysaccharides superior to those now in use for food applications in this country is greatly hindered by factors such as the time (years) and expense (millions of dollars) it takes to get the FDA's approval for human consumption. A sensible approach for both cost effectiveness and quick availability is to tailor mixed polysaccharide systems having desired functional properties. This exploits the synergism between inexpensive materials and the necessity of using an expensive ingredient already in vogue.

Several laboratories have reported interesting results from a series of physicochemical (Dea *et al.,* 1977: Cheetham and Mashimba, 1991; Doublier and Llamas, 1991; Shatwell *et al.,* 1991a,b,c; Lundin and Hermansson, 1995) and x-ray (Cairns *et al.,* 1986; Brownsey *et al.,* 1988; Millane and Wang, 1990) studies during the past 20 years on the synergistic interactions of at least four major complexes: κ-carrageenan:galactomannan, κ-carrageenan:glucomannan, agarose:glucomannan, and xanthan:galacto-

FIG. 33. Two probable molecular structures and packing arrangements of twofold araban helices. Stereo view of two unit cells roughly normal to the *bc*-plane. The helices in the front are in thick bonds and those in the back are in thin bonds: (a) C2′-*endo* and (c) C3′-*endo*. A *c*-axis projection of the unit cell: (b) C2′-*endo* and (d) C3′-*endo*.

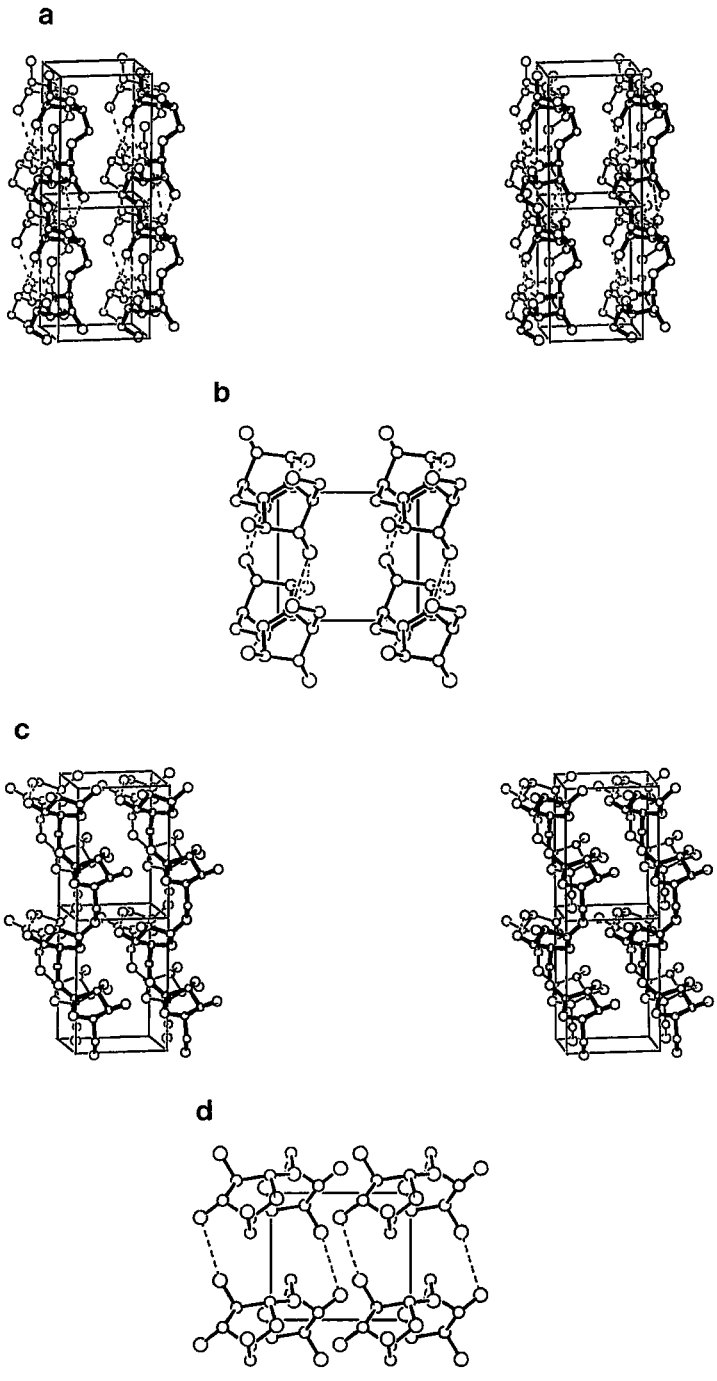
a
b
c
d

mannan systems. In each case, an anionic and a neutral polysaccharide are involved. No specific details on the molecular interactions have yet emerged. For the xanthan:galactomannan complex, it has long been believed that the backbone of xanthan helix associates with the naked region of galactomannan chain as inferred from schematic drawings (Cairns *et al.*, 1986; Cheetham and Mashimba, 1991). A recent modeling study guided by limited x-ray data has revealed preliminary molecular details of this complex for the first time (Chandrasekaran and Radha, 1997). The packing arrangement of cellulose I (Fig. 8) is one of the options that evokes backbone–backbone interactions between xanthan and galactomannan if both take up twofold helices like cellulose and mannan, respectively. An alternative is a fivefold double helix of pitch 47.4 Å in which a xanthan chain intertwines a galactomannan chain. Whether the strands are parallel or antiparallel, and whether the helix is right- or left-handed, are unresolved. One of the putative helices (Chandrasekaran and Radha, 1997) suggests that the hybrid may closely resemble the xanthan model depicted in Fig. 32. Since neither xanthan nor locust bean gum is known for gel formation, this type of intimate association is attractive with regard to onset of gelation observed for the complex.

V. MORPHOLOGY TO MACROSCOPIC PROPERTIES

The extended ribbon structures of cellulose and mannan enable them to strongly associate among themselves through hydrogen bonds. Such an effect prevents them from intimate interactions with solvents of any kind. This insolubility is essential for the integrity of cell walls in plants. Either structure is a valid model for the related glucomannan (konjac mannan), which is a $\beta(1\rightarrow4)$-linked random copolymer of glucose and mannose. In fact, the mannan II packing arrangement is viable for glucomannan also (Millane and Hendrixson, 1994). Introduction of side chains as in galactomannans and xanthan generates bumps along their main chains at regular or random intervals, creating big holes between neighboring polymer molecules to such an extent that polymer–solvent interactions exceed polymer–polymer interactions. As a result, an aqueous solution of either polymer becomes very viscous and is suitable for food applications. The same phenomenon is applicable to several cellulose derivatives, the strategy for the insoluble to soluble polymer conversion being the breakdown of the otherwise strong self-association.

It is quite remarkable that several polysaccharides, namely pectin, alginate, curdlan, carrageenan, and gellan, are known for their gelation proper-

ties and most of them are used in food applications. In principle, any gelling polysaccharide would do the job as well as any other; preferences are based on subtlety in behavior, availability, and above all economics.

Compatible with its function as a storage polysaccharide, amylose and its derivatives adopt a variety of structures including single and double helices. The ability to form a short and wide helix or a ring structure such as cyclodextrin is intended for capturing a spectrum of small molecules. The double helix is vital for the crystalline arrangement of amylopectin that gives robustness to starch granules.

Mixed-linkage (1→3), (1→4)-β-D-glucans, found in oat and barley cereals, are called soluble fibers or dietary fibers. While a detailed secondary structure of β-glucan is almost impossible to determine, it is not unthinkable that the (1→4) and (1→3) blocks might resemble the corresponding cellulose and curdlan structures previously described. A short stretch of an extended sixfold single helix of curdlan I (Okuyama *et al.,* 1991) is a probable motif for the latter block. The triple helix of curdlan III (Deslandes *et al.,* 1980) would require a cooperative association of three strands in the dietary fiber in proper register. The hexameric association of curdlan triple helices helps to form micelles (Fulton and Atkins, 1980). The existence of such a state in dietary fibers is realistic and consistent with the finding of micelle-like aggregation from light scattering experiments (Vårum *et al.,* 1992).

A comparison of the ordered structures of welan and *R. trifolii* CPS with those of galactomannans and predicted for xanthan gives mixed messages on the correlation between side chains and molecular morphology. The myth is that side chains interfere with helix formation, lateral organization, or both. This is consistent with the difficulty in inducing order in fibers of xanthan in which the main chains prefer extended ribbon structures and hydrogen-bonded sheets, but side chains have to be somehow accommodated. On the other hand, galactomannan, welan, and *R. trifolii* CPS helices require their side chains to promote helix stability and/or packing arrangement. These observations, taken together, point to the dual (constructive and destructive) roles of side chains to polymer geometry as well as to broader practical applications. Since flexibility prevails for long side chains, it is likely that backbone conformation is regular, but those of side chains are not. This leads to a partially ordered system. Similarly, several alternatives exhibiting different levels of ordering exist. Therefore, it is nearly impossible to correctly predict the structural behavior of branched polysaccharides in the solid state or in solution with currently available experimental and theoretical methods.

VI. SUMMARY

The morphologies of food polysaccharides described in this chapter illustrate the power of x-ray fiber diffraction in conjunction with computer modeling and sophisticated refinement techniques. On the other hand, the lack of information on structures such as xanthan reflects the inadequacy of the experimental techniques used to date. But the demands from academic and industrial sectors to investigate the molecular interactions in multicomponent systems, including protein–protein, protein–polysaccharide, polysaccharide–polysaccharide, and other complexes, are high and growing, because they have important food applications. These complexes are structurally more difficult than those solved in the past 40 years and it is improbable that any chosen system will be amenable for crystallographic investigation, crystals or fibers. Modern research facilities that include two-dimensional area detectors, millisecond exposures with synchrotron x-ray radiation, interactive computer graphics, sophisticated molecular dynamics calculations, unbelievably fast and inexpensive computers, and our own intellectual abilities are indispensable tools for the future of structural science in general and food polysaccharides in particular.

ACKNOWLEDGMENT

This work was supported by the Industrial Consortium of the Whistler Center for Carbohydrate Research.

REFERENCES

Arndt, E. R., and Stevens, E. S. 1996. Vacuum ultraviolet circular dichroism of gellan-family polymer films from water and dimethyl sulfoxide. *Carbohydr. Res.* **280,** 15–26.

Arnott, S., Scott, W. E., Rees, D. A., and McNab, C. G. A. 1974a. ι-Carrageenan: Molecular structure and packing of polysaccharide double helices in oriented fibers of divalent cation salts. *J. Mol. Biol.* **90,** 253–267.

Arnott, S., Fulmer, A., Scott, W. E., Dea, I. C. M., Moorhouse, R., and Rees, D. A. 1974b. The agarose double helix and its function in agarose gel structure. *J. Mol. Biol.* **90,** 269–284.

Atkins, E. D. T., Nieduszynski, I. A., Mackie, W., Parker, K. D., and Smolko, E. E. 1973a. Structural components of alginic acid. I. The crystalline structure of poly-β-D-mannuronic acid. Results of x-ray diffraction and polarized infrared studies. *Biopolymers* **12,** 1865–1878.

Atkins, E. D. T., Nieduszynski, I. A., Mackie, W., Parker, K. D., and Smolko, E. E. 1973b. Structural components of alginic acid. II. The crystalline structure of poly-α-L-guluronic acid. Results of x-ray diffraction and polarized infrared studies. *Biopolymers* **12,** 1879–1887.

Atkins, E. D. T., Farnell, S., Mackie, W., and Sheldrick, B. 1988. Crystalline structure and packing of mannan I. *Biopolymers* **27,** 1097–1105.

Baird, J. K., Talashek, T. A., and Chang, H. 1992. Gellan gum: Effect of composition on gel properties. *In* "Gums and Stabilisers for the Food Industry" (G. O. Phillips, P.A. Williams, and D. J. Wedlock, eds.), pp. 479–487. IRL Press, Oxford.

BeMiller, J. N. 1993. Starch-based gums. *In* "Industrial Gums: Polysaccharides and Their Derivatives" (R. L. Whistler and J. N. BeMiller, eds.), pp. 579–600. Academic Press, New York.

Biliaderis, C. G. 1991. The structure and interactions of starch with food constituents. *Can. J. Physiol. Pharmacol.* **69,** 60–78.

Biliaderis, C. G., and Galloway, G. 1989. Crystallization behavior of amylose-V complexes: Structure-property relationships. *Carbohydr. Res.* **189,** 31–48.

Biliaderis, C. G., Page, C. M., Slade, L., and Sirett, R. R. 1985. Thermal behavior of amylose-lipid complexes. *Carbohydr. Polym.* **5,** 367–389.

Bluhm, T. L., and Zugenmaier, P. 1979a. The crystal and molecular structure of tri-*O*-ethylamylose (TEA 3). *Carbohydr. Res.* **68,** 15–21.

Bluhm, T. L., and Zugenmaier, P. 1979b. Conformation and packing analysis of polysaccharides and derivatives: 6. Detailed refinement of tri-*O*-ethylamylose-solvent complexes TEA1-C1 and TEA1-DCM1. *Polymer* **20,** 23–30.

Bluhm, T. L., and Zugenmaier, P. (1981). Detailed structure of the V_h-amylose-iodine complex: a linear polyiodine chain. *Carbohydr. Res.* **89,** 1–10.

Bluhm, T. L., Deslandes, Y., Marchessault, R. H., Pérez, S., and Rinaudo, M. 1982. Solid-state and solution conformation of scleroglucan. *Carbohydr. Res.* **100,** 117–130.

Booy, F. P., Chanzy, H., and Sarko, A. 1979. Electron diffraction study of single crystals of amylose complexed with *n*-butanol. *Biopolymers* **18,** 2261–2266.

Branden, C., and Tooze, J. (eds.) 1991. "Introduction to Protein Structure." Garland Publishing, New York.

Brigand, G. 1993. Scleroglucan. *In* "Industrial Gums: Polysaccharides and Their Derivatives" (R. L. Whistler and J. N. BeMiller, eds.), pp. 461–474. Academic Press, New York.

Brownsey, G. J., Silvers, G. R., I'Anson, K., and Morris, V. J. 1984. Some observations (or problems) on the characterization of gellan gum solutions. *Int. J. Biol. Macromol.* **6,** 211–214.

Brownsey, G. J., Cairns, P., Miles, M. J., and Morris, V. J. 1988. Evidence for intermolecular binding between xanthan and the glucomannan konjac gum. *Carbohydr. Res.* **176,** 329–334.

Burchard, W. 1994. Light scattering techniques. *In* "Physical Techniques for the Study of Food Biopolymers" (S. B. Ross-Murphy, ed.), pp. 151–213. Blackie A & P, London.

Cairns, P., Miles, M. J., and Morris, V. J. 1986. Intermolecular binding of xanthan and carob gum. *Nature* **322,** 89–90.

Chandrasekaran, R., and Radha, A. 1995. Molecular architectures and functional properties of gellan gum and related polysaccharides. *Trends Food Sci. Technol.* **6,** 143–148.

Chandrasekaran, R., and Radha, A. 1997. Molecular modeling of xanthan:galactomannan interactions. *Carbohydr. Polym.* **32,** 201–208.

Chandrasekaran, R., and Thailambal, V. G. 1990. The influence of calcium ions, acetate and L-glycerate groups on the gellan double-helix. *Carbohydr. Polym.* **12,** 431–442.

Chandrasekaran, R., Millane, R. P., Arnott, S., and Atkins, E. D. T. 1988a. The crystal structure of gellan. *Carbohydr. Res.* **175,** 1–15.

Chandrasekaran, R., Puigjaner, L. C., Joyce, K., and Arnott, S. 1988b. Cation interactions in gellan: An x-ray study of the potassium salt. *Carbohydr. Res.* **181,** 23–40.

Chandrasekaran, R., Radha, A., and Thailambal, V. G. 1992. Roles of potassium ions, acetyl and L-glyceryl groups in native gellan double helix: An X-ray study. *Carbohydr. Res.* **224,** 1–17.

Chandrasekaran, R., Radha, A., and Lee, E. J. 1994a. Structural roles of calcium ions and side chains in welan: An x-ray study. *Carbohydr. Res.* **252,** 183–207.

Chandrasekaran, R., Radha, A., Lee E. J., and Zhang, M. 1994b. Molecular architecture of araban, galactoglucan and welan. *Carbohydr. Polym.* **25,** 235–243.

Chandrasekaran, R., Radha, A., and Okuyama, K. 1998. Morphology of galactomannans: An x-ray structure analysis of guaran. *Carbohydr. Res.*, in press.

Chanzy, H., Pérez, S., Miller, D. P., Paradossi, G., and Winter, W. T. 1987. An electron diffraction study of the mannan I crystal and molecular structure. *Macromolecules* **20,** 2407–2413.

Cheetham, N. W. H., and Mashimba, E. N. M. 1991. Conformational aspects of xanthan-galactomannan gelation. Further evidence from optical rotation studies. *Carbohydr. Polym.* **14,** 17–27.

Chien, Y. Y., and Winter, W. T. 1985. Accurate lattice parameters for tara gum. *Macromolecules* **18,** 1357–1359.

Chuah, C. T., Sarko, A., Deslandes, Y., and Marchessault, R. H. 1983. Triple-helical crystalline structure of curdlan and paramylon hydrates. *Macromolecules* **16,** 1375–1382.

Churms, S. C., Merrifield, E. H., Stephen, A. M., Walwyn, D. R., Polson, A., van der Merwe, K. J., Spies, H. S. C., and Costa, N. 1983. An L-arabinan from apple-juice concentrates. *Carbohydr. Res.* **113,** 339–344.

Clare, K. 1993. Algin. *In* "Industrial Gums: Polysaccharides and Their Derivatives" (R. L. Whistler and J. N. BeMiller, eds.), pp. 105–143. Academic Press, New York.

Clark, A. H. 1994. X-ray scattering and diffraction. *In* "Physical Techniques for the Study of Food Biopolymers" (S. B. Ross-Murphy, ed.), pp. 65–149. Blackie A & P, London.

Clarke, R. J., Coates, J. H., and Lincoln, S. F. 1988. Inclusion complexes of the cyclomaltooligosaccharides (cyclodextrins). *Adv. Carbohydr. Chem. Biochem.* **46,** 205–249.

Coffey, D. G., Bell, D. A., and Henderson, A. 1995. Cellulose and cellulose derivatives. In "Food Polysaccharides and Their Applications" (A. M. Stephen, ed.), pp. 123–153. Marcel Dekker, New York.

Cooper, J. M., McCleary, B. V., Morris, E. R., Richardson, R. K., Marrs, W. M., and Hart, R. J. 1992. Preparation, physical properties and potential food applications of enzymically-debranched araban from sugar beet. *In* "Gums and Stabilizers for the Food Industry 6" (G. O. Phillips, P. A. Williams, and D. J. Wedlock, eds.), pp. 451–460. IRL Press, Oxford.

Crescenzi, V., Dentini, M., Coviello, T., Paoletti, S., Cesàro, A., and Delben, F. 1987. On the solution and gelling behaviour of some bacterial polysaccharides. *Gazetta Chim. Ital.* **117,** 611–616.

Cros, S., Imberty, A., Bouchemal, N., Penhoat, C. H. D., and Pérez, S. 1994. Modeling of arabinofuranose and arabinan. II. NMR and conformational analysis of arabinobiose and arabinan. *Biopolymers* **34,** 1433–1437.

Dea, I. C. M., Morris, E. R., Rees, D. A., Welsh, E. J., Barnes, H. A., and Price, J. 1977. Associations of like and unlike polysaccharides: Mechanisms and specificity in galactomannans, interacting bacterial polysaccharides, and related systems. *Carbohydr. Res.* **57,** 249–272.

Deslandes, Y., Marchessault, R. H., and Sarko, A. 1980. Triple-helical structure of (1→3)-β-D-glucan. *Macromolecules* **13,** 1466–1471.

Desmarais, A. J., and Wint, R. F. (1993). Hydroxyalkyl and ethyl ethers of cellulose. *In* "Industrial Gums: Polysaccharides and Their Derivatives" (R. L. Whistler and J. N. BeMiller, eds.), pp. 505–535. Academic Press, New York.

Doublier, J-L., and Llamas, G. 1991. Flow and viscoelastic properties of mixed xanthan gum + galactomannan systems. *In* "Food Polymers, Gels and Colloids" (E. Dickinson, ed.), pp. 349–356. Royal Society of Chemistry, London.

Eliasson, A.-C. (ed.) 1996. "Carbohydrates in Food." Marcel Dekker, New York.

Feddersen, R. L., and Thorp, S. N. 1993. *In* "Industrial Gums: Polysaccharides and Their Derivatives" (R. L. Whistler and J. N. BeMiller, eds.), pp. 537–578. Academic Press, New York.

Foord, S. A., and Atkins, E. D. T. 1989. New x-ray diffraction results from agarose: Extended single helix structures and implications for gelation mechanism. *Biopolymers* **28,** 1345–1365.

Frei, E., and Preston, R. D. 1968. Non-cellulosic structural polysaccharides in algal cell walls. III. Mannan in siphoneous green algae. *Proc. R. Soc. London Ser. B* **169,** 127–145.

French, A. D., and Zobel, H. F. 1967. X-ray diffraction of oriented amylose fibers. I. Amylose dimethyl sulfoxide complex. *Biopolymers* **5,** 457–464.

French, D. 1984. Organization of starch granules. *In* "Starch: Chemistry and Technology" (R. L. Whistler, J. N. BeMiller, and E. F. Paschall, eds.), pp. 183–247. Academic Press, New York.

Fulton, W. S., and Atkins, E. D. T. 1980. The gelling mechanism and relationship to molecular structure of microbial polysaccharide curdlan. *Am. Chem. Soc. Symp. Ser.* **141,** 385–410.

Gardiner, E. S., and Sarko, A. 1985. Packing analysis of carbohydrates and polysaccharides. 16. The crystal structure of celluloses IV_I and IV_{II}. *Can. J. Chem.* **63,** 173–180.

Gardner, K. H., and Blackwell, J. 1974. The structure of native cellulose. *Biopolymers* **13,** 1975–2001.

Godet, M. C., Buléon, A., Tran, V., and Colonna, P. 1993a. Structural features of fatty acid-amylose complexes. *Carbohydr. Polym.* **21,** 91–95.

Godet, M. C., Tran, V., Delage, M. M., and Buléon, A. 1993b. Molecular modelling of the specific interactions involved in the amylose complexation by fatty acids. *Int. J. Biol. Macromol.* **15,** 11–16.

Godet, M. C., Bizot, H., and Buléon, A. 1995. Crystallization of amylose-fatty acid complexes prepared with different amylose chain lengths. *Carbohydr. Polym.* **27,** 47–52.

Grant, G. T., Morris, E. R., Rees, D. A., Smith, P. J. C., and Thom, D. 1973. Biological interactions between polysaccharides and divalent cations: The egg-box model. *FEBS Lett.* **32,** 195–198.

Grover, J. A. 1993. Methyl cellulose and its derivatives. *In* "Industrial Gums: Polysaccharides and Their Derivatives" (R. L. Whistler and J. N. BeMiller, eds.), pp. 475–504. Academic Press, New York.

Gunning, A. P., and Morris, V. J. 1990. Light scattering studies of tetramethylammonium gellan. *Int. J. Biol. Macromol.* **12,** 338–341.

Hamilton, W. C. 1965. Significance tests on crystallographic *R* factor. *Acta Crystallogr.* **18,** 502–510.

Harada, T., Terasaki, M., and Harada, A. 1993. Curdlan. *In* "Industrial Gums: Polysaccharides and Their Derivatives" (R. L. Whistler and J. N. BeMiller, eds.), pp. 427–445. Academic Press, New York.

Hermansson, A.-M., and Langton, M. 1994. Electron Microscopy. *In* "Physical Techniques for the Study of Food Biopolymers" (S. B. Ross-Murphy, ed.), pp. 277–341. Blackie A & P, London.

Hinkle, M. E., and Zobel, H. 1968. X-ray diffraction of oriented amylose fibers. III. The structure of amylose-*n*-butanol complexes. *Biopolymers* **6,** 1119–1128.

Imberty, A., and Pérez, S. 1988. A revisit to the three-dimensional structure of B-type starch. *Biopolymers* **27,** 1205–1221.

Imberty, A., and Pérez, S. 1989. Conformational analysis and molecular modelling of the branching point of amylopectin. *Int. J. Biol. Macromol.* **11,** 177–185.

Imberty, A., Chanzy, H., Pérez, S., Buléon, A., and Tran, V. 1988. The double-helical nature of the crystalline part of A-starch. *J. Mol. Biol.* **201,** 365–378.

Imberty, A., Buléon, A., Tran, V., and Pérez, S. 1991. Recent advances in knowledge of starch structure. *Starch/Stärke* **43,** 375–384.

IUPAC-IUB Commission on Biochemical Nomenclature. 1971. *Arch. Biochem. Biophys.* **145,** 405–421.

Jimenez-Barbero, J., Bouffar-Roupe, C., Rochas, C., and Pérez, S. 1989. Modelling studies of solvent effects on the conformational stability of agarobiose and neoagarobiose and their relationship to agarose. *Int. J. Biol. Macromol.* **11,** 265–272.

Kang, K. S., and Pettitt, D. J. 1993. Xanthan, gellan, welan and rhamsan. *In* "Industrial Gums: Polysaccharides and Their Derivatives" (R. L. Whistler and J. N. BeMiller, eds.), pp. 341–397. Academic Press, New York.

Kirby, A. R., and Morris, V. J. 1994. New microscopes feel their way. *Biologist* **41,** 9–13.

Kolpak F. J., and Blackwell, J. 1976. Determination of the structure of cellulose. II. *Macromolecules* **9,** 273–278.

Lee, E. J., and Chandrasekaran, R. 1991. X-ray and computer modeling studies on gellan-related polymers: Molecular structures of welan, S-657, and rhamsan. *Carbohydr. Res.* **214,** 11–24.

Lee, E. J., and Chandrasekaran, R. 1992. The "pseudo double-helical" structure of the gel-forming capsular polysaccharide from *Rhizobium trifolii*. *Carbohydr. Res.* **231,** 171–183.

Lundin, L., and Hermansson, A-M. 1995. Supermolecular aspects of xanthan-locust bean gum gels based on rheology and electron microscopy. *Carbohydr. Polym.* **26,** 129–140.

Mackie, W., Pérez, S., Rizzo, R., Taravel, F., and Vignon, M. 1983. Aspects of the conformation of polyguluronate in the solid state and in solution. *Int. J. Biol. Macromol.* **5,** 329–341.

Maier, H., Anderson, M., Karl, C., Magnuson, K., and Whistler, R. L. 1993. Guar, locust bean, tara, and fenugreek gums. *In* "Industrial Gums. Polysaccharides and Their Derivatives" (R. L. Whistler and J. N. BeMiller, eds.), pp. 181–226. Academic Press, New York.

Marchessault, R. H., Deslandes, Y., Ogawa, K., and Sundararajan, P. R. (1980). X-ray diffraction data for β-(1→3)-D-glucan. *Can. J. Chem.* **55,** 300–303.

Meyer, K. H., and Misch, L. 1937. Positions des atomes dans le nouveau modèle spatial de la cellulose. *Helv. Chim. Acta* **20,** 232–244.

Millane, R. P. 1989. Relating reflection boundaries in x-ray fiber diffraction patterns to specimen morphology and their use for intensity measurement. *J. Macromol. Sci. -Phys. B* **28,** 149–166.

Millane, R. P., and Arnott, S. 1985a. Background removal in x-ray fiber diffraction patterns. *J. Appl. Crystallogr.* **18,** 419–423.

Millane, R. P., and Arnott, S. 1985b. Digital processing of x-ray diffraction patterns from oriented fibers. *J. Macromol. Sci. -Phys. B* **24,** 193–227.

Millane, R. P., and Hendrixson, T. L. 1994. Crystal structures of mannans and glucomannans. *Carbohydr. Polym.* **25,** 245–251.

Millane, R. P., and Wang, B. 1990. A cellulose-like conformation accessible to the xanthan backbone and implications for xanthan synergism. *Carbohydr. Polym.* **13,** 57–68.

Millane, R. P., Chandrasekaran, R., Arnott, S., and Dea, I. C. M. 1988. The molecular structure of kappa-carrageenan and comparison with iota-carrageenan. *Carbohydr. Res.* **182,** 1–17.

Moorhouse, R., Walkinshaw, M. D., and Arnott, S. 1977. Xanthan gum—Molecular conformation and interactions. *Am. Chem. Soc. Symp. Ser.* **45,** 90–102.

Morris, E. R. 1994. Chiroptical methods. *In* "Physical Techniques for the Study of Food Biopolymers" (S. B. Ross-Murphy, ed.), pp. 15–64. Blackie A & P, London.

Morris, V. J. 1995. Bacterial polysaccharides. *In* "Food Polysaccharides and Their Applications" (A. M. Stephen, ed.), pp. 341–375. Marcel Dekker, New York.

Nieduzynski, I., and Marchessault, R. 1972. The crystalline structure of poly-β,D(1→4′)mannose: Mannan I. *Can. J. Chem.* **50,** 2130–2138.

Okuyama, K., Arnott, S., Moorhouse, R., Walkinshaw, M. D., Atkins, E. D. T., and Wolf-Ullish, Ch. 1980. Fiber diffraction studies of bacterial polysaccharides. *Am. Chem. Soc. Symp. Ser.* **145,** 411–427.

Okuyama, K., Otsubo, A., Fukuzawa, Y., Ozawa, M., Harada, T., and Kasai, N. 1991. Single-helical structure of native curdlan and its aggregation state. *J. Carbohydr. Chem.* **10,** 645–656.

Radha, A., and Chandrasekaran, R. 1997. X-ray and conformational analysis of arabinan. *Carbohydr. Res.* **298,** 105–115.

Rappenecker, G., and Zugenmaier, P. 1981. Detailed refinement of the crystal structure of V_h-amylose. *Carbohydr. Res.* **89,** 11–19.

Rolin, C. 1993. Pectin. *In* "Industrial Gums: Polysaccharides and Their Derivatives" (R. L. Whistler and J. N. BeMiller, eds.), pp. 257–293. Academic Press, New York.

Ross-Murphy, S. B. (ed.) 1994. "Physical Techniques for the Study of Food Biopolymers." Blackie A & P, London.

Saenger, W. 1984. *In* "Principles of Nucleic Acids Structure" (C. R. Cantor, ed.). Springer-Verlag, Berlin.

Sarko, A., and Biloski, A. 1980. Crystal structure of the KOH-amylose complex. *Carbohydr. Res.* **79,** 11–21.

Sarko, A., and Marchessault, R. H. 1967. The crystalline structure of amylose triacetate. I. A stereochemical approach. *J. Am. Chem. Soc.* **89,** 6454–6462.

Sarko, A., and Muggli, R. 1974. Packing analysis of carbohydrates and polysaccharides. III. *Valonia* cellulose and cellulose II. *Macromolecules* **7,** 486–494.

Sarko, A., and Zugenmaier, P. 1980. Crystal structures of amylose and its derivatives. *Am. Chem. Soc. Symp. Ser.* **141,** 459–482.

Sarko, A., Southwick, J., and Hayashi, J. 1976. Packing analysis of carbohydrates and polysaccharides. 7. Crystal structure of cellulose III_I and its relationship to other cellulose polymorphs. *Macromolecules* **9,** 857–863.

Scott, W. E., and Arnott, S. 1972. Accurate x-ray diffraction analysis of fibrous polysaccharides containing pyranose rings. Part I. The linked-atom approach. *J. Chem. Soc. Perkin Trans.* **II,** 324–335.

Selby, H. H., and Whistler, R. L. 1993. Agar. *In* "Industrial Gums: Polysaccharides and Their Derivatives" (R. L. Whistler and J. N. BeMiller, eds.), pp. 87–103. Academic Press, New York.

Shafer, S. E., and Stevens, E. S. 1995. A re-examination of the double-helix model for agarose gels using optical rotation. *Biopolymers* **36,** 103–108.

Shatwell, K. P., Sutherland, I. W., Ross-Murphy, S. B., and Dea, I. C. M. 1991a. Influence of the acetyl substituent on the interaction of xanthan with plant polysaccharides—I. Xanthan-locust bean systems. *Carbohydr. Polym.* **14,** 29–51.

Shatwell, K. P., Sutherland, I. W., Ross-Murphy, S. B., and Dea, I. C. M. 1991b. Influence of the acetyl substituent on the interaction of xanthan with plant polysaccharides—II. Xanthan-guar gum systems. *Carbohydr. Polym.* **14,** 115–130.

Shatwell, K. P., Sutherland, I. W., Ross-Murphy, S. B., and Dea, I. C. M. 1991c. Influence of the acetyl substituent on the interaction of xanthan with plant polysaccharides—III. Xanthan-konjac mannan systems. *Carbohydr. Polym.* **14,** 131–147.

Smith, P. J. C., and Arnott, S. 1978. LALS: A linked-atom least-squares reciprocal-space refinement system incorporating stereochemical restraints to supplement sparse diffraction data. *Acta Crystallogr. A* **34,** 3–11.

Stanley, N. F. 1995. Agars. *In* "Food Polysaccharides and Their Applications" (A. M. Stephen, ed.), pp. 187–204. Marcel Dekker, New York.

Stephen, A. M. (ed.) 1995. "Food Polysaccharides and Their Applications." Marcel Dekker, New York.

Stipanovic, A. J., and Sarko, A. 1976. Packing analysis of carbohydrates and polysaccharides. 6. Molecular and crystal structure of regenerated cellulose II. *Macromolecules* **9,** 851–857.

Stout, G. H., and Jensen, L. H. 1989. "X-Ray Structure Determination: A Practical Guide." Wiley Interscience, New York.

Therkelsen, G. H. 1993. Carrageenan. *In* "Industrial Gums: Polysaccharides and Their Derivatives" (R. L. Whistler and J. N. BeMiller, eds.), pp. 145–180. Academic Press, New York.

Vårum, K. M., Smidsrød, O., and Brant, D. A. 1992. Light scattering reveals micelle-like aggregation in the (1→4), (1→3)-β-D-glucans from oat aleurone. *Food Hydrocolloids* **5,** 497–511.

Walkinshaw, M. D., and Arnott, S. 1981a. Conformations and interactions of pectins. I. X-ray diffraction analysis of sodium pectate in neutral and acidified forms. *J. Mol. Biol.* **153,** 1055–1073.

Walkinshaw, M. D., and Arnott, S. 1981b. Conformations and interactions of pectins. II. Models for junction zones in pectinic acid and calcium pectate gels. *J. Mol. Biol.* **153,** 1075–1085.

Whistler, R. L., and BeMiller, J. N. (eds.) 1993. "Industrial Gums: Polysaccharides and Their Derivatives." Academic Press, New York.

Whistler, R. L., and BeMiller, J. N. (eds.) 1997. "Carbohydrate Chemistry for Food Scientists." Eagan, Minnesota.

Wild, D. L., and Blanshard, J. M. V. 1986. The relationship of the crystal structure of amylose polymorphs to the structure of the starch granule. *Carbohydr. Polym.* **6,** 121–143.

Winter, W. T., and Sarko, A. 1974a. Crystal and molecular structure of V-anhydrous amylose. *Biopolymers* **13,** 1447–1460.

Winter, W. T., and Sarko, A. 1974b. Crystal and molecular structure of the amylose-DMSO complex. *Biopolymers* **13,** 1461–1482.

Wu, H. C. H., and Sarko, A. 1977. The crystal structure of A-starch: Is it double helical? *Carbohydr. Res.* **54,** C3–C6.

Wu, H. C. H., and Sarko, A. 1978a. The double-helical molecular structure of crystalline A-amylose. *Carbohydr. Res.* **61,** 27–40.

Wu, H. C. H., and Sarko, A. 1978b. The double-helical molecular structure of crystalline B-amylose. *Carbohydr. Res.* **61,** 7–25.

Zobel, H. F., French, A. D., and Hinkle, M. E. 1967. X-Ray diffraction study of oriented amylose fibers. II. Structure of V amyloses. *Biopolymers* **5,** 837–845.

Zugenmaier, P., and Sarko, A. 1976. Packing analysis of carbohydrates and polysaccharides. IV. A new method for detailed crystal structure refinement of polysaccharides and its application to V-amylose. *Biopolymers* **15,** 2121–2136.

Zugenmaier, P., and Sarko, A. 1980. The variable virtual bond: Modeling technique for solving polymer crystal structures. *Am. Chem. Soc. Symp. Ser.* **141,** 225–237.

Zugenmaier, P., Kuppel, A., and Husemann, E. 1977. Detailed refinement of trimethylamylose. *Am. Chem. Soc. Symp. Ser.* **48,** 115–132.